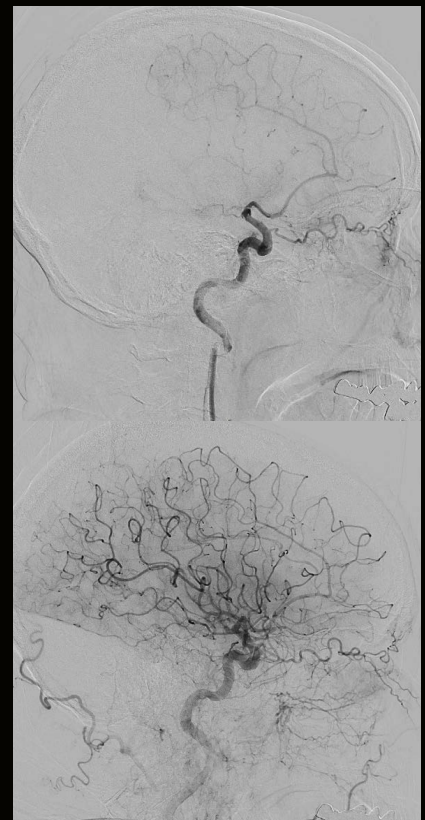
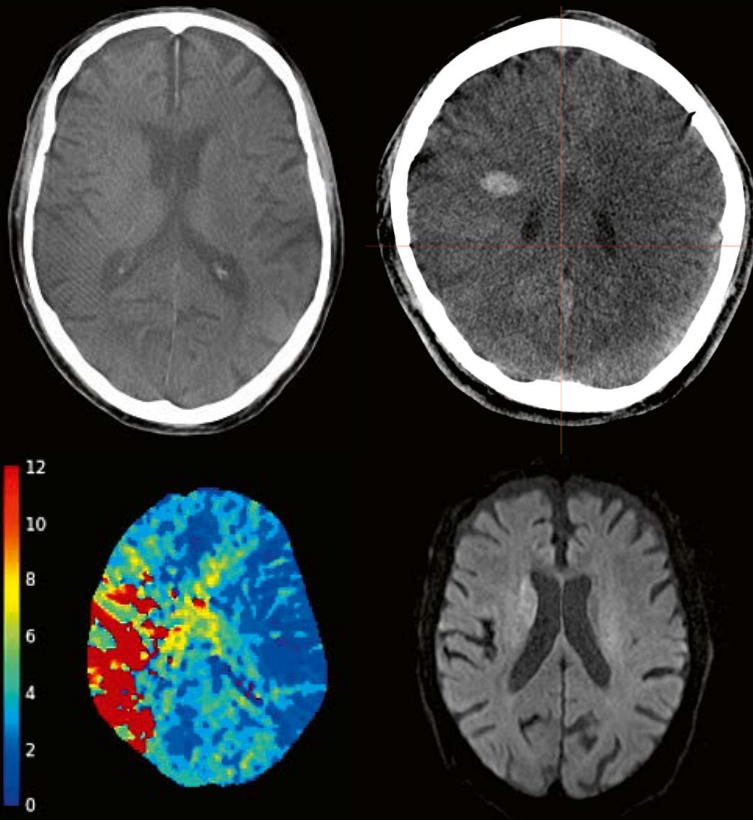
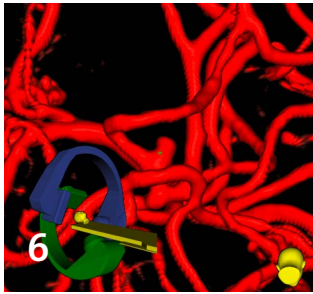


The Role of Imaging Along the Stroke Pathway

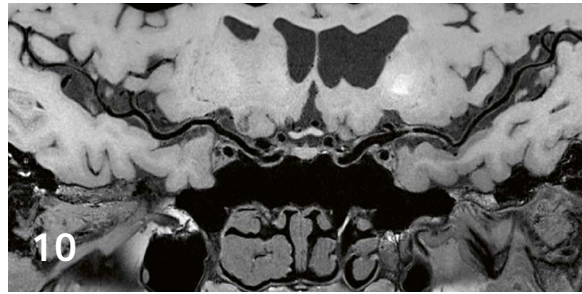
ESOC 2026

[siemens-healthineers.com/clinical-specialities/neurology/stroke-care](https://www.siemens-healthineers.com/clinical-specialities/neurology/stroke-care)

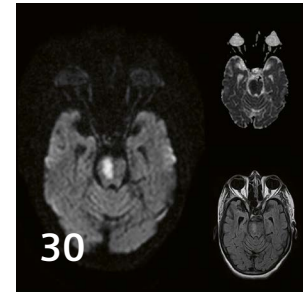




Automated head positioning



Vessel wall imaging



MRI in brainstem stroke

Editorial

4 The Evolving Role of Imaging in Stroke Care

Johannes Kaesmacher

University Hospital Bern, Inselspital, University of Bern,
Switzerland

Stroke Prevention

6 Automated Head Positioning to Optimize Biplane C-Arm Projections in Intracranial Aneurysm Treatment^{1,2}

Daniel Behme, et al.

University Clinic for Neuroradiology, University Hospital
Magdeburg, Germany

Research Campus STIMULATE, Otto-von-Guericke University,
Magdeburg, Germany

10 Updates on Advanced Whole-Brain Vessel Wall Imaging in Stroke Patients

Qi Yang, et al.

Department of Radiology, Beijing Chaoyang Hospital, Capital
Medical University, Beijing, China

16 How-I-do-it: Intracranial Vessel Wall MRI

Luigi Cirillo, et al.

Department of Biomedical and Neuromotor Sciences
(DIBINEM), University of Bologna, Italy

Acute Stroke Therapy

20 One-Stop Management Strategy for Acute Stroke Patients

Vera Aebischer and Marios-Nikos Psychogios

Department of Diagnostic and Interventional Neuroradiology,
University Hospital of Basel, Switzerland

24 Endovascular Treatment of an Unruptured Symptomatic Intracranial Aneurysm in a Toddler

Riitta Rautio, et al.

Turku University Hospital and University of Turku, Finland

Acute Stroke Imaging

30 Beyond the Clock: The Pivotal Role of Advanced MRI in Revolutionizing the Diagnosis and Management of Brainstem Stroke

Anirudda Deshpande, et al.

Department of Care of the Elderly & Stroke,
Altnagelvin Hospital, Londonderry, Northern Ireland, UK

33 Wake-Up Strokes: Advanced Imaging Solutions for Time-Sensitive Neurological Emergencies

Anirudda Deshpande, et al.

Department of Care of the Elderly & Stroke,
Altnagelvin Hospital, Londonderry, Northern Ireland, UK

¹ The information in this paper is based on research results that are not commercially available.

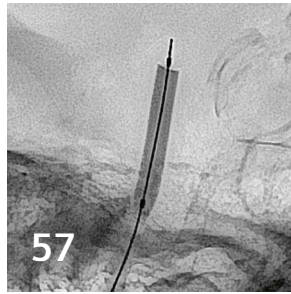
² Work in progress. The application is currently under development and is not for sale in the U.S. and in other countries. Its future availability cannot be ensured.

The statements by customers of Siemens Healthineers described herein are based on results that were achieved in the customer's unique setting. Since there is no "typical" hospital and many variables exist (e.g., hospital size, case mix, level of IT and/or automation adoption) there can be no guarantee that other customers will achieve the same results.

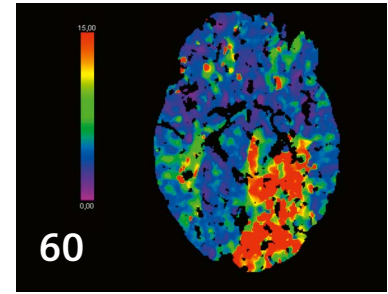
The products/features (mentioned herein) are not commercially available in all countries. Their future availability cannot be guaranteed.



Effect of copper filtration



Basilar artery brainstem perforators



Acute stroke with pcCT

38 Stroke Case Study Using a Lower-Field MRI System in a Tier 4 Town of Southern India

RG Jyothi, DNB; et al.

Jyothi Diagnostics, Madanapalle, India

40 One-Stop Management of Acute Ischemic Stroke Using an Angio-CT System¹

Michio Fujimoto

Dept. of Neurosurgery, Shin-Yurigaoka General Hospital, Kawasaki, Kanagawa, Japan

Therapy

46 The Distal Occlusion Tracker (DOT) Sign: A New Imaging Finding on Non-contrast DynaCT for the Detection of Remaining Vessel Occlusions After Mechanical Thrombectomy

Johannes Kaesmacher, et al.

University Hospital Bern, Inselspital, University of Bern, Switzerland

52 Effect of Copper Filtration on Radiation Dose in Cerebral 3D Rotational Angiography During Endovascular Aneurysm Treatment¹

Niclas Schmitt, Markus A Möhlenbruch, et al.

Department of Neuroradiology, Heidelberg University Hospital, Heidelberg, Germany

57 ARTIS icono Ultra-High-Resolution Cone-Beam Computed Tomography for Depiction of Basilar Artery Brainstem Perforators Prior to Stent Placement: A Short Case Report

Philippe Breiding

Department of Neurosurgery, University of Bern, Inselspital, Bern, Switzerland

Angiography

60 Optimizing Acute Stroke Diagnostics with Photon-counting CT: Balancing Multiphase CT Angiography, Perfusion, and Cardioembolic Assessment

Adrian Szum, et al.

Department of Clinical Neuroscience, Karolinska Institutet, Stockholm, Sweden

70 Flat-Panel CT Perfusion Imaging in the Angiography Suite to Assess Reperfusion Quality after Thrombectomy

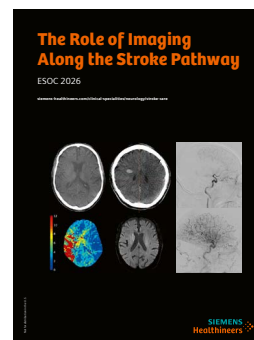
Adnan Mujanovic, et al.

Department of Diagnostic and Interventional Neuroradiology, University Hospital Bern, Inselspital, University of Bern, Switzerland

75 Pictorial Essay of Cerebral CT Angiographies in the Era of Photon-Counting CT

Matthias Lichy

Siemens Healthineers, Forchheim, Germany



Cover images

One-Stop Management Strategy for Acute Stroke Patients by Marios-Nikos Psychogios, et al. (Department of Diagnostic and Interventional Neuroradiology, University Hospital of Basel, Switzerland)



Johannes Kaesmacher is a clinician-scientist (M.D., Ph.D.) and interventional neuroradiologist with a clinical and academic focus on cerebrovascular diseases. After initial training in Munich, Germany, he is currently appointed as a senior physician at the University Hospital Bern and as an Associate Professor at the University of Bern as well as a Research Group Leader at the Stroke Research Center Bern, Switzerland. His research focuses on adjuvant medical therapies and new imaging techniques during acute interventional stroke treatment. He has been actively involved in multiple large international randomized stroke trials, including SWIFT DIRECT and IRIS, and is the sponsor of the recently finished TECNO trial. One of his specific research interests is detecting residual perfusion deficits after acute procedures to enable more individualized decision-making during acute patient care. He is actively involved in university-level training and education and serves on several committees of European medical societies (e.g. European Stroke Organisation, ESO; European Society of Minimal Invasive Neurological Therapy, ESMINT).

The Evolving Role of Imaging in Stroke Care

“The real voyage of discovery consists not in seeking new landscapes, but in having new eyes.”

Marcel Proust

One of the primary reasons proposed to explain the neutral results of the early endovascular stroke treatment trials was a lack of adequate imaging criteria for patient selection; specifically, the inclusion of patients without vessel occlusions and the failure to exclude those with large, likely irreversible, established infarcts.

We subsequently acquired “new eyes.” For every successful pivotal EVT trial for large vessel occlusion (LVO) stroke that followed, vessel imaging became mandatory, and all trials utilized some form of imaging proxy to exclude patients with extensive ischemic parenchyma. From there, the field enthusiastically evolved into an imaging-based expansion of indication criteria. This included wake-up and late-presenting strokes, yielding yet another resounding success for the field.

However, positive trial results using advanced imaging-based patient selection do not necessarily demonstrate true treatment effect heterogeneity. In other words, they do not prove that patients outside those strict imaging

criteria would not benefit. With the recent publication of late time window trials using simplified imaging criteria, alongside large-core trials and individual patient data meta-analyses consistently failing to establish clearly different responses to EVT based on advanced imaging phenotypes, a critical question emerges: Did we overdo it?

Growing evidence suggests we might have. The single most important factor seems to be swift diagnosis of an LVO with vessel imaging prompting urgent transfer to the angiography suite or to a comprehensive stroke center if no EVT can be performed at the local site. Models for automatic LVO detection are performing well and their implementation improved stroke-network time metrics and intervention volumes by automatic notifications and by increasing general awareness. Depending on a centers organization, direct-to-the-angiography transfers may constitute a reasonable alternative and trial results evaluating the diagnostic yield of flat-panel imaging in this scenario are eagerly awaited.

Along the clinico-scientific journey of more advanced imaging techniques, we have sharpened our eyes with knowledge, workflows, algorithms, and acquisition techniques that we can now repurpose. We must turn these tools toward frontiers where the risk-benefit profile is less clear than it is for the initial indication for EVT in LVO stroke.

The complexity of the distal frontier

The distal frontier remains complex. Recent trials on distal occlusion EVT yielded neutral results, likely due to overly simplistic inclusion criteria that failed to capture the heterogeneity of medium vessel occlusions. Here, the “advanced imaging” that has become less critical for proximal LVOs may find its renaissance. This is true for diagnosis, which is more complex for less specialized readers on vessel imaging alone. But also, in order to demonstrate benefit in distal territories, we probably require the more granular precision of perfusion imaging to distinguish patients who need interventions from those who will thrive with medical management. To achieve this, established thresholds must be rethought.

The AI-driven acceleration of MRI

While CT has long been the workhorse of acute stroke due to its speed, Artificial Intelligence is eroding that monopoly. Deep learning reconstruction and acceleration techniques are compressing MRI acquisition times to levels almost competitive with CT. This is a game-changer for the workup of milder strokes and the aforementioned distal occlusions. We are approaching a reality where the superior tissue contrast of MRI is available within the “stroke code” timeframe, offering a robust alternative.

The ultra-high field microscope

Parallel to the acute setting, the research domain is deepening its gaze. Ultra-high field MRI (7T and beyond) is disentangling pathophysiology that was previously invisible. In complex scenarios like primary angiitis of the CNS, incidental aneurysms, and intracranial atherosclerotic disease, ultra-High field provides an in vivo “histology.” It allows us to characterize vessel wall inflammation and plaque vulnerability with unprecedented clarity, moving us from morphological diagnosis to functional characterization of the disease state.

The Angio Suite as the decision cockpit

Finally, the decision-making timeline is shifting into the angiography suite itself. Real-time, decisions on rescue-stenting, additional maneuvers, intra-arterial thrombolytics and administration of antithrombotics are becoming paramount. We are seeing a surge in Flat-Panel CT capabilities, transforming the angio system from a purely therapeutic tool into an evolving diagnostic powerhouse. Coupled with newly described imaging findings and evolving techniques, interventionalists can now assess tissue-level perfusion¹, macrovascular vessel damage, blood-brain-barrier breakdown and tissue viability during the procedure, tailoring the aggressiveness of the recanalization strategy to the immediate pathophysiological reality of the patient.

Expansion to chronic cerebrovascular disease

Beyond the acute setting, the same AI tools and diagnostic software can be expanded to chronic cerebrovascular disease, where imaging-derived biomarkers already carry substantial prognostic and mechanistic information. Automated quantification of cerebral small vessel disease features and composite measures such as the SVD sum score allow standardized assessment of cumulative microvascular brain injury across populations and time. When integrated with longitudinal imaging, cognitive data, and clinical phenotypes, AI-driven models can help disentangle trajectories from covert vascular brain injury to overt (vascular) dementia, a domain characterized by substantial overlap with neurodegenerative processes. This opens the door to earlier risk stratification, refined trial enrichment, and individualized prevention strategies, effectively extending the paradigm of imaging-based precision medicine from hyperacute stroke care into the chronic and preclinical stages of cerebrovascular and cognitive disease.

Conclusion

We stand at a crossroads. For standard LVO strokes, we are learning that “less may be more.” However, for intra-procedural decision making, as well as for distal and complex pathologies, we are learning that we need to see more, faster, and deeper. By leveraging AI-accelerated MRI, Ultra-High Field insights, and real-time angio-suite diagnostics, we are not just imaging stroke; we are visualizing the future of personalized neurovascular care — in the hyperacute setting but also increasingly in primary and secondary prevention.

Acknowledgment

This text significantly benefited from feedback and suggestions by: PD Thomas R. Meinel, Ph.D., head of the neurological emergency department; Professor Urs Fischer, MD, MSc, director and chairman of neurology, and Professor Jan Gralla, MD, MSc, director and chairman of neuroradiology.



Johannes Kaesmacher

¹ The information in this paper is based on research results that are not commercially available.

Automated Head Positioning to Optimize Biplane C-Arm Projections in Intracranial Aneurysm Treatment

Stefan Klebingat, Ph.D.; Roland Schwab, M.D.; Daniel Behme, M.D.

University Clinic for Neuroradiology, University Hospital Magdeburg, Germany
Research Campus STIMULATE, Otto-von-Guericke University, Magdeburg, Germany

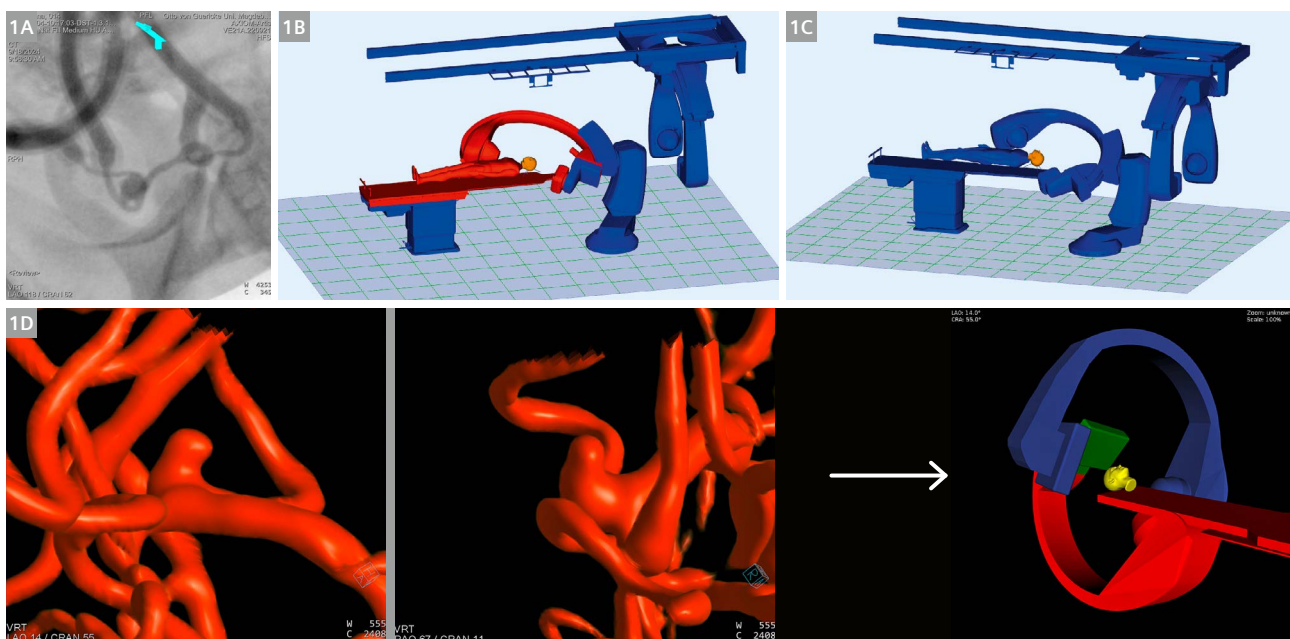
Introduction

The endovascular treatment of intracranial aneurysms has become a standard therapeutic option over the past three decades. Its success is closely linked to the quality of angiographic imaging, which not only enables diagnosis and procedural planning, but also provides the real-time guidance necessary for safe device deployment. Optimal imaging in this context does not merely mean standard anterior-posterior (AP) or lateral projections, but rather the identification of individualized “working projections” that provide unobstructed visualization of the aneurysm sac, the neck, and the parent vessels.

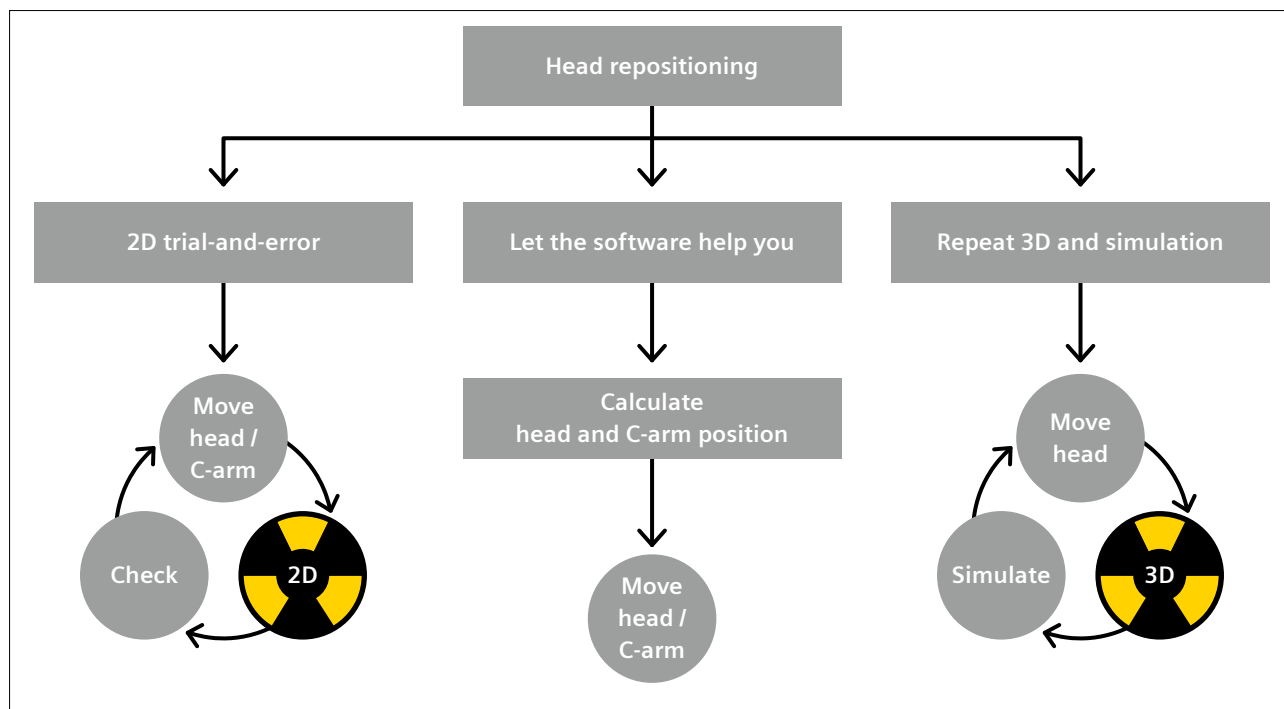
Traditionally, such projections were identified empirically, often requiring multiple 2D acquisitions in a trial-and-error fashion. The introduction of 3D rotational angiography and 3D digital subtraction angiography

(3D-DSA) has dramatically improved this process, allowing operators to plan projections on volumetric datasets before attempting them in the angiography suite. However, a persistent limitation remains: the mechanical restrictions of C-arm systems.

When an operator selects the theoretically optimal projection, it may not be physically achievable because of collision risks with the patient or the angiography table. This mismatch between imaging theory and clinical reality is a frequent bottleneck in neurointerventions. In some cases, it forces the use of suboptimal views, with potential consequences for device safety and procedural efficiency. In extreme cases, it may render an intended endovascular treatment technically impossible.



1 (1A) 3D display showing a perspective translucent mock rendering of a DSA scene. Users may select the optimal projection here. (1B) Simulation tool showing a collision issue with the selected ARTIS icono device angulation. (1C) Proposed solution, involving Head Movement and an attainable alternate angulation. (1D) The optimal projection for an MCA bifurcation aneurysm would cause a collision between the C-arm and the patient table.



2 Possible workflows for finding optimal working projections using (left) the traditional 2D-DSA trial-and-error method, (right) the repeated use of 3D-DSA and simulation, and (center) the one-time 3D-DSA and head-orientation simulation approach described in this article.

To address this gap, researchers at University Hospital Magdeburg have developed a prototype solution: automated calculation of optimized head positions¹. By adjusting the orientation of the patient's head, the anatomical relationship between the intracranial vessels and the C-arm geometry can be modified, creating feasible working projections that would otherwise be unattainable.

In close cooperation with Siemens Healthineers, the original prototype¹ is in the process of being further developed into an integrated solution with existing Siemens Healthineers angiography devices like the ARTIS icono or the ARTIS pheno.

Methods

The prototype software uses volumetric angiographic data as input. Based on operator-defined target projections, it calculates the C-arm angulations that would provide the desired view of the aneurysm. If these angulations are not feasible due to collision risks, the system simulates potential head repositioning maneuvers and determines new C-arm orientations that preserve the aneurysm visualization while avoiding collisions.

The software supports combined movements along three axes: flexion/extension ($\pm 30^\circ$), lateral tilt ($\pm 30^\circ$),

and rotation around the longitudinal axis (implemented but rarely required). The algorithm prioritizes solutions that minimize the extent of head movement required, preserving patient comfort and procedural workflow. Once an optimized head position is determined, the software outputs the necessary head angles and the corresponding new C-arm coordinates.

Validation was performed in vitro on 20 cases of anterior circulation aneurysms. Five experienced interventional neuroradiologists independently selected optimal working projections on a simulation platform, disregarding mechanical restrictions. This process yielded 100 candidate biplane working projections. Each candidate projection was then analyzed by the prototype.

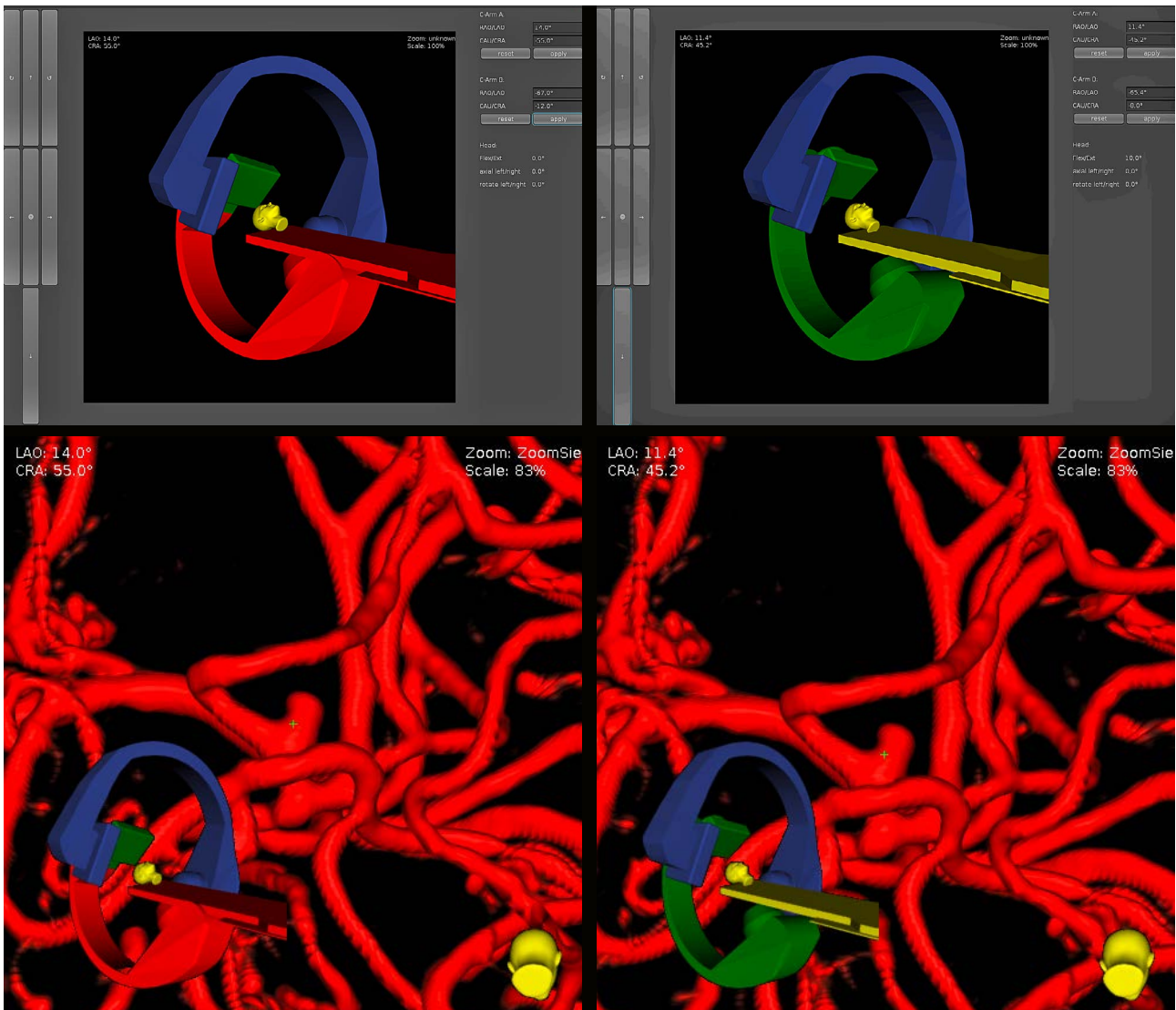
Results

Of the 100 candidate projections, 18 were not feasible on a real angiography system because of collision risks, primarily between the C-arm and the angiography table. In all 18 cases, the optimization tool successfully calculated head orientations that resolved the collisions while maintaining the desired aneurysm view.

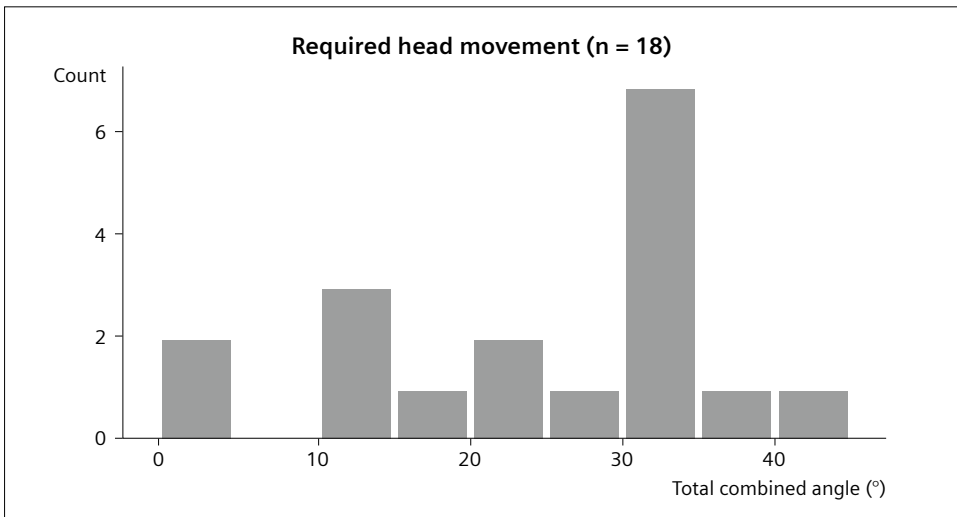
The required adjustments were modest: In several cases, a flexion or extension of only 10° was sufficient.

The information in this paper is based on research results that are not commercially available.

¹ Work in progress. The application is currently under development and is not for sale in the U.S. and in other countries. Its future availability cannot be ensured.



3 Example case showing an MCA bifurcation aneurysm in C-arm A projection before (left) and after (right) 10° flexion optimization.



4 Required head-orientation adjustments in degrees.

Importantly, all optimized projections could be reproduced on the angiography system in vitro, confirming the feasibility of the approach.

This finding highlights two key aspects: First, that head repositioning can systematically expand the range of achievable projections. Second, that the extent of movement required is small enough to be practical in real clinical conditions, even in patients under general anesthesia.

Supplementary analyses included visualizing the algorithm's calculated head-angle adjustments, examining consistency across operators, and reproducing the calculated C-arm positions on the angiography system. Across all operators, the tool demonstrated high reliability in identifying feasible solutions.

Discussion

This study demonstrates that automated head positioning can close the gap between theoretical planning and practical execution in neurointerventional imaging. By shifting the anatomical frame of reference through modest head movements, operators can access projections that would otherwise be excluded due to system collisions.

The clinical benefits of such a solution are substantial. First, it may reduce reliance on suboptimal views, which often compromise visualization of the aneurysm neck and parent vessel. Improved visualization can translate directly into safer and more effective device deployment, particularly for stent-assisted coiling or flow diverter placement. Second, it may shorten procedure time by reducing the need for repeated 3D acquisitions. Third, it may expand the treatability of certain aneurysm cases that would otherwise be deemed unsuitable for endovascular therapy.

At the same time, several important limitations and questions remain. The feasibility of specific head movements in real patients, especially in combination, is not well characterized in the literature. The required precision of head orientation to replicate the simulated working projection also requires systematic evaluation. Ergonomic aspects, including airway management and anesthesia safety, must be carefully considered before clinical implementation. Finally, it remains to be tested whether real-time feedback on head positioning can be seamlessly integrated into workflows without prolonging procedures.

Comparison with the existing literature underscores the novelty of this approach. While anecdotal reports describe manual head repositioning to improve projections, this is the first systematic, software-assisted framework for doing so. Early in vitro validation provides strong feasibility data, but prospective clinical trials will be required to determine the true impact on safety and outcomes.

Conclusion

Automated head positioning represents a promising new dimension of procedural planning in neurointerventions. By systematically leveraging patient head orientation to resolve C-arm collision issues, it may expand the range of feasible working projections, improve visualization, and enable safer and more efficient aneurysm treatments.

The prototype developed at University Hospital Magdeburg in cooperation with Siemens Healthineers demonstrates that such solutions are technically feasible and reproducible. With further clinical validation, automated head positioning could become an integral part of neurointerventional workflows, bridging the gap between theoretical planning and clinical reality.

References

- 1 Dowlati E, Zhou T, Stewart J, Felbaum DR, Liu AH, Mai JC, et al. Head Repositioning during Neurointerventional Procedures to Optimize Biplanar Imaging. *J Neuroimaging*. 2020;30(5):603–608.
- 2 Klebingat S, Schwab R, Thormann M, Behme D. Towards automatically suggested head positions to optimize biplane C-arm projections for intracranial aneurysm treatment. 6th Conference on Image-Guided Interventions. Abstract Book. 2023;11:56–57.
- 3 Klebingat S, Schwab R, Thormann M, Behme D. Optimization of biplane C-arm projections using a 3D head positioning tool. 58. Jahrestagung der Deutschen Gesellschaft für Neuroradiologie e. V. *Clin Neuroradiol*. 2023;33(Suppl 1):S107–S106.



Contact

Stefan Klebingat, Ph.D.
University Clinic for Neuroradiology
University Hospital Magdeburg
Leipziger Straße 44 (Haus 60b)
39120 Magdeburg
Germany
Tel.: +49 391 67-21989
stefan.klebingat@med.ovgu.de



Roland Schwab, M.D.
University Clinic for Neuroradiology
University Hospital Magdeburg
Leipziger Straße 44 (Haus 60b)
39120 Magdeburg
Germany
Tel.: +49 391 67-21608
roland.schwab@med.ovgu.de



Professor Daniel Behme, M.D.
University Clinic for Neuroradiology
University Hospital Magdeburg
Leipziger Straße 44 (Haus 60b)
39120 Magdeburg
Germany
Tel.: +49 391 67-21608
daniel.behme@med.ovgu.de

Updates on Advanced Whole-Brain Vessel Wall Imaging in Stroke Patients

Fang Wu, M.D.¹; Yuehong Liu, M.D.²; Qi Yang, M.D., Ph.D.²

¹ Department of Radiology and Nuclear Medicine, Xuanwu Hospital, Capital Medical University, Beijing, China

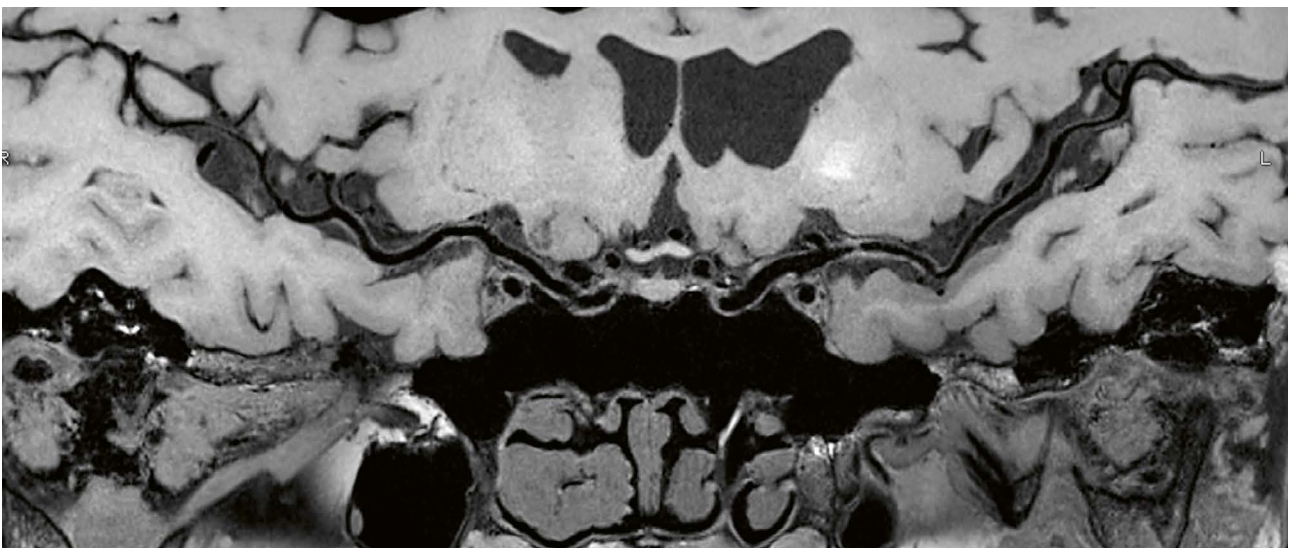
² Department of Radiology, Beijing Chaoyang Hospital, Capital Medical University, Beijing, China

Abstract

Intracranial artery stenosis is one of the common causes of ischemic stroke in Asia. Advances in vessel wall imaging techniques now make it possible to directly visualize the intracranial vessel wall. Several single-center studies have suggested that intracranial vessel wall magnetic resonance imaging (VW-MRI) may provide insights into stroke etiology, vascular pathogenesis, and the risk of recurrent stroke. However, the robustness of intracranial VW-MRI as a valuable tool for the assessment of various cerebrovascular diseases still needs to be validated in a large-scale multicenter study. Thus, our research group initiated a multicenter study in China on February 1, 2017. This study aimed to investigate the clinical utility of whole-brain intracranial VW-MRI in assessing the etiologies in patients with ischemic stroke.

Introduction

Stroke is one of the most common causes of death and disability in the world, which usually causes an abrupt onset of a neurological deficit [1, 2]. Intracranial artery stenosis has been considered a major cause of ischemic stroke, especially in Asia [3]. Traditionally, intracranial vascular diseases have been evaluated with invasive luminal imaging techniques, such as catheter angiography or non-invasive luminal imaging techniques (MR angiography or CT angiography). However, these techniques indirectly visualize vessel wall abnormalities, and many cerebral vasculopathies may have similar luminal narrowing. VW-MRI has been applied as the only non-invasive technique to directly assess the intracranial vessel wall structure [4, 5]. It can provide derived vessel wall characteristics to help clinicians determine stroke etiology, estimate atherosclerotic plaque burden or vasculitis activity, as well as future cerebrovascular events [6].



1 Curved-planar reformation of three-dimensional vessel wall magnetic resonance imaging (VW-MRI).

Field strength and pulse sequences

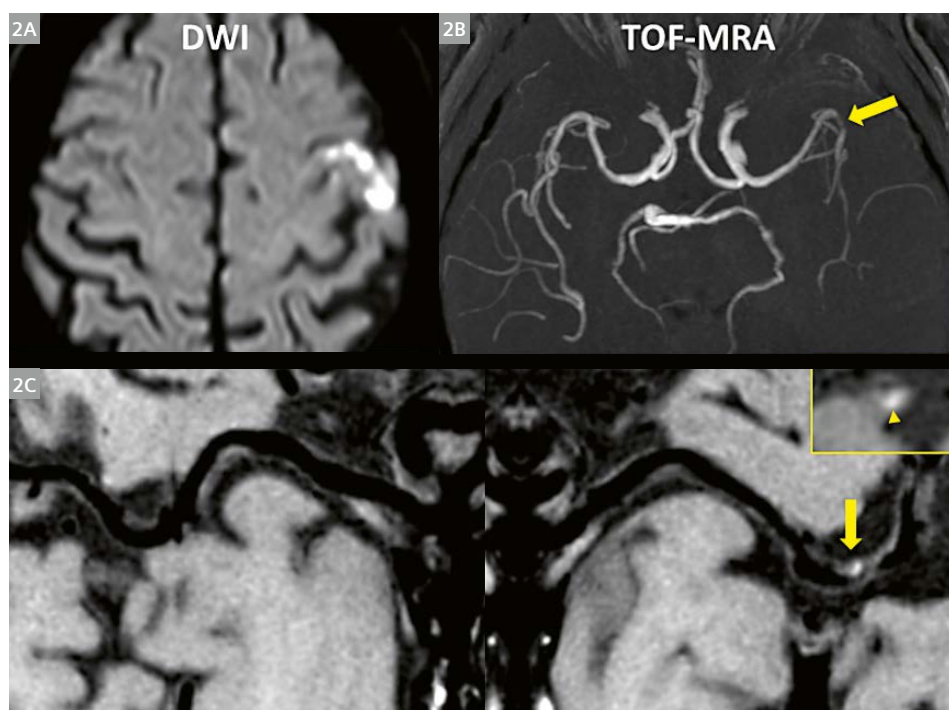
Currently, VW-MRI for intracranial arteries is performed on 3T MRI systems at most centers. Considering the small caliber of intracranial arteries, ultra-high field MRI (7T) may provide an additional value for evaluating intracranial atherosclerotic plaques, as it allows for a high signal-to-noise ratio (SNR), spatial resolution, and contrast-to-noise ratio. Although the feasibility of intracranial VW-MRI at 7T has been demonstrated in several *in-vivo* and *ex-vivo* studies [7, 8], more evidence of additional clinical value of 7T MRI is needed before being used in routine clinical practice. The selection of pulse sequences and protocols remains variable across sites and vendors. To clearly depict the inner and outer boundaries of vessel walls, adequate spatial resolution, as well as excellent blood and cerebrospinal fluid (CSF) suppression are essential for intracranial vessel wall imaging techniques. A two-dimensional (2D) sequence can provide a better in-plane spatial resolution (a voxel size of $0.4 \times 0.4 \times 2.0 \text{ mm}^3$) for targeted vessel wall lesions. However, it is unable to achieve a more global depiction of multiple vessels and detect lesions without luminal stenosis. Literature shows a shift from 2D to 3D volumetric acquisitions. 3D isotropic imaging with a larger coverage of whole-brain vessels makes it possible to perform multi-planar and curved-planar reformations, as well as assess plaque burden and distribution of major intracranial arteries from various perspectives (Fig. 1) [9]. There are numerous technical developments for VW-MRI pulse sequences aimed to reduce blood and CSF flow artifacts.

Vascular pathologies and their depiction with VW-MRI

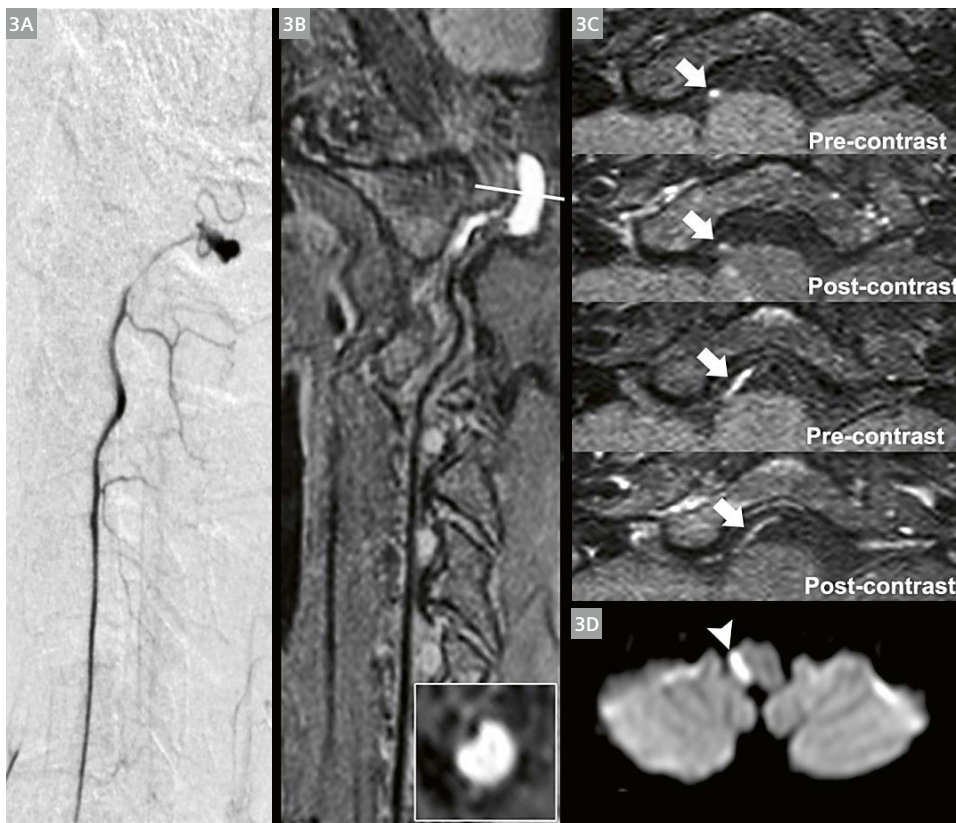
The most important recommendation for intracranial VW-MRI in clinical practice is to assess and differentiate intracranial vasculopathies, such as intracranial atherosclerotic plaque, vasculitis, reversible cerebral vasoconstriction syndrome, arterial dissection, and other causes of intracranial arterial narrowing. Diagnosis of cerebrovascular disease has relied on luminal imaging. However, different vasculopathies usually have similar morphological features on luminal imaging. The advent of VW-MRI offers insights into the pathogenesis of cerebrovascular disease. Furthermore, high diagnostic accuracy of VW-MRI for distinguishing a range of vasculopathies has been presented in several studies [4, 10].

Atherosclerotic plaque

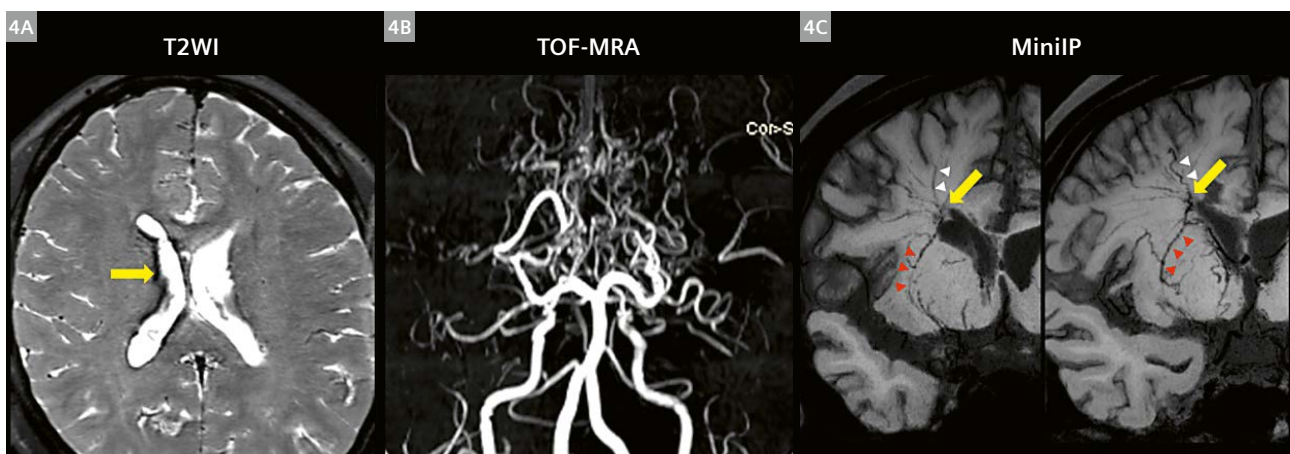
VW-MRI of intracranial atherosclerotic plaque typically demonstrates arterial wall thickening, which eccentrically (nonuniformly) involves the circumference of the arterial wall. Intraplaque hemorrhage (IPH), fissured fibrous cap, lipid-rich necrotic core, neovascularization, and inflammation are considered common features of vulnerable plaques and symptomatic lesions. Identification of plaque components with VW-MRI has the potential to identify vulnerable plaque and predict the risk of rupture and events (Fig. 2). For intracranial atherosclerosis, MRI-pathology correlation was explored in limited studies of postmortem artery specimens. Chen et al. reported that



2 70-year-old male patient. (2A) Diffusion-weighted imaging (DWI) showed disseminated spotty high signal intensity lesions in the left cortico-subcortical area of the MCA territory; (2B) time-of-flight magnetic resonance angiography (TOF-MRA) showed severe stenosis on the relevant MCA (arrow); (2C) curved multiplanar reconstruction of pre-contrast VW-MRI showed hyperintense plaque (arrow and arrowhead) on the MCA.



3 A 35-year-old female patient with cervicocranial artery dissection with lateral dorsal medulla syndrome. **(3A)** Digital subtraction angiography showed a severe stenosis and occlusion of the V3-V4 segment of the right vertebral artery; **(3B)** curved planar reformation of VW-MRI demonstrated intramural hematoma (white line) in the vessel wall of the V3 segment of right vertebral artery; **(3C)** axial VW-MRI detected a distal intraluminal thrombus (arrows) without contrast enhancement of the right vertebral artery; **(3D)** DWI showed a single infarction in the right part of the medulla oblongata (arrowhead).



4 A 21-year-old female moyamoya disease patient with right intraventricular hemorrhage. **(4A)** T2-weighted imaging (T2WI) demonstrated that the origin of hemorrhage was in the right periventricular area (yellow arrow); **(4B)** TOF-MRA detected occlusion of bilateral MCAs; **(4C)** minimum intensity projection (MinIP) of VW-MRI revealed an anastomosis (yellow arrow) between the LSAs (red arrowheads) and the medullary arteries (white arrowheads).

high signal on T1-weighted images in specimens at 1.5T was IPH as pathologically-verified in a postmortem case of a Chinese adult [11]. The correlation between the lipid core assessed on histology and low signal on T1-weighted fat-suppressed images within intracranial vessel walls has also been explored [12].

A postmortem study demonstrated that neovascularity can be found in middle cerebral artery (MCA) atherosclerotic plaque and that it was associated with ipsilateral infarction [13]. Gadolinium enhancement of carotid plaques was proven to be associated with vulnerable plaque, neovascularization, macrophages, and loose fibrosis correlating with histopathology [14]. Using VW-MRI, intracranial plaque enhancement can be evaluated and the relationship between plaque enhancement and recent infarction has been established [15].

Arterial dissection

Intracranial arterial dissection most often occurs as an extension of a cervical artery dissection. Simultaneous high-resolution 3D carotid and intracranial imaging has the potential to identify dissected vessels in the head and neck. VW-MRI features of intracranial arterial dissection include a curvilinear hyperintensity on T2-weighted images (intimal flap), separating the true lumen from the false lumen, and crescent-shaped arterial wall thickening with the signal characteristics of blood (intramural hematoma). Early detection of high-risk imaging characteristics of cervicocranial artery dissection may be useful to aid in the preventive treatment of patients with cervicocranial artery dissection without stroke but at higher risk. In a previous study, we investigated the imaging features that are associated with ischemic stroke in patients with cervicocranial artery dissection. We found that the presence of irregular surface and intraluminal thrombus were related to stroke occurrence in these patients (Fig. 3). Integrated head/neck VW-MRI might give insights into the pathogenesis of ischemic stroke in cervicocranial artery dissection. It may be useful for individual prediction of ischemic stroke early in cervicocranial artery dissection [16].

Vasculitis and reversible cerebral vasoconstriction syndrome

VW-MRI often demonstrates smooth and concentric arterial wall thickening and enhancement in patients with central nervous system vasculitis, in comparison with the typical eccentric wall thickening of atherosclerotic plaque. Reversible cerebral vasoconstriction syndrome (RCVS) can also result in concentric arterial wall thickening, but the vessel wall in RCVS is typically nonenhancing (or mildly enhancing) compared with the typical intense wall enhancement in active vasculitis [10]. Early differentiation

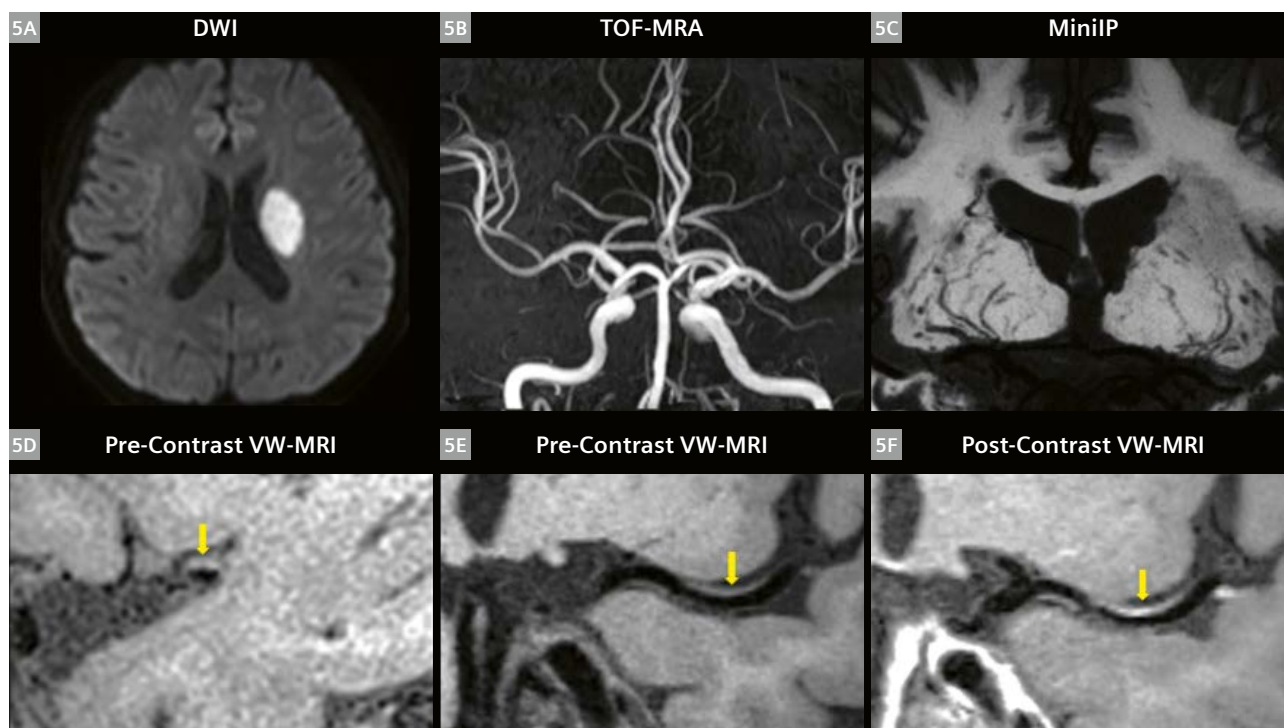
between vasculitis and RCVS is important: RCVS is treated with observation or calcium channel blockers, whereas vasculitis is treated with steroids and immunosuppressive drugs.

Moyamoya disease

VW-MRI holds significant value in differentiating moyamoya disease and atherosclerotic moyamoya syndrome, which have a significant overlap in luminal morphological patterns. Focal eccentric wall thickening or enhancement was observed in the involved arteries in atherosclerotic moyamoya syndrome, which was different from concentric wall thickening or enhancement in moyamoya disease. Intracranial hemorrhage is one of the most severe complications in patients with moyamoya disease. Moyamoya vessels are the dilated and proliferative perforating arteries serving as collateral circulation, which are more prone to rupture and might be closely associated with intracranial hemorrhage. In a previous study, we investigated the association between dilation, proliferation, and anastomosis of perforating arteries, and intracranial hemorrhage in moyamoya disease patients using VW-MRI. We found that choroidal anastomosis is a valuable imaging biomarker for predicting hemorrhagic events in adult patients with moyamoya disease (Fig. 4). Whole-brain VW-MRI can visualize not only the abnormal collateral vessels but also the anatomy of the parenchymal structure, which may facilitate risk estimates of bleeding in moyamoya disease [17].

Lenticulostriate artery imaging

The lenticulostriate artery (LSA) supplies blood to the basal ganglia and its vicinity in the brain. Impairment of the LSA is associated with ischemic stroke and small-vessel disease. Visualization of the LSA is essential for understanding the mechanisms of microvascular pathologies and potential guiding therapeutic intervention. Using the T1 VW-MRI technique, we have obtained detailed black-blood angiographic delineation of the LSAs [18]. Single subcortical infarctions with a nonstenotic middle cerebral artery have been considered to be caused by lipohyalinosis and fibrinoid degeneration in small-vessel disease, commonly called lacunar strokes. However, large-artery atherothrombosis that blocks the orifice of the perforating artery may also be an important cause of single subcortical infarctions. Jiang et al. used VW-MRI to quantitatively evaluate the associations between the distribution and characteristics of middle cerebral artery plaque and morphological changes to LSAs in the symptomatic and asymptomatic sides of single subcortical infarction patients. They found that superiorly distributed middle cerebral artery plaques at the LSA origin are closely



5 A 68-year-old male patient with right limb weakness. **(5A)** DWI showed a single subcortical infarction in the left LSA territory; **(5B)** TOF-MRA showed mild stenosis on the relevant MCA; **(5C)** coronal minimum intensity projection (MiniIP) revealed shorter lengths of left lenticulostriate arteries (LSAs) compared with the right side; **(5D)** the cross-section view of pre-contrast VW-MRI demonstrated a superiorly located plaque (arrow) of MCA; **(5E, F)** curved multiplanar reconstruction of pre- and post-contrast VW-MRI showed an isointensity plaque with contrast enhancement (arrow).

associated with morphological changes to the LSA in symptomatic middle cerebral arteries, suggesting that the distribution, rather than the inherent features of plaques, determines the occurrence of single subcortical infarctions (Fig. 5) [19].

Setup of our multicenter study

VW-MRI holds promise of improving our pathological understanding of intracranial artery stenotic disease. The robustness of this technique as a valuable tool for the assessment of various cerebrovascular diseases still needs to be validated in a large-scale multicenter study. We also used the sequence successfully in a multicenter study comprising nine hospitals in China that was initiated by Professor Qi Yang in February 2017. The aim of this study was to accurately classify the etiology of stroke through the scientific research cooperation of various partners, and at the same time carry out early screening and accurate diagnosis of high-risk plaques, thereby providing a new imaging method for the clinical diagnosis and treatment of stroke. The imaging technique used in this project is whole-brain VW-MRI based on sampling perfection with application-optimized contrast using different flip angle evolutions (SPACE) combined with nonselective excitation

and a trailing magnetization flip-down module [20, 21]. This imaging technique in combination with a uniform protocol setting on 3T scanners (MAGNETOM Prisma, MAGNETOM Skyra, Siemens Healthcare, Erlangen, Germany) can perform high-resolution imaging of the intracranial vessel wall, clearly depicting the morphology of the vessel wall and distinguishing high-risk vulnerable plaques. In this multi-center study, each participating site carried out imaging studies ranging from intracranial large arterial to perforating arteriole lesions, focusing on cerebrovascular diseases of different etiologies. Several results of this research have been published [22–26].

Outlook

The technology of whole-brain VW-MRI has become a new method for stroke classification. The research performed by our group and other groups presents a first step in designing focused trials on individualized treatment and prevention strategies of intracranial stenosis. Further studies are required to investigate the use of selected biomarkers in randomized control trials of secondary prevention and treatment of intracranial artery stenotic disease.

References

- 1 GBD 2016 Stroke Collaborators. Global, regional, and national burden of stroke, 1990-2016: a systematic analysis for the Global Burden of Disease Study 2016. *Lancet Neurol.* 2019;18:439-458.
- 2 Powers WJ. Acute Ischemic Stroke. *N Engl J Med.* 2020;383:252-260.
- 3 Wu S, Wu B, Liu M, et al. Stroke in China: Advances and challenges in epidemiology, prevention, and management. *The Lancet. Neurology.* 2019;18:394-405.
- 4 Mandell DM, Matouk CC, Farb RI, et al. Vessel wall MRI to differentiate between reversible cerebral vasoconstriction syndrome and central nervous system vasculitis: Preliminary results. *Stroke.* 2012;43:860-862.
- 5 Fan Z, Zhang Z, Chung YC, et al. Carotid arterial wall MRI at 3T using 3D variable-flip-angle turbo spin-echo (TSE) with flow-sensitive dephasing (FSD). *J Magn Reson Imaging.* 2010;31:645-654.
- 6 Mandell DM, Mossa-Basha M, Qiao Y, et al. Intracranial vessel wall MRI: Principles and expert consensus recommendations of the American society of neuroradiology. *AJNR Am J Neuroradiol.* 2017;38:218-229.
- 7 Hartevelde AA, van der Kolk AG, van der Worp HB, et al. High-resolution intracranial vessel wall MRI in an elderly asymptomatic population: comparison of 3T and 7T. *Eur Radiol.* 2017;27:1585-1595.
- 8 van der Kolk AG, Zwanenburg JJ, Denswil NP, et al. Imaging the intracranial atherosclerotic vessel wall using 7T MRI: initial comparison with histopathology. *AJNR Am J Neuroradiol.* 2015;36:694-701.
- 9 Qiao Y, Guallar E, Suri FK, et al. MR Imaging Measures of Intracranial Atherosclerosis in a Population-based Study. *Radiology.* 2016;280:860-868.
- 10 Mossa-Basha M, Shibata DK, Hallam DK, et al. Added value of vessel wall magnetic resonance imaging for differentiation of nonocclusive intracranial vasculopathies. *Stroke.* 2017;48:3026-3033.
- 11 Chen XY, Wong KS, Lam WW, et al. High signal on T1 sequence of magnetic resonance imaging confirmed to be intraplaque haemorrhage by histology in middle cerebral artery. *Int J Stroke.* 2014;9(4):E19.
- 12 Yang WJ, Chen XY, Zhao HL, et al. Postmortem Study of Validation of Low Signal on Fat-Suppressed T1-Weighted Magnetic Resonance Imaging as Marker of Lipid Core in Middle Cerebral Artery Atherosclerosis. *Stroke.* 2016;47:2299-2304.
- 13 Chen XY, Wong KS, Lam WW, et al. Middle cerebral artery atherosclerosis: histological comparison between plaques associated with and not associated with infarct in a postmortem study. *Cerebrovasc Dis.* 2008;25:74-80.
- 14 Millon A, Bousset L, Brevet M, et al. Clinical and histological significance of gadolinium enhancement in carotid atherosclerotic plaque. *Stroke.* 2012;43:3023-3028.
- 15 Qiao Y, Zeiler SR, Mirbagheri S, et al. Intracranial plaque enhancement in patients with cerebrovascular events on high-spatial-resolution MR images. *Radiology.* 2014;271:534-542.
- 16 Wu Y, Wu F, Liu Y, et al. High-Resolution Magnetic Resonance Imaging of Cervicocranial Artery Dissection: Imaging Features Associated With Stroke. *Stroke.* 2019;50:3101-3107.
- 17 Wu F, Han C, Liu Y, et al. Validation of Choroidal Anastomosis on High-Resolution Magnetic Resonance Imaging as Imaging Biomarker in Hemorrhagic Moyamoya Disease. *Eur Radiol.* 2021;31:4548-4556.
- 18 Zhang Z, Fan Z, Kong Q, et al. Visualization of the lenticulostriate arteries at 3T using black-blood T1-weighted intracranial vessel wall imaging: comparison with 7T TOF-MRA. *Eur Radiol.* 2019;29:1452-1459.
- 19 Jiang S, Yan Y, Yang T, et al. Plaque Distribution Correlates With Morphology of Lenticulostriate Arteries in Single Subcortical Infarctions. *Stroke.* 2020;51:2801-2809.
- 20 Fan Z, Yang Q, Deng Z, et al. Whole-brain intracranial vessel wall imaging at 3 Tesla using cerebrospinal fluid-attenuated T1-weighted 3D turbo spin echo. *Magn Reson Med.* 2017;77:1142-1150.
- 21 Yang Q, Deng Z, Bi X, et al. Wholebrain vessel wall MRI: a parameter tune-up solution to improve the scan efficiency of three-dimensional variable flip-angle turbo spin-echo. *J Magn Reson Imaging.* 2017;46:751-757.
- 22 Liu Y, Li S, Wu Y, et al. The Added Value of Vessel Wall MRI in the Detection of Intraluminal Thrombus in Patients Suspected of Craniocervical Artery Dissection. *Aging & Dis.* 2021; Doi:10.14336/AD.2021.0502.
- 23 Jiang S, Yan Y, Yang T, et al. Plaque Distribution Correlates With Morphology of Lenticulostriate Arteries in Single Subcortical Infarctions. *Stroke.* 2020;51(9):2801-2809.
- 24 Wu Y, Wu F, Liu Y, Yang Q, et al. High-Resolution Magnetic Resonance Imaging of Cervicocranial Artery Dissection: Imaging Features Associated with Stroke. *Stroke.* 2019; 50(11):3101-3107.
- 25 Wu F, Ma Q, Song H, et al. Differential Features of Culprit Intracranial Atherosclerotic Lesions: A Whole-Brain Vessel Wall Imaging Study in Patients With Acute Ischemic Stroke. *J Am Heart Assoc.* 2018 Jul 22;7(15).
- 26 Wu F, Song H, Ma Q, et al. Hyperintense plaque on intracranial vessel wall magnetic resonance imaging as a predictor of artery-to-artery embolic infarction. *Stroke.* 2018; 49(4):905-911.



Contact

Professor Qi Yang, M.D., Ph.D.
 Vice Chair
 Department of Radiology
 Beijing Chaoyang Hospital
 Capital Medical University
 No. 8 Gongti South Road
 Chaoyang District
 Beijing 100020, China
 Phone: +86 (0) 10-8523-1928
 yangyangqiqi@gmail.com

Intracranial Vessel Wall MRI

Luigi Cirillo*^{1,2,3}; Arianna Rustici*^{1,3,4}; Tommaso Kaswalder²; Ciro Princiotta²; Massimo Dall'Olio²; Caterina Tonon^{1,3}; Domenico Zacà⁵; Raffaele Lodi^{1,6}

¹ Department of Biomedical and Neuromotor Sciences (DIBINEM), University of Bologna, Italy

² UOC di Neuroradiologia, IRCCS Istituto delle Scienze Neurologiche di Bologna, Italy

³ Programma Neuroimmagini Funzionali e Molecolari, IRCCS Istituto delle Scienze Neurologiche di Bologna, Italy

⁴ UO di Neuroradiologia OM, IRCCS Istituto delle Scienze Neurologiche di Bologna, Italy

⁵ Siemens Healthcare Srl, Milano, Italy

⁶ IRCCS Istituto delle Scienze Neurologiche di Bologna, Italy

* These authors contributed equally and share first authorship.

Introduction

To date, MR is the only clinically available imaging modality that allows to image the brain vessels beyond the 'lumen techniques', depicting both the lumen and the vessel walls with high sensitivity and low invasiveness [1]. Besides standard MR angiography (MRA) sequences, some MR sequences for vessel wall imaging have been introduced into clinical practice [2]. These MR sequences allow to depict the vessel walls at high resolution, and are becoming emerging techniques for evaluating cerebrovascular diseases.

Although vessel wall MRI (VW MRI) sequences are widely reported to be effective and efficient [3], there are no commercially available sequences optimized for intracranial imaging. In fact, VW MRI requires a very complex signal because the signal from both the blood inside the lumen and from the outer cerebrospinal fluid (CSF) must be suppressed.

This article describes the technical aspects of our VW MRI sequence¹ so that other institutions can develop their own sequence for the diagnosis and follow-up of cerebrovascular pathologies.

Technique

We developed our optimized protocol on a 3T MAGNETOM Skyra system (Siemens Healthcare, Erlangen, Germany). It is based on a T1-weighted 3D SPACE sequence. Specific parameters have been modified to achieve sufficient signal-to-noise ratio (SNR) and contrast-to-noise ratio (CNR) for vessel wall imaging. Moreover, we set parameters to obtain isotropic 3D imaging, achieve good suppression of CSF and blood, and reduce scan time (to avoid artifacts caused by patient motion) [4, 5]. The total scan time is 7 minutes 10 seconds.

Sequence parameter	
Acquisition time	7:10 min
Orientation	Coronal
Type	3D
Slice for slab	80
Slice oversampling	10.0%
Slice thickness	0.60 mm
FOV read (mm)	160 mm
FOV phase (%)	82.8%
Phase oversampling	20%
Phase resolution	100%
Voxel size	0.3 × 0.3 × 0.6
TR (ms)	1000 ms
TE (ms)	38 ms
ETL	211 ms
Flip angle (°)	T1 variable
Bandwidth (Hz/pixel)	514 Hz/Px
k-space filling	Interpolation with zero-filling
PAT mode	GRAPPA
Accel. factor PE	2
Ref. lines PE	24
Fat suppression	None
Dark blood	Off

Table 1: Our sequence parameters for vessel wall MRI at 3T.

¹ Work in progress. The application is still under development and not commercially available. Its future availability cannot be ensured.

Our VW MRI sequence is a 3D multi-slab acquisition (80 slices per slab, each with 0.60 mm slice thickness) acquired in coronal plane, with a rectangular field of view (FOV read = 160 mm; FOV phase = 82.8%) (Table 1). To reduce the slab boundary artifact, we use oversampling in the slice direction (slice oversampling = 10.0%). To avoid the wrap-around artifact, we use phase oversampling (phase oversampling = 20%; phase resolution = 100%).

With spin echo (SE) sequences, it is possible to adjust the TR (repetition time) and TE (echo time) to suit specific needs. We therefore set the TR to 1000 ms and the TE to 38 ms (Table 1), to achieve a CSF darkening effect by tailoring image contrast to T1 weighting and proton-density (PD) weighting (Table 2).

The black-blood effect is achieved by the intravoxel dephasing of moving blood spins within a long echo train length (ETL = 211 ms). A variable refocusing flip angle is used to compensate for the signal decay inherent in the long ETL.

The difference in the precession frequencies of the spins inside the voxels at the extremities of the FOV is set at 514 Hz/Px (bandwidth).

To reduce scan time, a parallel imaging acquisition technique (iPAT) called GRAPPA (Generalized Autocalibrating Partially Parallel Acquisitions) is used, with an acceleration factor (R) of 2, and 24 reference lines in the phase-encoding direction, to compensate for the under-sampling of the *k*-space (Table 1).

With those parameters, there is no need for an inferior outer volume suppression pulse to limit the inflow effects of blood, and no need for a fat-saturation pulse (Tables 1 and 2).

Discussion

Intracranial VW MRI is a complex technique that requires elevated spatial and contrast resolution, and the ability to detect contrast enhancement after the administration of contrast medium.

Correctly visualizing the intracranial vessel walls relies on the suppression of the outer and inner structures. The signal of both the blood inside the lumen and of the outer CSF must therefore be suppressed. Although both structures are fluids, different suppression techniques are required because of their different properties. MR vendors have developed many different fluid-suppression techniques, each with some limitations [6, 7].

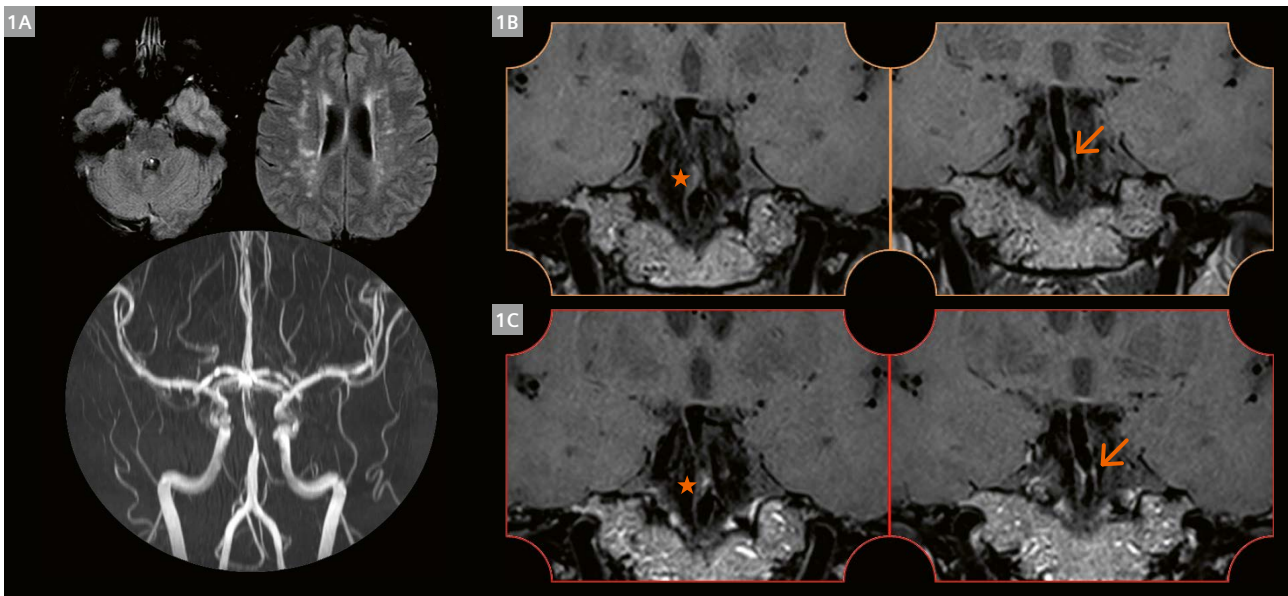
Due to the difficulty of generating one signal while suppressing others, and to the heterogeneity of scanners and coils, no sequences optimized for intracranial imaging are commercially available [8].

The basis of our VW MRI sequence is a 3D SPACE sequence, which is a spin-echo sequence. As all spin-echo sequences are pulsed sequences, they allow us to obtain different weighting based on predefined timing parameters, such as TR and TE. We decided to maintain the contrast of our sequence intermediate between the T1 and PD weighting. This is because the T1-weighted sequences have the advantage of clearer enhancement after the administration of contrast medium, whereas PD-weighted sequences provide a higher SNR [8] (Table 2). Moreover, an intermediate T1/PD weighting achieves the required CSF suppression, due to its long T1 relaxation time (Table 2).

Many different and complex techniques have been developed to suppress flowing blood. Each of them has some limitations [6, 7]. The most commonly used suppression methods are the black-blood techniques [6]. They can be broadly classified as either flow-dependent or flow-independent [7]. Although blood-suppression techniques are not the subject of this paper, it must be noted that the black-blood techniques have several limitations and could lead to artifacts [7], the most common of which is the presence of a residual blood signal, which is due to insufficient blood suppression and can mimic or obscure vascular pathologies. This can occur in cases of stagnant, slow, or retrograde blood flows, and typically with flow-dependent techniques.

	T1-weighted	PD-weighted	T2-weighted
CSF	Dark	Light gray	Bright
Blood inside vessels	Bright	Dark	Dark
Advantages	<ul style="list-style-type: none"> • High anatomical detail • High contrast to Gd • Relatively short lead times 	<ul style="list-style-type: none"> • High SNR • High anatomical detail 	<ul style="list-style-type: none"> • High tissue contrast
Disadvantages	<ul style="list-style-type: none"> • Low tissue contrast 	<ul style="list-style-type: none"> • Reduced contrast enhancement • Reduced suppression of CSF 	<ul style="list-style-type: none"> • Mid-level anatomical detail • Long standard sequences

Table 1: Signal intensity, with advantages and disadvantages, for each MR weighting.



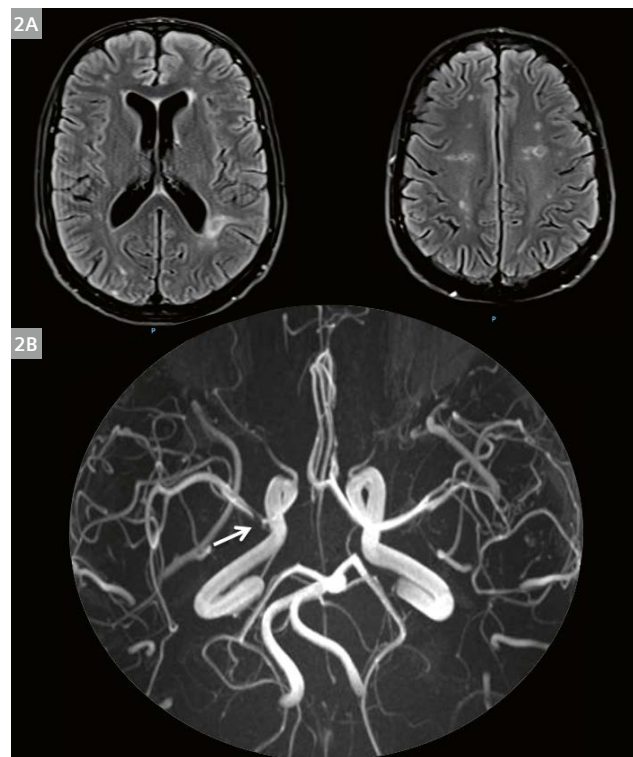
1 (1A) A 55-year-old female patient with recent worsening of chronic headache underwent an MRI study. The FLAIR axial images showed multiple chronic embolic lesions in both the posterior and anterior circulation; the time-of-flight (TOF) sequence showed the presence of multiple caliber alterations in the intracranial arterial circulation, the worst of which was on the basilar artery. (1B, C) Pre- and post-contrast high-resolution vessel wall imaging, with the coronal reconstruction of the 3D acquisition showing a focal atheromatous plaque and wall thickening (arrow), and the absence of wall enhancement after the administration of contrast medium (star).

Regardless of the suppression technique used, VW MRI does have pitfalls that should be noted [7]. For example, it is impossible to assess the presence of wall enhancement in the cavernous segment of the internal carotid artery. This is due to diffuse enhancement inside the cavernous sinus after contrast-agent administration [7].

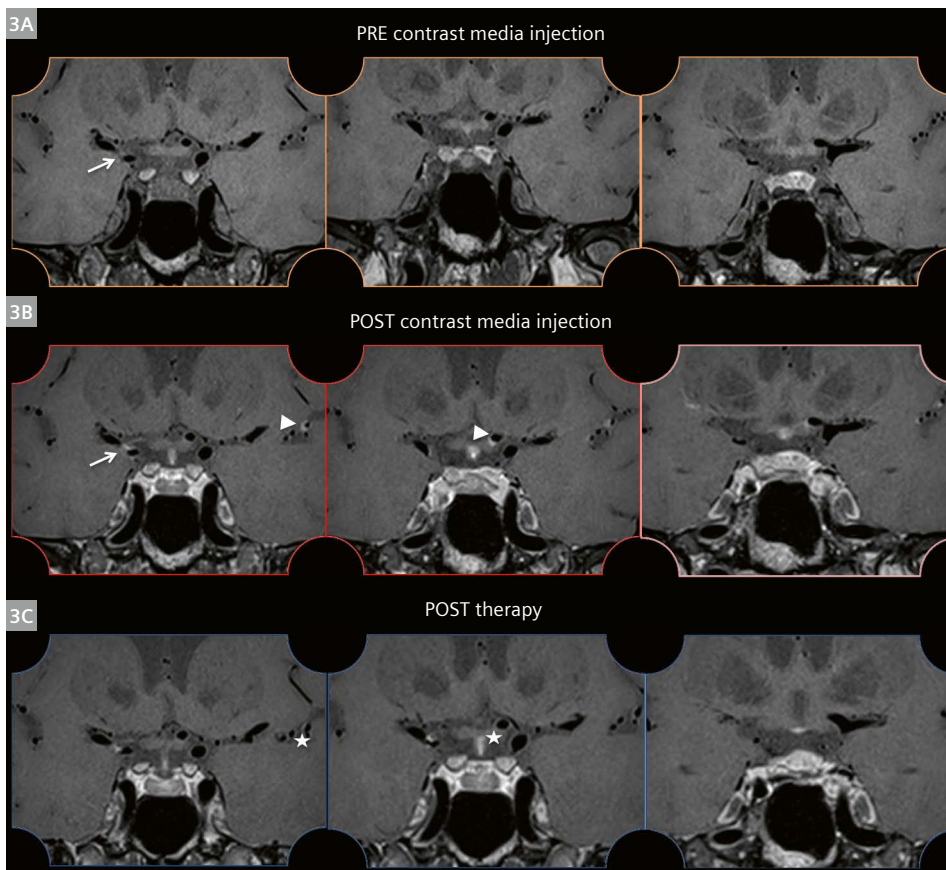
Aside from contrast resolution, the scan time is also important, because using sequences with long acquisition times in clinical practice may cause motion-induced artifacts. It is therefore necessary to reduce the scan time. MR vendors have provided various parallel imaging techniques to achieve this.

We have reported our experience with a VW MRI sequence, a novel imaging tool that has been evolving in recent years. Its purpose is to diagnose and support treatment decisions for various cerebrovascular pathologies, such as CNS vasculitis (Fig. 1), reversible cerebral vasoconstriction syndrome (RCVS), intracranial atherosclerosis (Figs. 2, 3), aneurysms, dissections, moyamoya disease, and moyamoya-like diseases.

After performing more than 200 VW MRI examinations with the aforementioned sequence, we found it to be useful in the diagnosis of more than 97.1% of cases (31.7% of our VW MRI examinations were determined to be positive for vessel wall pathologies, while 65.4% were negative). The VW MRI was inconclusive in less than 3% of cases, due to motion artifacts or blood-suppression artifacts.



2 (2A) A 48-year-old male patient with recent worsening of chronic headache. FLAIR axial images showed multiple chronic embolic lesions. (2B) MR angiography showed a focal stenosis of the right M1 segment at origin (arrow).



- 3** Vessel wall MRI study before (3A) and after (3B) the administration of contrast media showed the presence of a slight circumferential enhancement in correspondence of the right M1 origin segment (arrow). Other pathological vessel wall enhancements were noticed on the left A1–A2 angle and the M2–M3 segments of the left middle cerebral artery (arrowheads). The laboratory test was positive for a T. pallidum infection, so the final diagnosis is a luetic CNS vasculitis. An MR control performed one month after medical therapy (3C) showed the disappearance of the pathological enhancement at the left A1–A2 angle of the anterior cerebral artery and the M2–M3 segments (stars).

Compared to other VW MRI sequences reported in the literature, ours has the advantage of being as simple as possible, since it uses no blood-suppression techniques, which avoids suppression-related artifacts.

References

- Jung SC, Kang DW, Turan TN. Vessel and Vessel Wall Imaging. *Front Neurol Neurosci*. 2016;40:109–123.
- Bhogal P, Uff C, Makalanda HL. Vessel wall MRI and intracranial aneurysms. *J Neurointerv Surg*. 2016;8(11):1160–1162.
- Young CC, Bonow RH, Barros G, Mossa-Basha M, Kim LJ, Levitt MR. Magnetic resonance vessel wall imaging in cerebrovascular diseases. *Neurosurg Focus*. 2019;47(6):E4.
- Rustici A, Merli E, Cevoli S, Donato MD, Pierangeli G, Favoni V, et al. Vessel-wall MRI in thunderclap headache: A useful tool to answer the riddle? *Interv Neuroradiol*. 2021;27(2):219–224.
- Pensato U, Cevoli S, Cirillo L. Vessel Wall Imaging in Thunderclap Headache: A Reversible Cerebral Vasoconstriction Syndrome (RCVS) Case. *Headache*. 2020;60(10):2633–2635.
- Henningsson M, Malik S, Botnar R, Castellanos D, Hussain T, Leiner T. Black-Blood Contrast in Cardiovascular MRI. *J Magn Reson Imaging*. 2022;55(1):61–80.
- Lindenholz A, van der Kolk AG, Zwanenburg JJM, Hendrikse J. The Use and Pitfalls of Intracranial Vessel Wall Imaging: How We Do It. *Radiology*. 2018;286(1):12–28.
- Mandell DM, Mossa-Basha M, Qiao Y, Hess CP, Hui F, Matouk C, et al. Intracranial vessel wall MRI: Principles and Expert Consensus Recommendations of the American Society of Neuroradiology. *AJNR Am J Neuroradiol*. 2017;38(2):218–229.



Contact

Luigi Cirillo
Associate Professor of Neuroradiology
Alma Mater Studiorum —
University of Bologna
IRCCS Istituto delle Scienze
Neurologiche di Bologna
Via Altura 3
40133 Bologna
Italy
luigi.cirillo2@unibo.it

One-Stop Management for Acute Ischemic Stroke Patients

Vera Aebischer, M.D.; Marios-Nikos Psychogios, M.D.

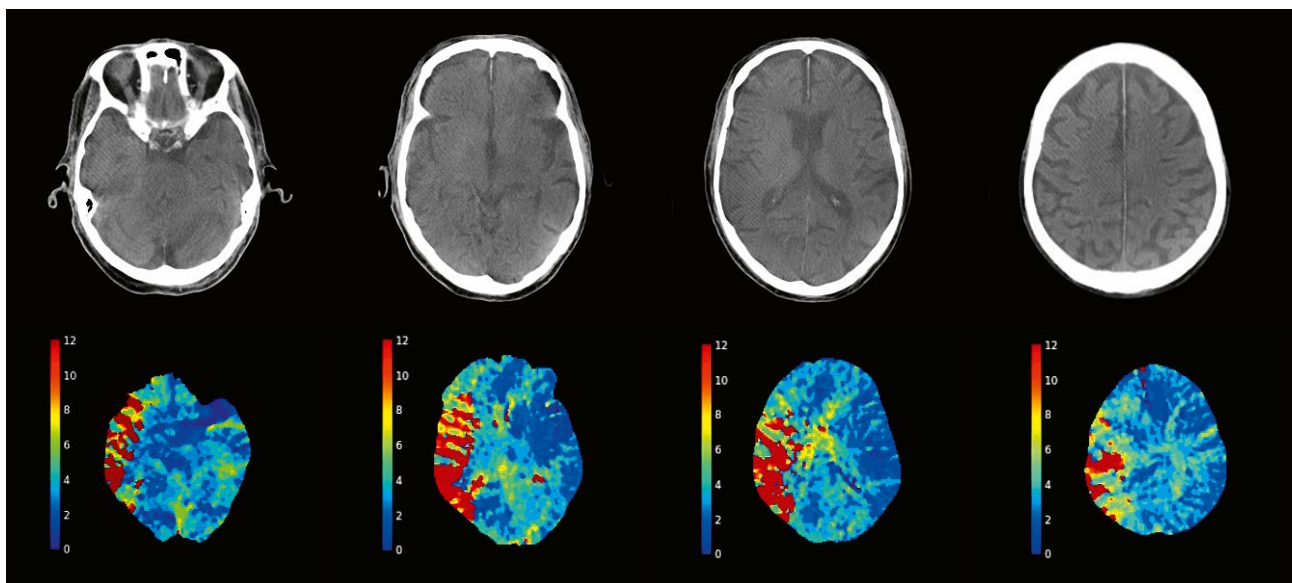
Department of Diagnostic and Interventional Neuroradiology, University Hospital Basel, Switzerland

Background

Fast and successful reperfusion of occluded vascular territories is the main objective in reperfusion therapies for stroke patients with confirmed vessel occlusions [1]. Following the publication of several randomized trials, a combination of endovascular treatment and intravenous thrombolysis has been established as the standard of care in patients with acute ischemic stroke [2–4]. Despite efforts to expedite reperfusion, door-to-groin times have consistently exceeded one hour. One contributor to this is the absence of a rapid, reliable, and cost-effective prehospital screening tool for stroke, akin to the electrocardiogram for acute coronary syndrome patients.

To address the delays in stroke treatment within hospital settings, a non-invasive triage method using an angiography suite equipped with a flat-detector computed tomography (FDCT) system has been introduced. This approach offers a comprehensive one-stop management strategy by integrating intravenous thrombolysis and endovascular treatment in a single space and holds promise for

substantial reductions in door-to-groin and door-to-reperfusion times [5, 6]. Further studies have demonstrated the efficacy of a straightforward and commercially available non-enhanced FDCT protocol for detecting intracranial hemorrhage (ICH) with a sensitivity comparable to that of non-contrast multidetector CT (MDCT) imaging [7, 8]. The non-inferiority of non-contrast *syngo* DynaCT Sine Spin FDCT compared to MDCT imaging for detecting ICH is evaluated by the SPINNERS trial (NCT05458908). Data obtained from a single-center randomized trial show that one-stop management can improve functional outcomes compared to traditional workflows [9]. Furthermore, two multicenter randomized trials, WE-TRUST and GET-FAST (NCT04701684, NCT07052045), are currently recruiting participants to investigate the effect of one-stop management on long-term functional outcomes. Lastly, FDCT angiography has been shown to reliably identify large vessel occlusions and grade collaterals [10, 11].



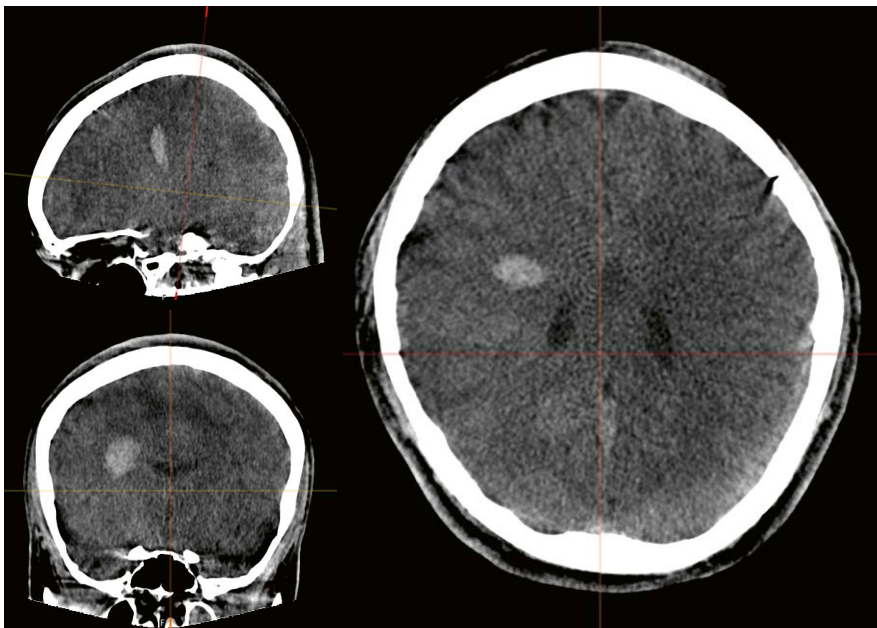
1 FDCT and processed FDCT (i.e., Tmax maps) acquired with an ARTIS icono system using the one-stop protocol for a patient with an acute M1 occlusion of the right middle cerebral artery. The patient presented with a NIHSS score of 12 and RACE score of 7. Onset-to-door time was 50 minutes, and door-to-imaging time was 15 minutes.

In conclusion, advances in FDCT such as FDCTA and FDCTP technology broaden the spectrum of imaging information that can be retrieved. The technology therefore plays a valuable role in therapeutic decision-making in acute ischemic stroke. Moreover, it influences the interventional strategy. Overall, FDCT technology has the potential to mitigate complications and reduce both pre-treatment workflows and intervention times.

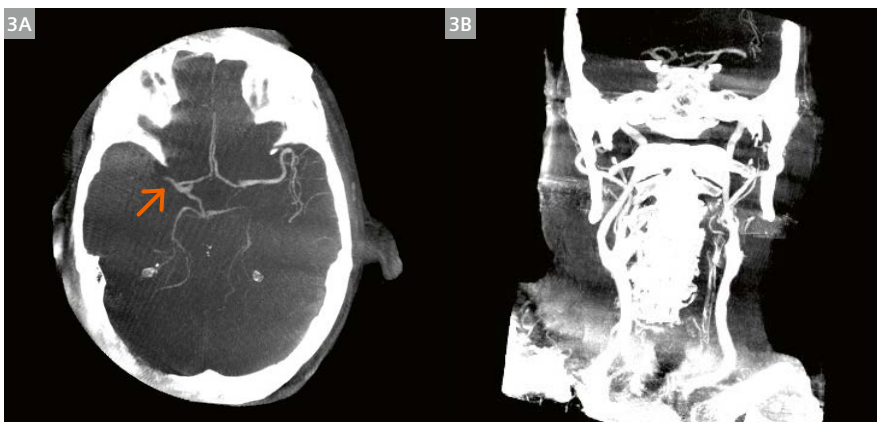
One-stop workflow

- The hospital is pre-notified of a patient arriving with a high probability of stroke. The notification uses the Rapid Arterial occlusion Evaluation (RACE) score [12] and the National Institutes of Health Stroke Scale (NIHSS) score:

- RACE ≥ 5 or NIHSS ≥ 9
- Only non-trauma and non-wake-up setting
- The patient arrives at the angio suite and is transferred to the angio table, where they are positioned with their head inclined on the specially designed head rest. Cables, glasses, and other possible sources of artifact are removed.
- FDCT imaging of the head is acquired using *syngo* DynaCT Sine Spin (Fig. 1, top row).
- The on-call interventionist and neurologist evaluate the images. If an intracranial hemorrhage (Fig. 2) has been excluded, intravenous thrombolysis can be administered.



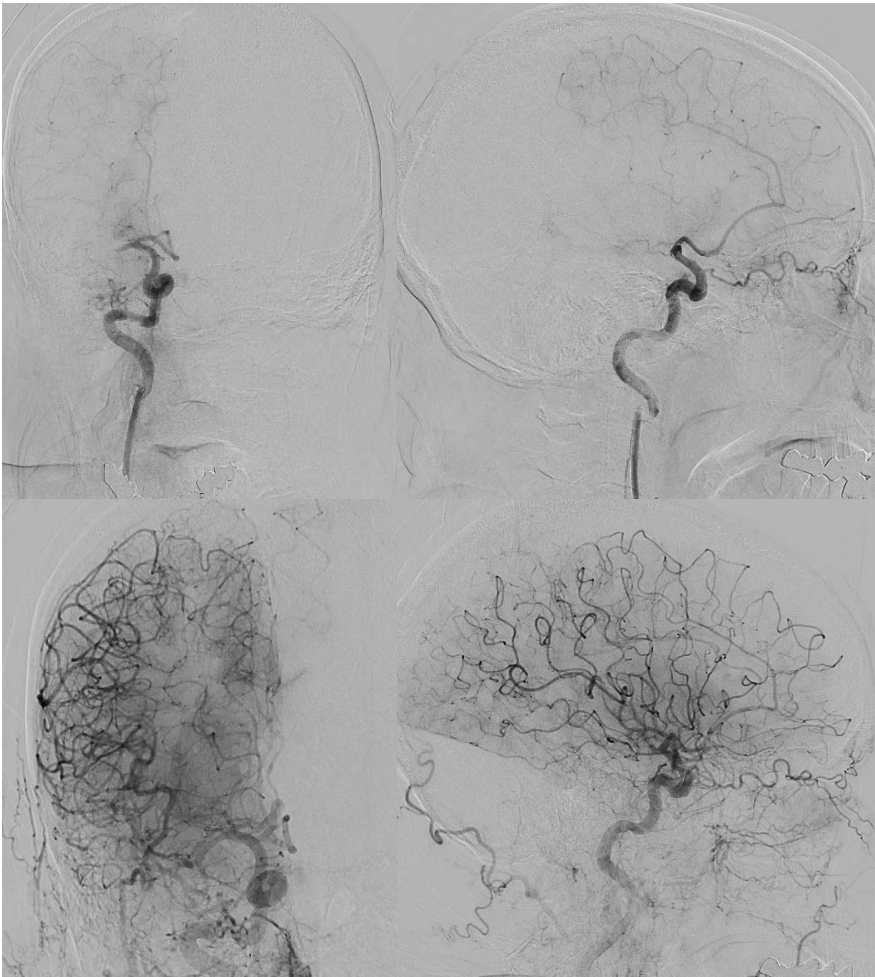
2 Identification of intracerebral hemorrhage using the one-stop protocol on an ARTIS icono system.



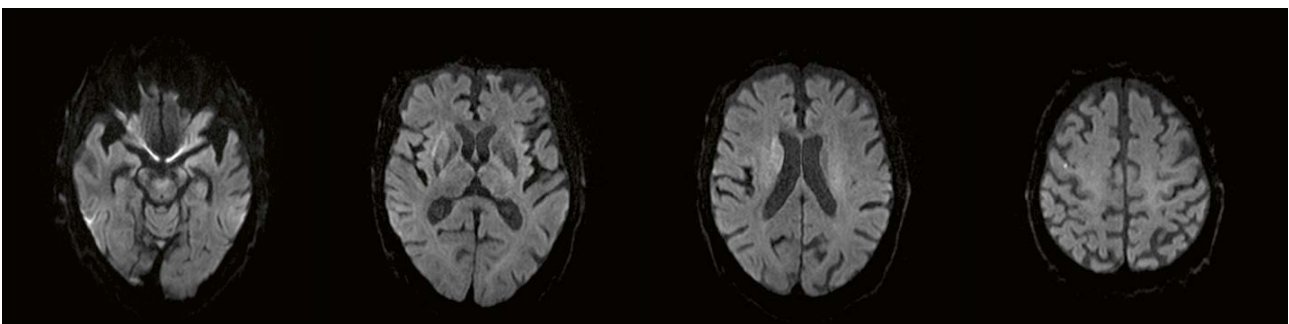
3 Intracranial FDCTA with maximum intensity projection (**3A**) and long-object orientation (**3B**); the latter allows the visualization of the aortic arch and extracranial vessels. The arrow indicates the M1 occlusion of the right middle cerebral artery.

- At the same time, intravenous contrast agent is administered. A 90° turn of the detector on plane A achieves a larger cranio-caudal field of view (Portrait mode). This allows the acquisition of an angiogram of the supra-aortic vessels, enabling evaluation of the aortic arch

type, as well as the cervical vessels for high-grade stenoses, plaques, or elongations. If these are identified, another set of materials or a different approach can be planned (Fig. 3).



- 4** Pre- and post-thrombectomy angiographic images with the ARTIS icono system. After one pass, complete reperfusion was achieved (modified Treatment in Cerebral Infarction score 3). Groin-to-reperfusion time was 20 minutes, resulting in a door-to-reperfusion time of 49 minutes.



- 5** This 24-hour follow-up imaging shows a diffusion restriction in the basal ganglia and a pinpoint lesion in the precentral gyrus. NIHSS at discharge was 1.

- FDCT perfusion imaging with evaluation for mismatch is then performed (Fig. 1, bottom row). This allows further processing of perfusion raw data to ultimately estimate the mismatch volume and to detect occlusions of more distal branches.

One-stop protocol

1. Native FDCT imaging using *syngo* DynaCT Sine Spin
2. Single-phase, long-object FDCT angiography (FDCTA).
 - IV injection of 60 mL contrast agent (300 mg) followed by a 60 mL NaCl bolus on the contrast pump
 - AltAcquisition (special acquisition protocol to be used in conjunction with a native 3D protocol) for bolus-watching phase to monitor contrast media arrival in carotid siphon
 - Start of 3D acquisition as soon as contrast media is visible in the carotid siphon
 - One run of the C-arm
3. FDCT perfusion with simultaneous triggering of contrast pump and CT imaging

References

- 1 Saver JL, Goyal M, van der Lugt A, Menon BK, Majoie CB, Dippel DW, et al. Time to Treatment With Endovascular Thrombectomy and Outcomes From Ischemic Stroke: A Meta-analysis. *JAMA*. 2016;316(12):1279–88.
- 2 Goyal M, Menon BK, van Zwam WH, Dippel DW, Mitchell PJ, Demchuk AM, et al. Endovascular thrombectomy after large-vessel ischaemic stroke: a meta-analysis of individual patient data from five randomised trials. *Lancet*. 2016;387(10029):1723–31.
- 3 Turc G, Bhogal P, Fischer U, Khatri P, Lobotesis K, Mazighi M, et al. European Stroke Organisation (ESO) - European Society for Minimally Invasive Neurological Therapy (ESMINT) Guidelines on Mechanical Thrombectomy in Acute Ischemic Stroke. *J Neurointerv Surg*. 2023;15(8):e8.
- 4 Prabhakaran S, Gonzalez NR, Zachrisson KS, Adeoye O, Alexandrov AW, Ansari SA, et al. 2026 Guideline for the Early Management of Patients With Acute Ischemic Stroke: A Guideline From the American Heart Association/American Stroke Association. *Stroke*. 2026. doi: 10.1161/STR.0000000000000513. Epub ahead of print.
- 5 Psychogios MN, Behme D, Schregel K, Tsogkas I, Maier IL, Leyhe JR, et al. One-Stop Management of Acute Stroke Patients: Minimizing Door-to-Reperfusion Times. *Stroke*. 2017;48(11):3152–3155.
- 6 Brehm A, Tsogkas I, Maier IL, Eisenberg HJ, Yang P, Liu JM, et al. One-Stop Management with Perfusion for Transfer Patients with Stroke due to a Large-Vessel Occlusion: Feasibility and Effects on In-Hospital Times. *AJNR Am J Neuroradiol*. 2019;40(8):1330–1334.
- 7 Leyhe JR, Tsogkas I, Hesse AC, Behme D, Schregel K, Papageorgiou I, et al. Latest generation of flat detector CT as a peri-interventional diagnostic tool: a comparative study with multidetector CT. *J Neurointerv Surg*. 2017;9(12):1253–1257.
- 8 Petroulia VD, Kaesmacher J, Piechowiak EI, Dobrocky T, Pilgram-Pastor SM, Gralla J, et al. Evaluation of Sine Spin flat detector CT imaging compared with multidetector CT. *J Neurointerv Surg*. 2023;15(3):292–297.
- 9 Requena M, Olivé-Gadea M, Muchada M, Hernández D, Rubiera M, Boned S, et al. Direct to Angiography Suite Without Stopping for Computed Tomography Imaging for Patients With Acute Stroke: A Randomized Clinical Trial. *JAMA Neurol*. 2021;78(9):1099–1107.
- 10 Hoelter P, Goelitz P, Lang S, Luecking H, Kalmuenzer B, Struffert T, et al. Visualization of large vessel occlusion, clot extent, and collateral supply using volume perfusion flat detector computed tomography in acute stroke patients. *Acta Radiol*. 2019;60(11):1504-1511.
- 11 Maier IL, Scalzo F, Leyhe JR, Schregel K, Behme D, Tsogkas I, et al. Validation of collateral scoring on flat-detector multiphase CT angiography in patients with acute ischemic stroke. *PLoS One*. 2018;13(8):e0202592.
- 12 Pérez de la Ossa N, Carrera D, Gorchs M, Querol M, Millán M, Gomis M, et al. Design and validation of a prehospital stroke scale to predict large arterial occlusion: the rapid arterial occlusion evaluation scale. *Stroke*. 2014;45(1):87–91.



Contact

Professor Marios-Nikos Psychogios, M.D.
Department of Diagnostic and
Interventional Neuroradiology
University Hospital Basel
Petersgraben 4
4031 Basel
Switzerland
marios.psychogios@usb.ch



Vera Aebischer, M.D.
Department of Diagnostic and
Interventional Neuroradiology
University Hospital Basel
Petergraben 4
4031 Basel
Switzerland
vera.aebischer@usb.ch

Endovascular Treatment of an Unruptured Symptomatic Intracranial Aneurysm in a Toddler

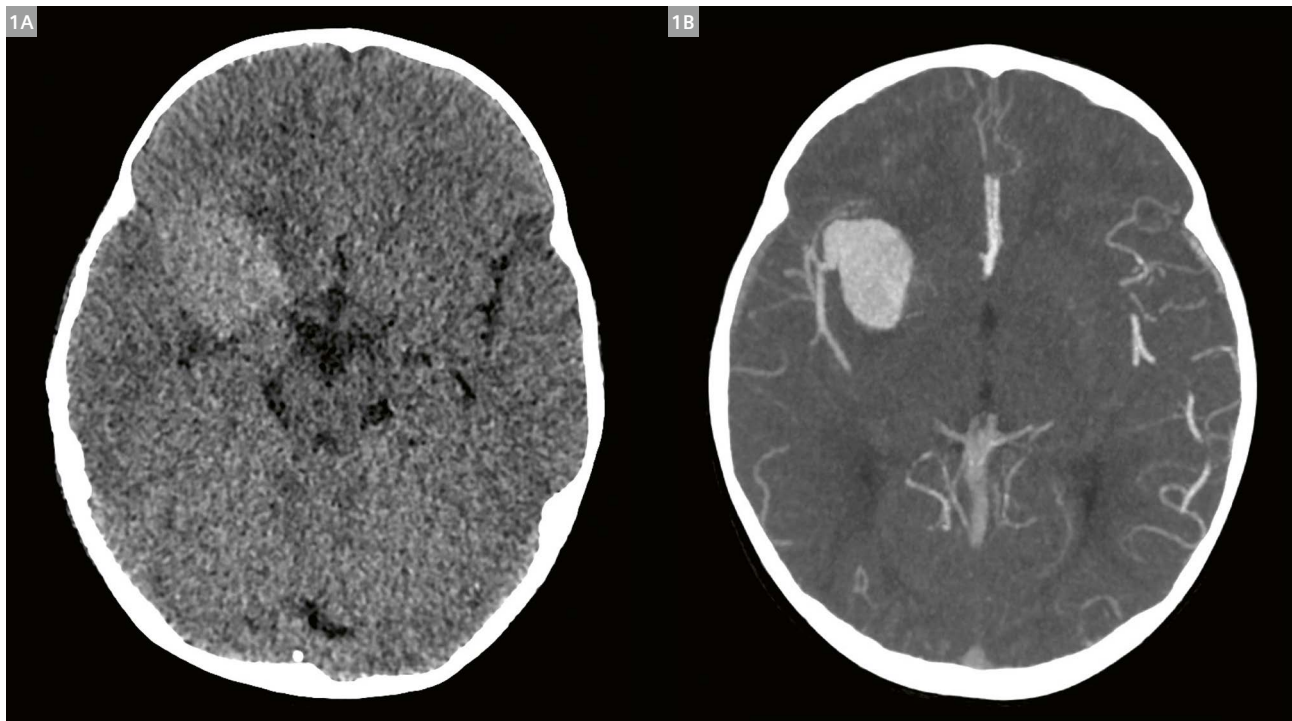
Riitta Rautio, M.D., Ph.D.; Johanna Pekkola M.D., Ph.D.; Matias Sinisalo, M.D.
Turku University Hospital and University of Turku, Finland

History

A previously healthy 20-month-old boy appeared normal after waking up in the morning. He was eating breakfast cereal when his parents noticed left-sided paresis and slurred speech. After the child was transported by ambulance to the university hospital, the left-side weakness persisted with a score of 4 on the National Institutes of Health Stroke Scale (NIHSS).

Diagnostic imaging and work-up

An MRI scan would have required anesthesia, but the patient had just eaten breakfast so an emergency head CT (computed tomography) and CTA (computed tomography angiography) were performed. The native CT showed no evidence of acute intracranial hemorrhage (Fig. 1A), but the CTA revealed a large fusiform aneurysm arising from the M1 segment of the right middle cerebral artery (MCA) (Fig. 1B). The aneurysm had a maximum diameter of 32 mm. There was also edema in the brain parenchyma surrounding the aneurysm (Fig. 1A).



1 (1A) Axial non-contrast CT scan performed at admission revealing an aneurysm with mild surrounding edema in the right MCA distribution. (1B) The CTA confirms the presence of a large right MCA aneurysm.

Conventional digital subtraction angiography (DSA) was performed the same day. DSA demonstrated a large fusiform dissecting aneurysm that was partially thrombosed on the right. The fusiform portion extended from the distal M1 segment and continued to the lower M2 branch. Distal MCA branches showed signs of arterial delay (Fig. 2).



2 Anteroposterior cerebral angiogram demonstrates a large fusiform dissecting-type aneurysm involving the right M1–M2 segment.

An attempt at reconstructive endovascular treatment was made during the initial DSA procedure, but microcatheterization through the fusiform aneurysm from the M1 to the lower M2 branch was unsuccessful.

Clinical course

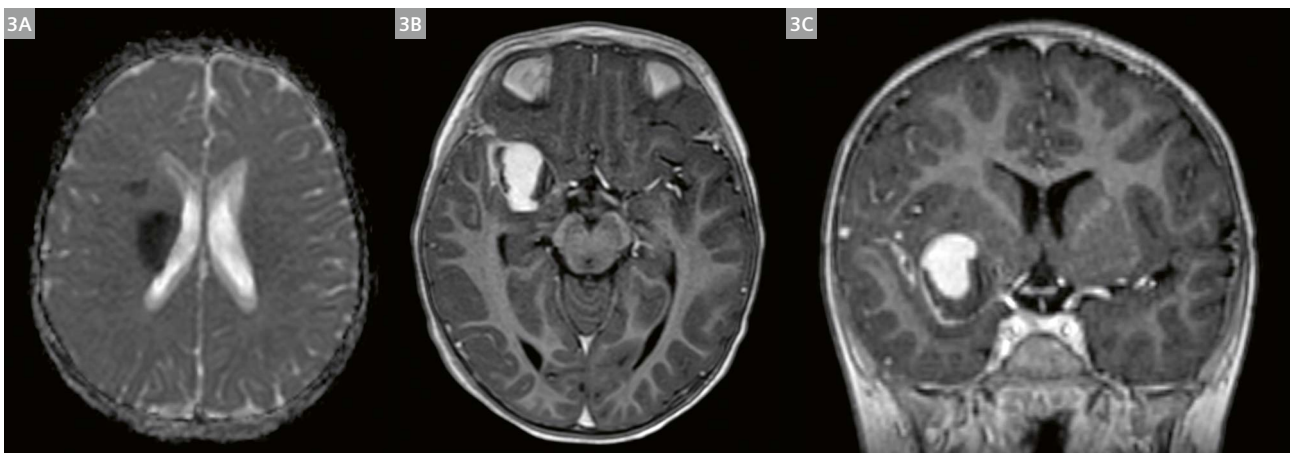
The patient's¹ clinical condition remained unchanged in the following days. He suffered from partial hemiparesis without aphasia. An MRI exam revealed fresh infarcts in the right hemisphere and partial thrombosis of the aneurysm (Figs 3A–3C). Rehabilitation was initiated, and the patient was discharged on daily enoxaparin. A follow-up MRI exam and temporary balloon occlusion test were planned once the patient had recovered from the initial infarcts to assess possible collateral leptomeningeal circulation.

Follow-up

The patient made a single emergency visit four weeks after the onset of symptoms, due to a transient weakness in the left leg. An MRI scan showed no change in aneurysm size and no new infarcts.

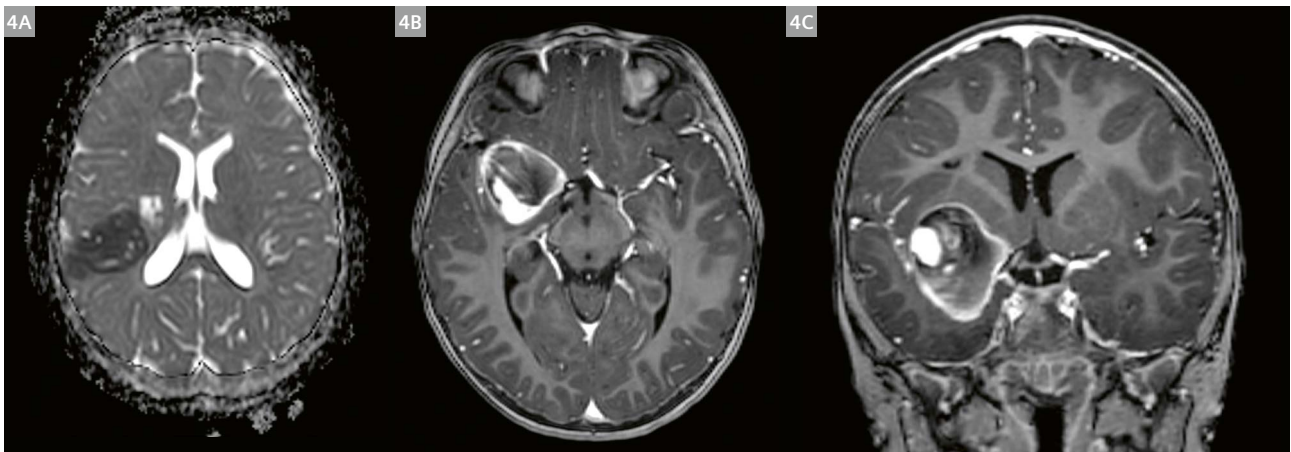
On the three-month follow-up MRI scan, the aneurysm had grown up to 40 mm in diameter and new infarcts were noted (Figs 4A–C). Flow to the distal MCA branches had decreased. However, the patient's clinical condition had improved significantly.

Due to the aneurysm's growth and the occurrence of new infarcts, a decision was made to attempt another endovascular treatment.

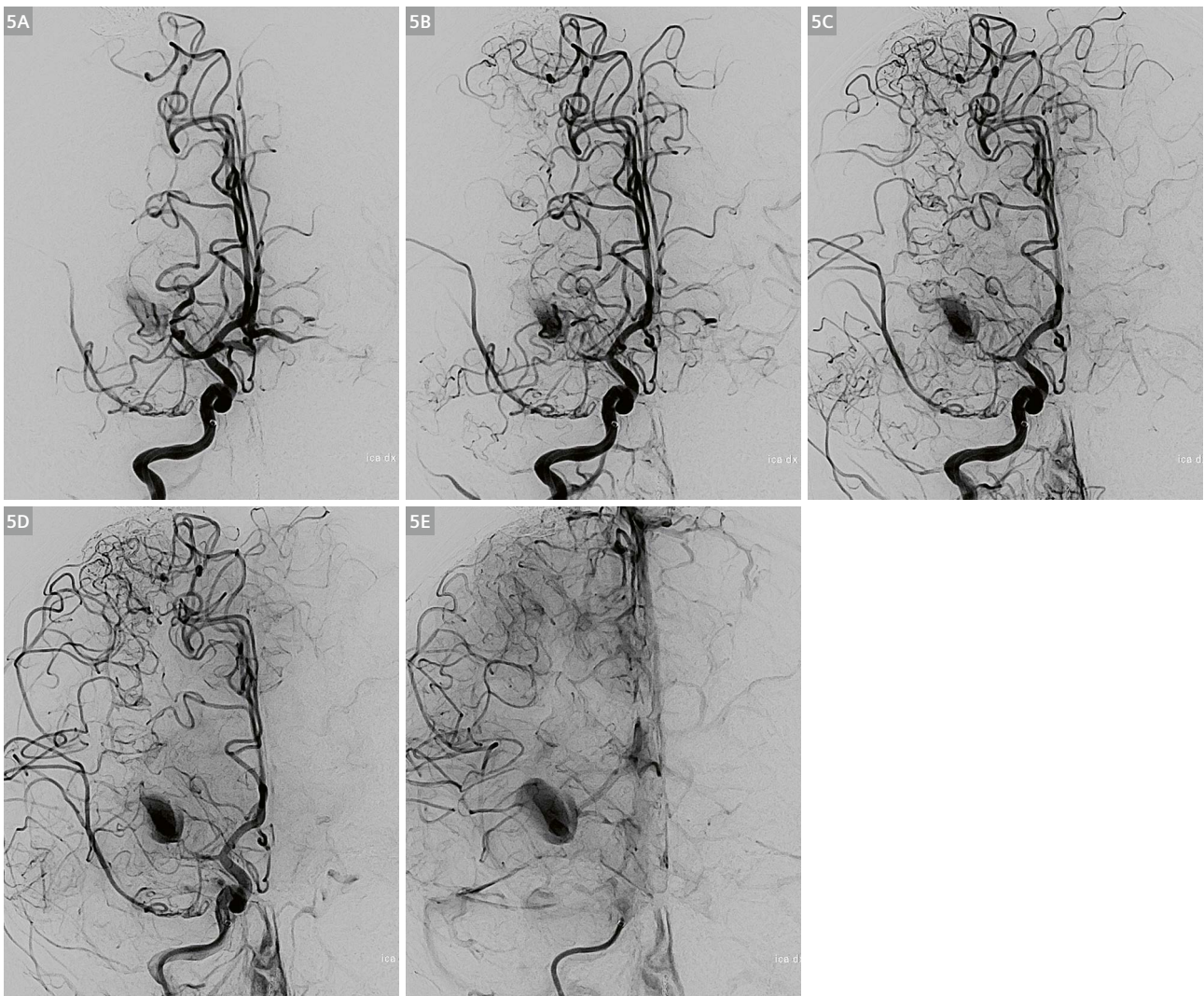


3 An MRI scan was performed on the second hospital day. Acute stroke is seen on the right in the putamen on the ADC map (3A). Axial (3B) and coronal (3C) post-contrast T1-weighted MR images show the partially thrombosed MCA aneurysm with a maximum diameter of 32 mm in axial plane. Images acquired on a 3T MAGNETOM Skyra MRI scanner (Siemens Healthineers, Erlangen, Germany).

¹ MR scanning has not been established as safe for imaging fetuses and infants less than two years of age. The responsible physician must evaluate the benefits of the MR examination compared to those of other imaging procedures.



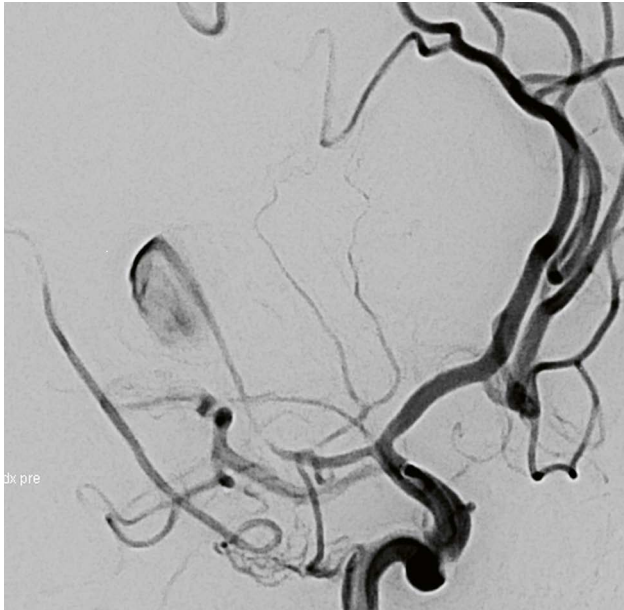
4 MRI scan performed three months later shows new stroke on the right, as well as the old infarct in the putamen (4A). Axial (4B) and coronal (4C) post-contrast T1-weighted MR images show that the partially thrombosed MCA aneurysm has grown. The maximum diameter is now 40 mm in coronal plane.



5 (5A–5E) Anteroposterior DSA images before endovascular treatment demonstrate the slow filling of the aneurysm and the rich collateral network.

New DSA findings and endovascular treatment

In the follow-up DSA, the filling of the aneurysm was slower, and the collateral network had expanded (Figs. 5A–5E). Collaterals were visible from the temporal branch, as well as from the pericallosal artery and the posterior circulation. The distal M1 segment appeared thinner than in the original DSA (Fig. 6). It was observed that the lenticulostriate artery branches were not arising from the aneurysm sac.



6 Working projection for the endovascular parent vessel occlusion visualizes the narrowed distal M1 vessel.

Since the loss of parent vessel flow was proven to be well compensated by natural collaterals, a decision was made to proceed with parent vessel occlusion after thorough discussion with the neurosurgeon. The distal M1 segment was occluded with two coils (1.5 mm × 4 cm and 1 mm × 10 mm) distal to the orifice of the temporal branch (Fig. 7A, 7B).

Postprocedural care

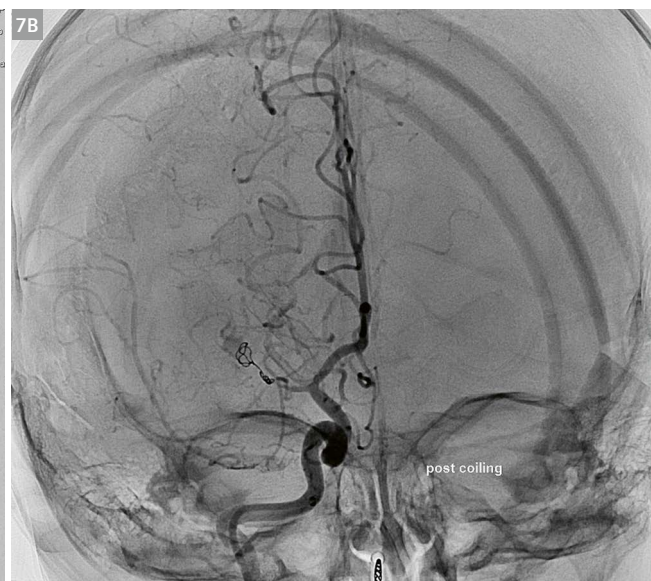
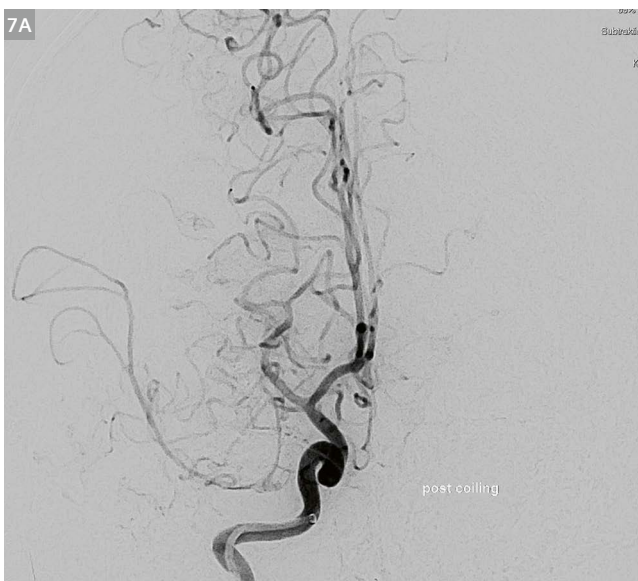
After the procedure, the patient's blood pressure was maintained at 20% above baseline in order to support the collateral circulation. The patient received intravenous aspirin during the procedure, which was continued on a daily basis for one month following the intervention.

Between the original DSA and the final endovascular procedure, our neuroangiography equipment was upgraded to the ARTIS icono biplane system. This change is reflected in the DSA images. To minimize radiation exposure, a CARE program was implemented, ensuring that image quality was not compromised.

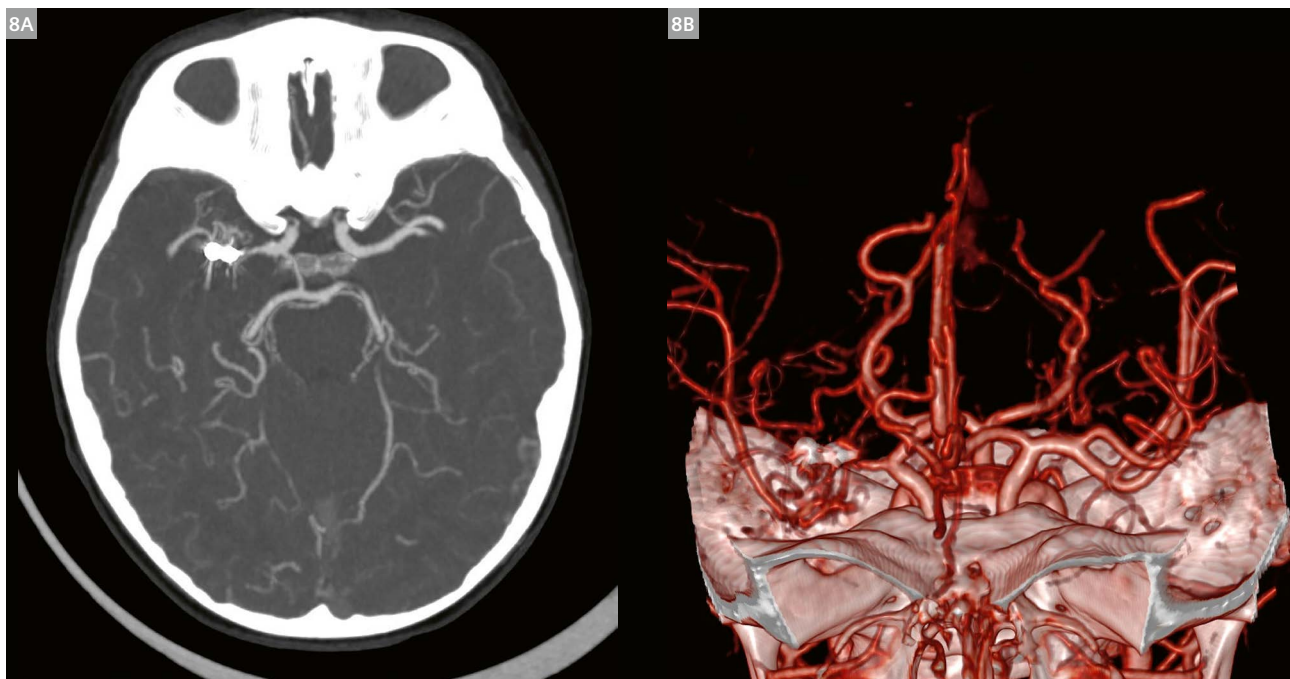
Outcome and follow-up

The patient woke up without any new neurological symptoms. He was initially monitored in the intensive care unit and then transferred to the pediatric ward. Rehabilitation continued, and a follow-up CTA was performed five months later. The CTA showed no visible aneurysm sac, and there were no new infarcts (Figs. 8A, 8B).

One year after the endovascular treatment, the patient still experiences partial left-sided upper extremity hemiplegia, but there has been continuous improvement.



7 Subtracted (7A) and unsubtracted (7B) DSA image after coil embolization of the distal M1.



8 CTA (8A) and 3D CTA (8B) reconstruction images show no visible residual aneurysm sac. The collateral supply to the occluded middle cerebral artery is well established.

Discussion

Pediatric intracranial aneurysms are rare, representing only 1% to 7% of all intracranial aneurysms [1]. Of these aneurysms, 75% are located in the anterior circulation, with the remaining 25% found in the posterior circulation. The internal carotid artery is the most commonly affected site, constituting 27% of cases, followed by the middle cerebral artery (26%) [2]. Occasionally, aneurysms are discovered in more distal locations.

The cause of aneurysm formation remains unclear in many cases [3]. Various conditions have been associated with an increased risk of aneurysm development, including infections, hypertension, collagen disorders, autosomal dominant polycystic kidney disease, neurofibromatosis, tuberous sclerosis, aortic coarctation, AV malformations, trauma, cranial irradiation, metastatic atrial myxoma, moyamoya disease, and prior surgery for craniopharyngioma [4].

There are no consensus recommendations for the treatment of pediatric intracranial aneurysms regarding indications or treatment modalities. The decision to treat is typically based on a risk-to-benefit evaluation, following thorough discussions with pediatric neurosurgeons and interventional neuroradiologists. Surgical treatment, reconstructive endovascular treatment, parent vessel occlusion, and conservative treatment should all be considered on an individual basis. The family must be clearly informed about the risks and benefits of each treatment option. In our case, the patient showed rapid aneurysm growth, and the aneurysm was symptomatic, providing a clear indication for active treatment. Due to the presence of a rich collateral vasculature, endovascular parent vessel occlusion was considered the safest treatment approach.

Informed written consent was obtained from the family for the publication of this case.

References

- 1 Ghali MGZ, Srinivasan VM, Cherian J, Wagner KM, Chen SR, Johnson J, et al. Multimodal Treatment of Intracranial Aneurysms in Children: Clinical Case Series and Review of the Literature. *World Neurosurg.* 2018;111:e294–e307.
- 2 Beez T, Steiger HJ, Hänggi D. Evolution of Management of Intracranial Aneurysms in Children: A Systematic Review of the Modern Literature. *J Child Neurol.* 2016;31(6):773–83.
- 3 Mohotti JE, Carter NS, Zhang VJW, Lai LT, Xenos C, Asadi H, et al. Neonatal intracranial aneurysms: case report and review of the literature. *J Neurosurg Pediatr.* 2018;21(5):471–477.
- 4 Jain PK, Mehta VS. Anterior communicating artery aneurysm in a 3-year-old girl. *Childs Nerv Syst.* 2002;18(1–2):71–3.

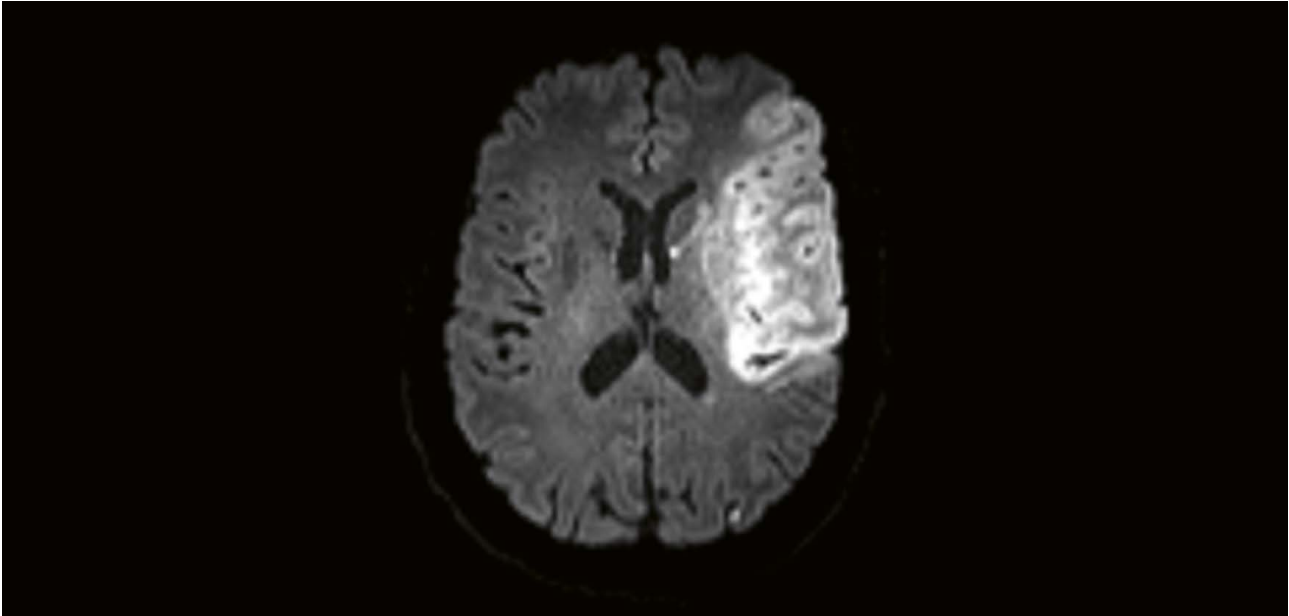
Contact

Associate Professor Riitta Rautio, M.D., Ph.D.
Head of the Department of Interventional Radiology
Turku University Hospital
Kiiinamyllynkatu 4-8
FI-20520 Turku
Finland
Riitta.Rautio@tyks.fi



Speed up stroke care for your patients.

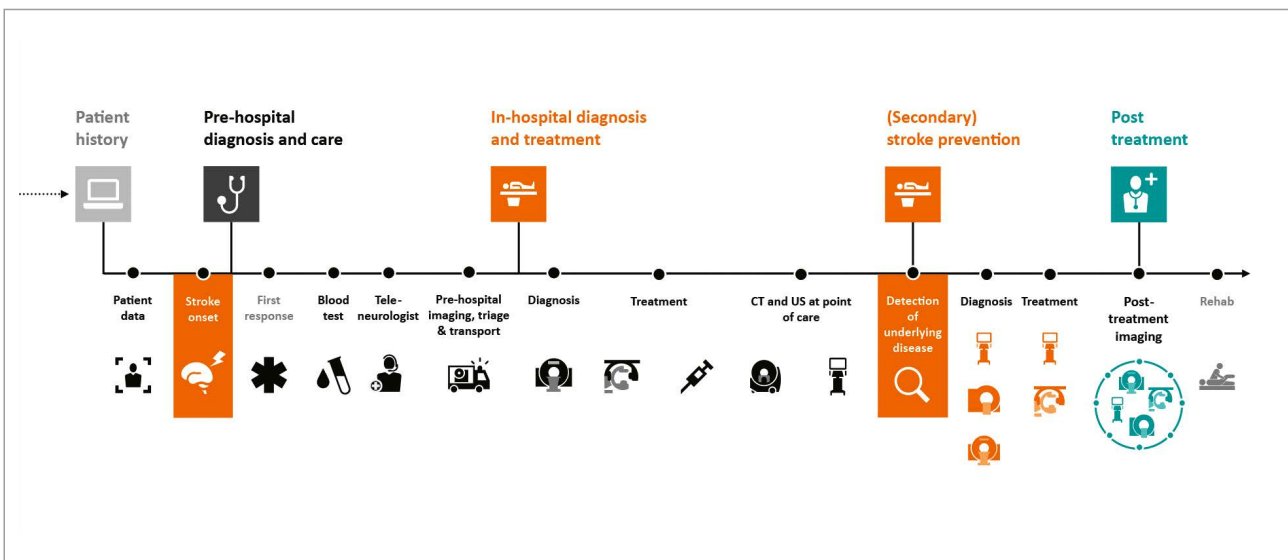
Explore our comprehensive offering for stroke care.



As your partner in stroke management, we keep you ahead of your time. Our advanced technologies let you speed up stroke care and transform care delivery along the entire

pathway — from stroke screening and pre-hospital diagnosis and care to in-hospital diagnosis and treatment. Explore our offerings for stroke care!

Optimal treatment across all steps of the clinical pathway is crucial for good patient outcome



Visit us at

<https://www.siemens-healthineers.com/clinical-specialities/neurology/stroke-care>

Beyond the Clock: The Pivotal Role of Advanced MRI in Revolutionizing the Diagnosis and Management of Brainstem Stroke

Anirudda Deshpande, M.D., DM, DNB, FRCP, SCE Neurology¹; Vikram Khardenavis, MBBS, DM²; Aakash Shetty, MBBS, M.D., DM, DNB³; Ganesh Samudrala, MBBS⁴; Alla Dinesh, MBBS⁵

¹ Department of Care of the Elderly & Stroke, Altnagelvin Hospital, Londonderry, Northern Ireland, UK

² Department of Neurology, Madurai Medical College, Alwarpuram, Madurai, Tamil Nadu, India

³ Department of Neurology, University of Alberta, Edmonton, Canada

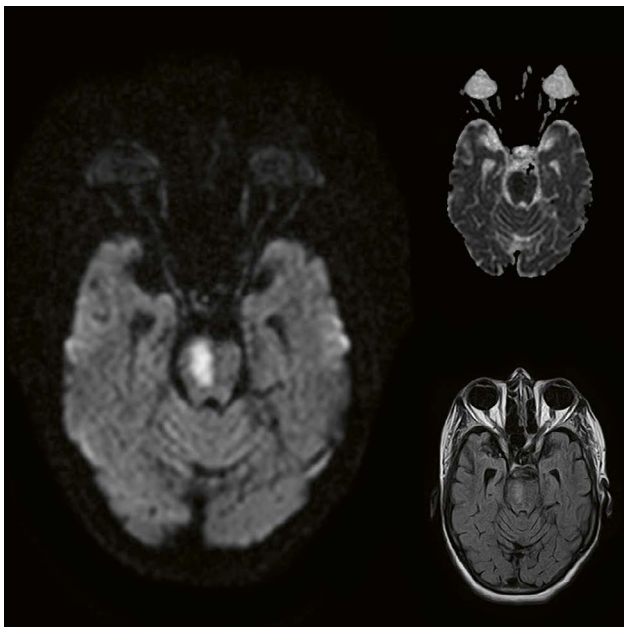
⁴ Medisure Diagnostics, Warangal, Telangana, India

⁵ Salus Medical Diagnostics, Hyderguda, Hyderabad, Telangana, India

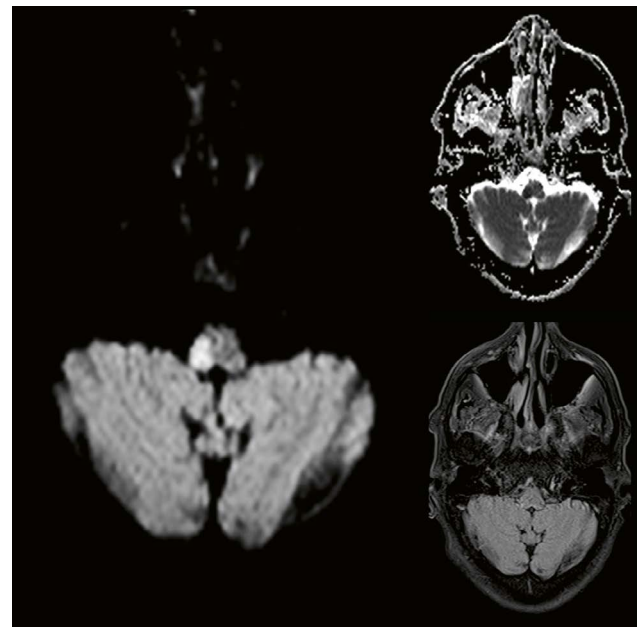
Abstract

The brainstem, a compact neural structure housing critical life-sustaining nuclei and white matter tracts, presents a unique diagnostic challenge when ischemic injury occurs. Its anatomical complexity and the non-specific nature of presenting symptoms often lead to diagnostic delays or misdiagnosis. Computed tomography is notoriously insensitive to acute brainstem ischemia. This review articulates the indispensable role of advanced magnetic resonance imaging (MRI) as the unequivocal gold standard for diagnosing brainstem stroke. We detail how specific

MRI sequences — particularly high-resolution diffusion-weighted imaging on modern platforms like the MAGNETOM systems — enable precise anatomical localization, facilitate differential diagnosis, and provide prognostic information. Furthermore, we explore the emerging potential of advanced techniques like diffusion tensor imaging and high-resolution vessel wall imaging in refining our understanding of brainstem stroke pathophysiology and in guiding future therapeutic strategies.



1 DWI, ADC, and FLAIR images of acute right paramedian pontine infarction.



2 DWI, ADC, and FLAIR images of right lateral medullary infarction.

1. Introduction: The diagnostic conundrum of brainstem stroke

Brainstem strokes, accounting for 10%–15% of all ischemic strokes, are neurological emergencies of the highest order [1]. Their presentation can be misleading: vertigo, nausea, diplopia, ataxia, and crossed sensory-motor deficits can easily be mistaken for peripheral vestibulopathies, metabolic disorders, or even psychological events. This diagnostic ambiguity, coupled with the profound limitations (due to bone artifact) of non-contrast computed tomography (CT) in visualizing the posterior fossa, creates a perilous gap in early care. The advent of magnetic resonance imaging (MRI) has fundamentally closed this gap, transforming brainstem stroke from a clinical enigma into a precisely imageable entity.

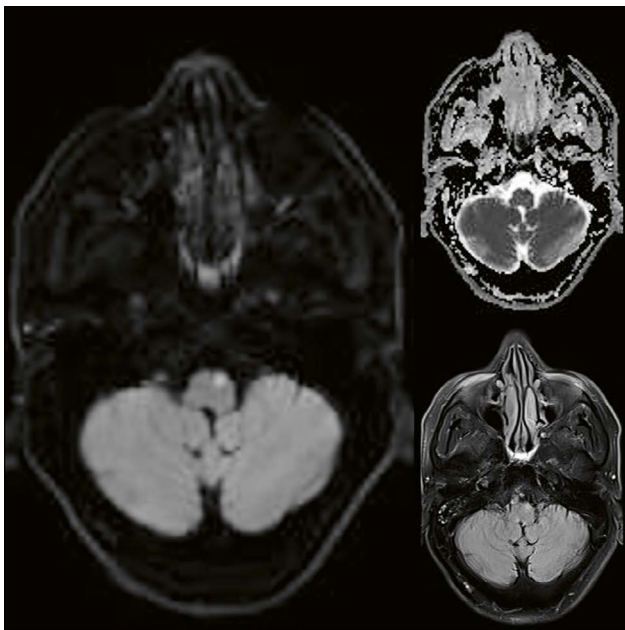
2. The armamentarium of MRI sequences: A tailored approach

A comprehensive MRI protocol is critical. Modern scanners offer optimized sequences that are pivotal for assessment.

2.1. Diffusion-weighted imaging (DWI): The cornerstone of acute diagnosis

DWI is the most critical sequence in the acute setting (< 24 hours), revealing restricted diffusion as hyperintensity within minutes of ischemia onset [2]. Its value in brainstem stroke is unparalleled:

- **Unmatched sensitivity:** DWI sensitivity for acute brainstem infarction exceeds 95%, compared to < 50% for CT, and lower for standard MRI sequences [3].



3 DWI, ADC, and FLAIR images of left medial medullary infarction.

- **Anatomical precision:** The high resolution of modern DWI sequences (e.g., using RESOLVE to minimize echo-planar imaging (EPI) distortion) allows clinicians to pinpoint the infarct to specific structures — e.g., the medial medulla (anterior spinal artery (ASA) territory) versus the lateral medulla (posterior inferior cerebellar artery (PICA) territory) — directly informing the vascular etiology and prognosis.

2.2. Fluid-attenuated inversion recovery (FLAIR) and T2-weighted imaging

While less sensitive than DWI in the hyperacute phase, these two sequences become positive after several hours and are excellent for depicting subacute and chronic infarcts. They provide essential context, helping to distinguish acute from chronic lesions.

2.3. High-resolution 3D T2-weighted sequences (SPACE, CISS)

Sequences like sampling perfection with application-optimized contrasts using different flip angle evolution (SPACE) and constructive interference in steady state (CISS) provide exquisite anatomical detail of the brainstem parenchyma and surrounding cisterns. They are invaluable for ruling out non-ischemic mimics like demyelination, infection, or compressive tumors.

2.4. Magnetic resonance angiography (MRA)

Time-of-flight (TOF) MRA non-invasively assesses the vertebrobasilar circulation, which is the lifeblood of the brainstem. Identifying basilar artery occlusion (an often fatal but treatable emergency) or vertebral artery dissection is a critical component of the MRI exam, which directly guides urgent endovascular therapy.

3. The clinical impact: From diagnosis to prognosis

Several clinical examples are shown in Figures 1–3. They all highlight DWI and FLAIR which are the most utilized contrasts in the acute brainstem stroke setting. However, all capabilities of MRI contribute to the diagnosis as well as prognosis of the patient.

3.1. Resolving diagnostic uncertainty

The most immediate impact of MRI is ending diagnostic doubt. A patient with vertigo and nystagmus can have a definitive diagnosis of lateral medullary stroke (Wallenberg syndrome) confirmed by a tiny DWI hyperintensity. This prevents misdiagnosis as benign positional vertigo and ensures that appropriate secondary prevention is initiated.

3.2. Informing etiology and management

The pattern of infarction on MRI points to the underlying mechanism:

- **Large artery atherosclerosis:** Infarcts in the proximal vascular territory
- **Small penetrating artery disease (lacunar):** Small, deep infarcts (< 1.5 cm) in the pons or midbrain
- **Artery-to-artery embolism:** Larger, wedge-shaped cortical-subcortical infarcts
- **Vertebral artery dissection:** An infarct in the lateral medulla or PICA territory with a crescent sign on axial T1-weighted fat-saturated images of the vertebral artery

This etiological classification is essential for tailoring long-term management, such as selecting dual antiplatelet therapy for minor stroke, or high-intensity statins for atherosclerosis.

3.3. Prognostic implications

The location and extent of the lesion on MRI are powerful prognostic indicators. A small, unilateral pontine lacune carries a vastly different prognosis than a large, bilateral “locked-in” pontine infarct or “top of the basilar” syndrome affecting the midbrain and thalami.

4. Future directions and advanced techniques

The evolution of MRI continues to refine our understanding of brainstem stroke. **Diffusion tensor imaging (DTI)** can map the disruption of critical white matter tracts (e.g., corticospinal tracts), providing biomarkers for motor recovery potential. **High-resolution vessel wall imaging** can directly visualize plaque inflammation or dissection flaps in the vertebrobasilar system, offering insights into pathophysiology that lumenography (MRA/CTA) cannot. Modern MR scanners are usually equipped with susceptibility-weighted imaging (SWI) which is very sensitive to T2* variations and, hence, can detect microbleeds, a sign of cerebral small vessel disease that may influence anticoagulation decisions.

Quantitative susceptibility mapping (QSM)¹ will take SWI one step further by quantifying the susceptibility variation. This may have potential benefits for hemorrhagic stroke

patients [6] and may also enable new insights into the complex processes following acute ischemic stroke [7].

5. Conclusion

Advanced MRI has changed the landscape of brainstem stroke management. It has evolved from a mere diagnostic tool to a comprehensive guidance system for acute triage, etiological classification, and prognostic stratification.

By leveraging a multimodal protocol on a technologically advanced MRI platform, clinicians can overcome the inherent challenges of brainstem anatomy, ensure accurate and timely diagnosis, and provide patients with highly informed and effective care pathway. The continued integration of these sophisticated imaging techniques into clinical protocols is essential for further improving outcomes in this complex patient population.

References

- 1 Saposnik G, Barinagarrementeria F, Brown RD Jr, Bushnell CD, Cucchiara B, Cushman M, et al. Diagnosis and Management of Cerebral Venous Thrombosis: A Statement for Healthcare Professionals From the American Heart Association/American Stroke Association. *Stroke*. 2011;42(4):1158–92. Epub 2011 Feb 3.
- 2 Lövblad KO, Bassetti C, Schneider J, Guzman R, El-Koussy M, Remonda L, et al. Diffusion-weighted mr in cerebral venous thrombosis. *Cerebrovasc Dis*. 2001;11(3):169–76.
- 3 Oppenheim C, Domingo V, Gauvrit JY, Lamy C, Mackowiak-Cordoliani MA, Pruvo JP, et al. Subarachnoid hemorrhage as the initial presentation of dural sinus thrombosis. *AJNR Am J Neuroradiol*. 2005;26(2):614–7.
- 4 van der Knaap N, Franx BAA, Majoie CBML, van der Lugt A, Dijkhuizen RM; CONTRAST consortium. Implications of Post-recanalization Perfusion Deficit After Acute Ischemic Stroke: a Scoping Review of Clinical and Preclinical Imaging Studies. *Transl Stroke Res*. 2024;15(1):179–194.
- 5 Hwang DY, Silva GS, Furie KL, Greer DM. Comparative sensitivity of computed tomography vs. magnetic resonance imaging for detecting acute posterior fossa infarct. *J Emerg Med*. 2012;42(5):559–65. Epub 2011 Nov 3.
- 6 Wang S, Lou M, Liu T, Cui D, Chen X, Wang Y. Hematoma Volume Measurement in Gradient Echo MRI Using Quantitative Susceptibility Mapping. *Stroke*. 2013;44(8):2315–2317.
- 7 Probst J, Rohner M, Zahn M, Piccirelli M, Pangalu A, Luft A, et al. Quantitative susceptibility mapping in ischemic stroke patients after successful recanalization. *Scientific Reports*. 2021;11(1):16038.

Contact

Anirudda Deshpande, M.D., DM, DNB, FRCP, SCE Neurology
Consultant, Department of Care of the Elderly & Stroke
Altnagelvin Hospital
Glenshane Road
Londonderry, Northern Ireland, BT47 6SB
United Kingdom
anirudda.deshpande@westerntrust.hscni.net



¹ Work in progress. QSM is currently under development and is not for sale in the U.S. and in other countries. Its future availability cannot be ensured.

Wake-Up Strokes: Advanced Imaging Solutions for Time-Sensitive Neurological Emergencies

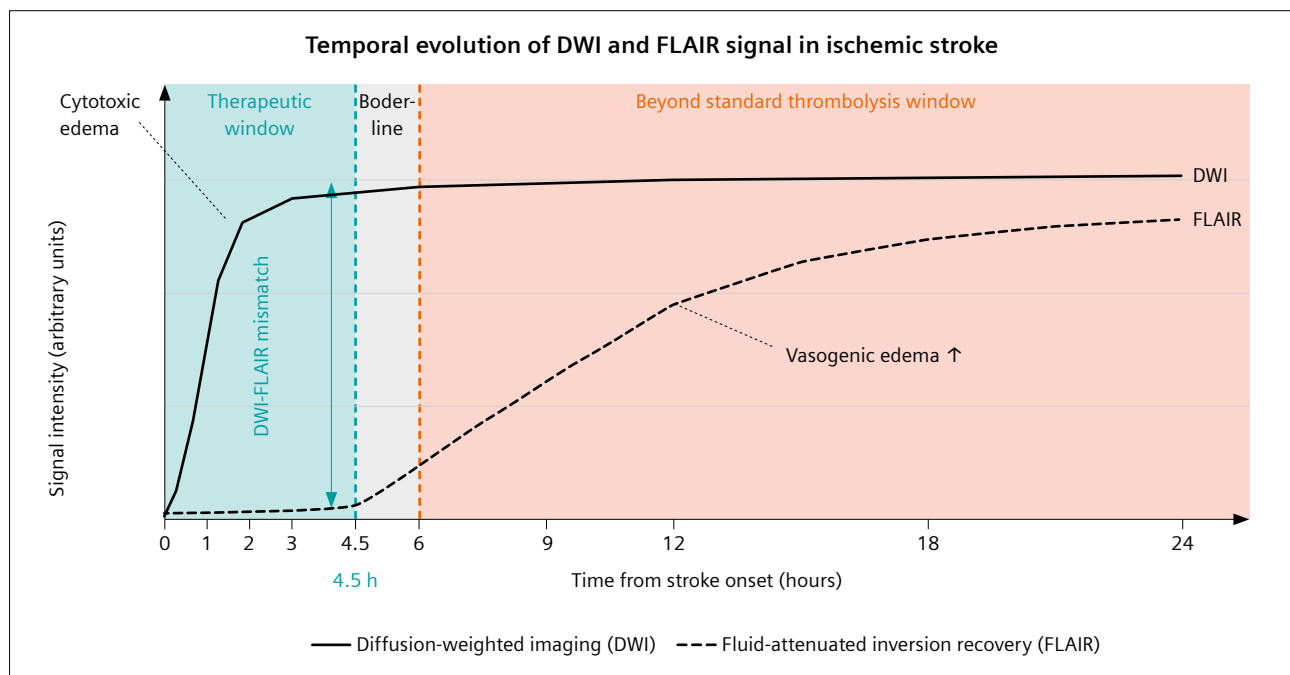
Anirudda Deshpande, M.D., DM, DNB, FRCP, SCE Neurology

Department of Care of the Elderly & Stroke, Altnagelvin Hospital, Londonderry, Northern Ireland, UK

Wake-up strokes, which account for 14%–28% of all ischemic strokes, present a unique diagnostic challenge [1]: In wake-up stroke, patients first notice neurological deficits when they awaken, making it impossible to precisely determine the onset time of the stroke. This uncertainty has historically excluded these patients from thrombolytic therapy, as traditional protocols required confirmed symptom onset within 4.5 hours [3]. However, advanced neuroimaging has revolutionized treatment paradigms, enabling tissue-based rather than time-based treatment decisions [4, 5].

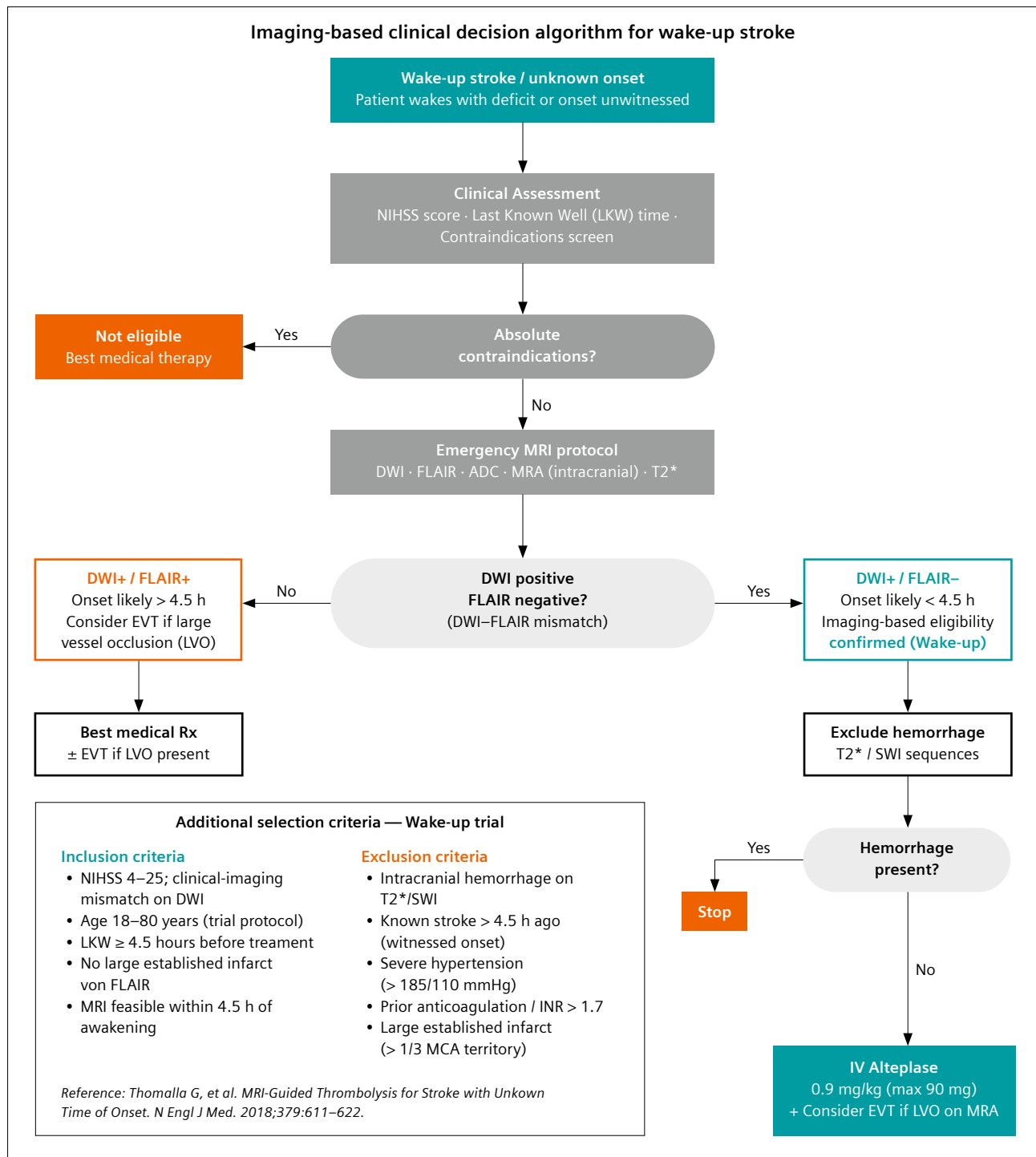
The clinical challenge

Wake-up strokes are when individuals go to sleep neurologically intact and awaken with established deficits. The last-known normal time is bedtime, but the actual time of stroke onset remains unknown. Traditional stroke management follows the principle that time is brain — every minute of ischemia destroys approximately 1.9 million neurons [2]. Alteplase, a tissue plasminogen activator, offers benefit only within narrow time windows. This creates an impossible situation for wake-up stroke patients, who, even with rapid emergency response, fall outside traditional eligibility criteria due to the unknown onset time [3].



1 Temporal evolution of DWI and FLAIR signal intensity following acute ischemic stroke onset.

Schematic graph illustrating the divergent time courses of diffusion-weighted imaging (DWI; solid line) and fluid-attenuated inversion recovery (FLAIR; dashed line) signal intensity following ischemic stroke onset. DWI signal rises rapidly within minutes of onset as cytotoxic edema — driven by failure of the Na^+/K^+ -ATPase and subsequent intracellular water accumulation — restricts water diffusion in the infarcted core. FLAIR signal elevation, reflecting vasogenic edema from blood–brain barrier disruption, is delayed by several hours, typically beyond 3–4.5 hours from onset. The interval during which DWI is positive and FLAIR remains negative (petrol shaded zone) constitutes the DWI–FLAIR mismatch window, underpinning the imaging-based patient selection strategy employed in the WAKE-UP randomized controlled trial. The borderline zone (4.5–6 hours, orange shading) reflects inter-individual variation in the rate of FLAIR signal emergence; treatment decisions in this range require individual risk–benefit evaluation.



2 Imaging-guided clinical decision algorithm for acute management of wake-up stroke.

Stepwise decision algorithm for the management of wake-up and unknown-onset ischemic stroke, based on the imaging selection criteria of the WAKE-UP trial [5]. Following clinical assessment and exclusion of absolute contraindications, emergency MRI is performed (DWI, FLAIR, ADC map, MRA, T2*/susceptibility-weighted imaging). Confirmation of DWI-FLAIR mismatch (DWI-positive, FLAIR-negative) — indicating a high likelihood of onset within 4.5 hours — combined with exclusion of intracranial hemorrhage on T2* sequences, supports eligibility for intravenous alteplase at 0.9 mg/kg (maximum 90 mg). The presence of DWI-FLAIR concordance (both sequences positive) suggests onset beyond the standard window, with management directed toward best medical therapy or endovascular thrombectomy where large vessel occlusion is confirmed on MRA. The inset table summarizes key inclusion and exclusion criteria from the WAKE-UP trial protocol.

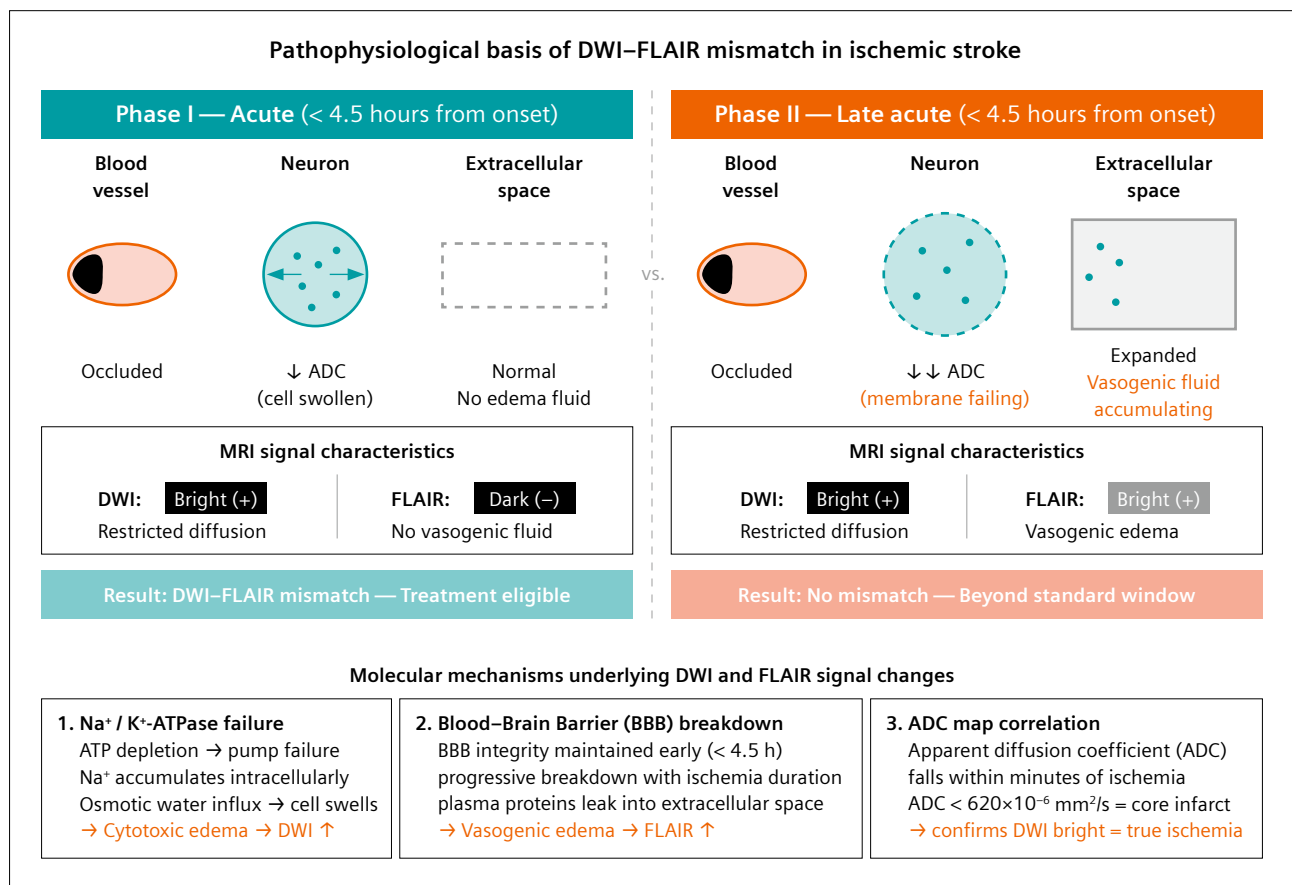
Abbreviations: LKW = last known well; NIHSS = National Institutes of Health Stroke Scale; LVO = large vessel occlusion; EVT = endovascular thrombectomy; IV = intravenous; INR = international normalized ratio

MRI-guided treatment selection

With modern magnetic resonance imaging (MRI), clinicians can employ diffusion-weighted imaging (DWI) and fluid-attenuated inversion recovery (FLAIR) sequences as biological clocks. DWI detects acute ischemic changes within minutes by measuring restricted water diffusion in swollen cells. FLAIR imaging suppresses cerebrospinal fluid signal while highlighting edema, but these changes develop more slowly, typically requiring several hours. When stroke appears bright on DWI but shows no corresponding FLAIR changes, the mismatch indicates recent onset, typically within the therapeutic window [4]. This imaging signature provides the timing information that a clinical history cannot offer.

Clinical evidence and treatment protocols

The landmark WAKE-UP trial (2018) enrolled 503 wake-up stroke patients with DWI-FLAIR mismatch, and randomly assigned them to receive either alteplase or a placebo. The results demonstrated favorable outcomes in 53.3% of the alteplase group, compared to 41.8% in the placebo group, without increased hemorrhagic complications [5]. The EXTEND trial reinforced these findings using perfusion imaging. It showed benefit up to 9 hours from last-known well in selected patients [6]. These studies established that imaging-guided patient selection enables safe, effective thrombolysis regardless of clock time [10].



3 Pathophysiological basis of DWI-FLAIR mismatch in ischemic stroke.

Cellular and molecular mechanisms underlying DWI and FLAIR signal changes in early and late acute ischemic stroke. **Phase I (left panel, < 4.5 hours from onset):** ischemia causes rapid depletion of adenosine triphosphate (ATP), leading to failure of the Na⁺/K⁺-ATPase pump. Sodium accumulates intracellularly, drawing water osmotically into the cell — cytotoxic (intracellular) edema. Restricted intracellular water diffusion generates DWI hyperintensity and a reduced apparent diffusion coefficient (ADC < 620×10⁻⁶ mm²/s). Blood-brain barrier integrity is maintained at this stage, preventing extracellular fluid accumulation; FLAIR signal therefore remains negative. **Phase II (right panel, > 4.5 hours from onset):** progressive ischemic injury disrupts tight junctions of the blood-brain barrier, allowing plasma proteins and fluid to accumulate in the extracellular space (vasogenic edema). This extracellular water accumulation is detected by FLAIR as hyperintensity, eliminating the DWI-FLAIR mismatch. **Column 3 (lower panel):** the ADC map provides quantitative confirmation of true cytotoxic ischemia and assists in differentiation from T2 shine-through artefact.

Abbreviations: ADC = apparent diffusion coefficient; ATP = adenosine triphosphate; BBB = blood-brain barrier; DWI = diffusion-weighted imaging; FLAIR = fluid-attenuated inversion recovery

Contemporary protocols integrate MRI into streamlined workflows. Following rapid neurological assessment and non-contrast CT imaging to exclude hemorrhage [12], patients undergo MRI with DWI and FLAIR sequences. Stroke neurologists and neuroradiologists evaluate mismatch patterns in real time. Positive mismatch without contraindications prompts immediate alteplase administration. Large-vessel occlusions may proceed to mechanical thrombectomy, the window for which has been extended in recent trials to 24 hours for appropriately selected patients [7, 8].

Implementation and technical factors

Successful implementation requires optimized imaging protocols, expert interpretation, and efficient workflows. DWI sequences employ b-values of 1000 s/mm² for optimal sensitivity. Both 1.5T and 3T MRI systems can effectively demonstrate mismatch, although 3T offers superior signal-to-noise ratios. Interpretation demands specialized expertise to distinguish acute changes from chronic white-matter disease and to avoid motion artifacts. Leading centers have achieved door-to-MRI times of less than 20 minutes by using dedicated stroke imaging slots, direct ambulance-to-scanner protocols, and immediate notification of radiologists [13].

Patient selection balances treatment benefit against hemorrhage risk. Inclusion criteria typically require a disabling neurological deficit, a last-known normal time between 4.5 and 24 hours prior, confirmed DWI-FLAIR or perfusion-diffusion mismatch, and absence of hemorrhage. Standard contraindications for thrombolysis remain applicable and include recent surgery, active bleeding, uncontrolled hypertension, and a large established infarction exceeding one-third of the middle cerebral artery territory [9, 14].

Current challenges and future directions

Despite remarkable progress, challenges persist. Advanced MRI capabilities remain concentrated in comprehensive stroke centers, creating geographic disparities. Approximately 10% of patients cannot undergo MRI due to pacemakers, defibrillators, or claustrophobia, although CT perfusion imaging offers an alternative [13]. Imaging protocols, mismatch definitions, and treatment thresholds vary across institutions. Artificial intelligence may eventually enable automated mismatch detection, thereby reducing variability and accelerating decision-making [11].

With approximately 180,000 wake-up strokes occurring annually in the United States alone [1], imaging-guided therapy can potentially benefit tens of thousands of patients who were previously excluded from treatment. Public education remains critical — many people believe that waking up with symptoms means treatment is impossible. Healthcare campaigns must emphasize that immediate evaluation is essential, regardless of symptom onset time. This shifts the paradigm from “time is brain” to “tissue is brain,” with salvageable tissue mattering more than elapsed clock time [9].

Conclusion

Advanced neuroimaging has transformed wake-up strokes from untreatable conditions to intervention opportunities. The shift from rigid time windows to flexible tissue windows guided by sophisticated MRI techniques exemplifies the power of technology in overcoming clinical barriers. Successful intervention requires integrated emergency response, rapid imaging capabilities, expert interpretation, streamlined protocols, and robust monitoring. Innovations in medical technology — including high-field MRI systems, accelerated sequences, automated analysis software, and algorithms — continue to expand access to evidence-based treatment.

For healthcare systems, investing in advanced imaging infrastructure and specialized teams directly translates into improved outcomes. For patients, stroke symptoms require immediate medical attention regardless of onset time. Wake-up strokes no longer automatically exclude patients from treatment. Through continued collaboration among clinicians, researchers, and medical-technology innovators, the 14%–28% of stroke patients whose symptoms begin during sleep can increasingly receive interventions that preserve brain tissue and function.

References

- 1 Mackey J, Kleindorfer D, Sucharew H, Moomaw CJ, Kissela BM, Alwell K, et al. Population-based study of wake-up strokes. *Neurology*. 2011;76(19):1662–7.
- 2 Saver JL. Time is brain—quantified. *Stroke*. 2006;37(1):263–6.
- 3 Hacke W, Kaste M, Bluhmki E, Brozman M, Dávalos A, Guidetti D, et al. Thrombolysis with alteplase 3 to 4.5 hours after acute ischemic stroke. *N Engl J Med*. 2008;359(13):1317–29.
- 4 Thomalla G, Cheng B, Ebinger M, Hao Q, Tourdias T, Wu O, et al. DWI-FLAIR mismatch for the identification of patients with acute ischaemic stroke within 4.5 h of symptom onset (PRE-FLAIR): a multicentre observational study. *Lancet Neurol*. 2011;10(11):978–86.

- 5 Thomalla G, Simonsen CZ, Boutitie F, Andersen G, Berthezene Y, Cheng B, et al. MRI-Guided Thrombolysis for Stroke with Unknown Time of Onset. *N Engl J Med.* 2018;379(7):611–622.
- 6 Ma H, Campbell BCV, Parsons MW, Churilov L, Levi CR, Hsu C, et al. Thrombolysis Guided by Perfusion Imaging up to 9 Hours after Onset of Stroke. *N Engl J Med.* 2019;380(19):1795–1803.
- 7 Nogueira RG, Jadhav AP, Haussen DC, Bonafe A, Budzik RF, Bhuva P, et al. Thrombectomy 6 to 24 Hours after Stroke with a Mismatch between Deficit and Infarct. *N Engl J Med.* 2018;378(1):11–21.
- 8 Albers GW, Marks MP, Kemp S, Christensen S, Tsai JP, Ortega-Gutierrez S, et al. Thrombectomy for Stroke at 6 to 16 Hours with Selection by Perfusion Imaging. *N Engl J Med.* 2018;378(8):708–718.
- 9 Powers WJ, Rabinstein AA, Ackerson T, Adeoye OM, Bambakidis NC, Becker K, et al. Guidelines for the Early Management of Patients With Acute Ischemic Stroke: 2019 Update to the 2018 Guidelines for the Early Management of Acute Ischemic Stroke. *Stroke.* 2019;50(12):e344–e418.
- 10 Campbell BCV, Ma H, Ringleb PA, Parsons MW, Churilov L, Bendszus M, et al. Extending thrombolysis to 4.5–9 h and wake-up stroke using perfusion imaging: a systematic review and meta-analysis of individual patient data. *Lancet.* 2019;394(10193):139–47.
- 11 Yoo AJ, Chaudhry ZA, Nogueira RG, Lev MH, Schaefer PW, Schwamm LH, et al. Infarct volume is a pivotal biomarker after intra-arterial stroke therapy. *Stroke.* 2012;43(5):1323–30.
- 12 Heit JJ, Iv M, Wintermark M. Imaging of Intracranial Hemorrhage. *J Stroke.* 2017;19(1):11–27.
- 13 Bivard A, Levi C, Krishnamurthy V, McElduff P, Miteff F, Spratt NJ, et al. Perfusion computed tomography to assist decision making for stroke thrombolysis. *Brain.* 2015;138(Pt 7):1919–31.
- 14 Hernandez-Perez M, Pérez de la Ossa N, Aleu A, Millán M, Gomis M, Dorado L, et al. Natural history of acute stroke due to occlusion of the middle cerebral artery and intracranial internal carotid artery. *J Neuroimaging.* 2014;24(4):354–8.
- 15 Fiebach JB, Schellinger PD, Gass A, Kucinski T, Siebler M, Villringer A, et al. Stroke magnetic resonance imaging is accurate in hyperacute intracerebral hemorrhage: a multicenter study on the validity of stroke imaging. *Stroke.* 2004;35(2):502–506.
- 16 Albers GW, Thijs VN, Wechsler L, Kemp S, Schlaug G, Skalabrin E, et al. Magnetic resonance imaging profiles predict clinical response to early reperfusion: the diffusion and perfusion imaging evaluation for understanding stroke evolution (DEFUSE) study. *Ann Neurol.* 2006;60(5):508–517.
- 17 Simonsen CZ, Madsen MH, Schmitz ML, Mikkelsen IK, Fisher M, Andersen G. Sensitivity of diffusion- and perfusion-weighted imaging for diagnosing acute ischemic stroke is 97.5%. *Stroke.* 2015;46(1):98–101.



Contact

Aniruddha Deshpande, M.D., DM, DNB, FRCP,
SCE Neurology
Consultant, Department of Care
of the Elderly & Stroke
Altnagelvin Hospital
Glenshane Road
Londonderry, Northern Ireland, BT47 6SB
United Kingdom
aniruddha.deshpande@westerntrust.hscni.net

Stroke Case Study Using a Lower-Field MRI System in a Tier 4 Town of Southern India

Dr. Jyothi Reddy Govindappagari, DNB¹; Dr. Peda Mamtha, M.D.¹; Dr. Bysani Navin Kumar, M.D.²

¹ Jyothi Diagnostics, Madanapalle, India

² Suraksha Hospital, Madanapalle, India

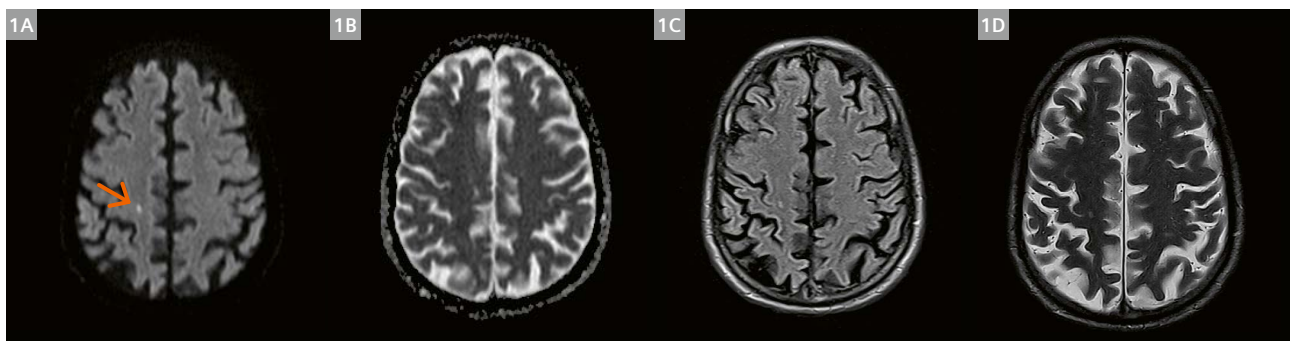
Stroke is a significant global health problem and a major cause of mortality and morbidity around the world [1, 2]. Current estimates indicate that life expectancy in India is over 60 years of age [3, 4]. This has resulted in an increase in age-related, noncommunicable diseases including stroke. Therefore, it is of no surprise that stroke is a leading cause of death and disability in India [5]. As “time is brain” is the core idea for acute stroke management, appropriate cerebral imaging is required to determine the type of stroke, which in turn determines the strategies for managing the patient’s condition.

According to data released by the Indian government for the 2011 census, Madanapalle is an urban agglomeration that is classified as a Class I UA/Town. Madanapalle is located in the Annamayya district of Andhra Pradesh. It is both a town and a municipality with a population of roughly 0.2 million inhabitants. Jyothi Diagnostics is the first diagnostic imaging facility of the town to have a superconductive 0.55T MRI scanner that is capable of advanced MR imaging — including DWI with ADC mapping,

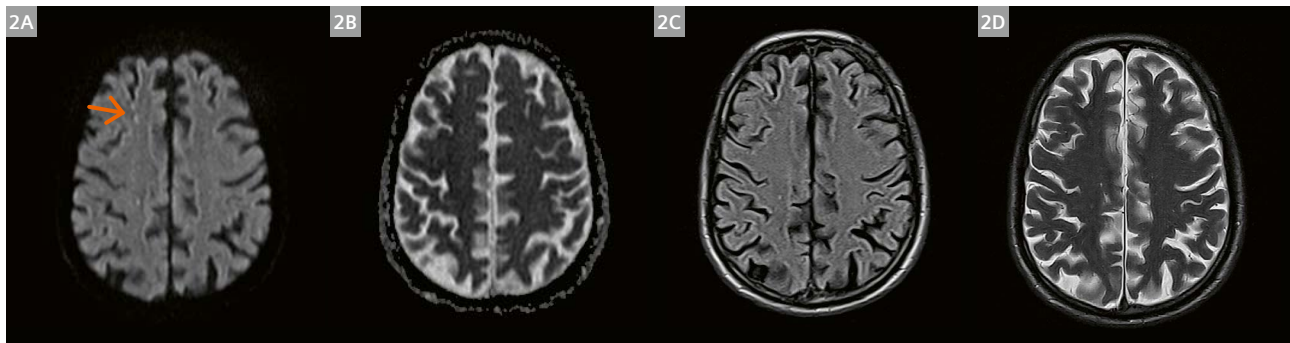
non-contrast MRA, and SWI — to characterize acute stroke. In this paper, we present a case study in which our MAGNETOM Free.Star MRI was able to pick up a tiny infarct efficiently.

Patient history and sequence details

An 80-year-old male patient presented with weakness in his left upper and lower limbs that had lasted for three hours. He underwent an MRI examination immediately. The scan sequences include axial SWI, DWI, T1, T2, T2-FLAIR, coronal T2- and sagittal T1-weighted imaging. A well-defined T2-FLAIR hyperintense lesion is seen in Figure 1 in the white matter of the right high parietal lobe, which is also reflected in a restricted diffusion on DWI. This is suggestive of a tiny T2-FLAIR acute infarct. A few periventricular white matter ischemic changes and age-related cerebral atrophy are also seen. In light of these findings, the patient was put on appropriate treatment, which led to a significant improvement in his symptoms.



1 An 80-year-old male patient with left-side weakness (for three hours). (1A) Restricted diffusion (red arrow) on axial DWI; (1B) corresponding ADC map; (1C) axial T2-weighted FLAIR; and (1D) T2-weighted image showing a hyperintense lesion suggestive of a tiny acute infarct.



2 A different slice from the same acquisition: **(2A)** Two foci showing restricted diffusion (red arrow) on axial DWI; **(2B)** corresponding ADC map; **(2C)** axial T2-weighted FLAIR; and **(2D)** T2-weighted image suggestive of ischemic changes.

Conclusions

The 0.55T MAGNETOM Free.Star scanner was found to be capable of accurately picking up even tiny findings (an acute infarct in this case), which can be critical in improving the patient outcomes. The scanner is also an important tool for providing access to care in small towns across the country.

Acknowledgments

We would like to acknowledge the support that Rishi Awasthi, PhD, of Siemens Healthineers provided for this article.

References

- 1 Feigin VL, Forouzanfar MH, Krishnamurthi R, Mensah GA, Connor M, Bennett DA, et al. Global and regional burden of stroke during 1990-2010: findings from the Global Burden of Disease Study 2010. *Lancet*. 2014;383(9913):245–54. Erratum in: *Lancet*. 2014;383(9913):218.
- 2 GBD 2017 Causes of Death Collaborators. Global, regional, and national age-sex-specific mortality for 282 causes of death in 195 countries and territories, 1980–2017: a systematic analysis for the Global Burden of Disease Study 2017. *Lancet*. 2018;392(10159):1736–1788. Erratum in *Lancet*. 2019;393(10190):e44.
- 3 Horton R, Das P. Indian health: the path from crisis to progress. *Lancet*. 2011;377(9761):181–3.
- 4 Yamunadevi A, Sulaja S. Old age mortality in India — an exploration from life expectancy at age 60. *Int J Asian Social Sci*. 2016;6(12):698–704.
- 5 Directorate General of Health Services: Ministry of Health and Family Welfare. National Programme for Prevention and Control of Cancer, Diabetes, Cardiovascular Diseases and Stroke. July 13, 2019. Accessed September 21, 2020. <https://main.mohfw.gov.in/Major-Programmes/non-communicable-diseases-injury-trauma/Non-Communicable-Disease-III-National-Programme-for-Prevention-and-Control-of-Cancer-Diabetes-Cardiovascular-diseases-and-Stroke-NPCDCS>
- 6 Naik KR. Challenges in delivering stroke care in India. *Ind J Health Sci Biomed Res (KLEU)*. 2016;9(3):245–246.



Contact

Dr. RG Jyothi, DNB
Jyothi Diagnostics
HG55+F73
RRN Colony
Madanapalle,
Andhra Pradesh 517325
India
Tel.: +91 91007 52753

One-Stop Management of Acute Ischemic Stroke Using an Angio-CT System: A Case Report

Michio Fujimoto, M.D., Ph.D.

Department of Neurosurgery, Shin-Yurigaoka General Hospital, Kawasaki, Kanagawa, Japan

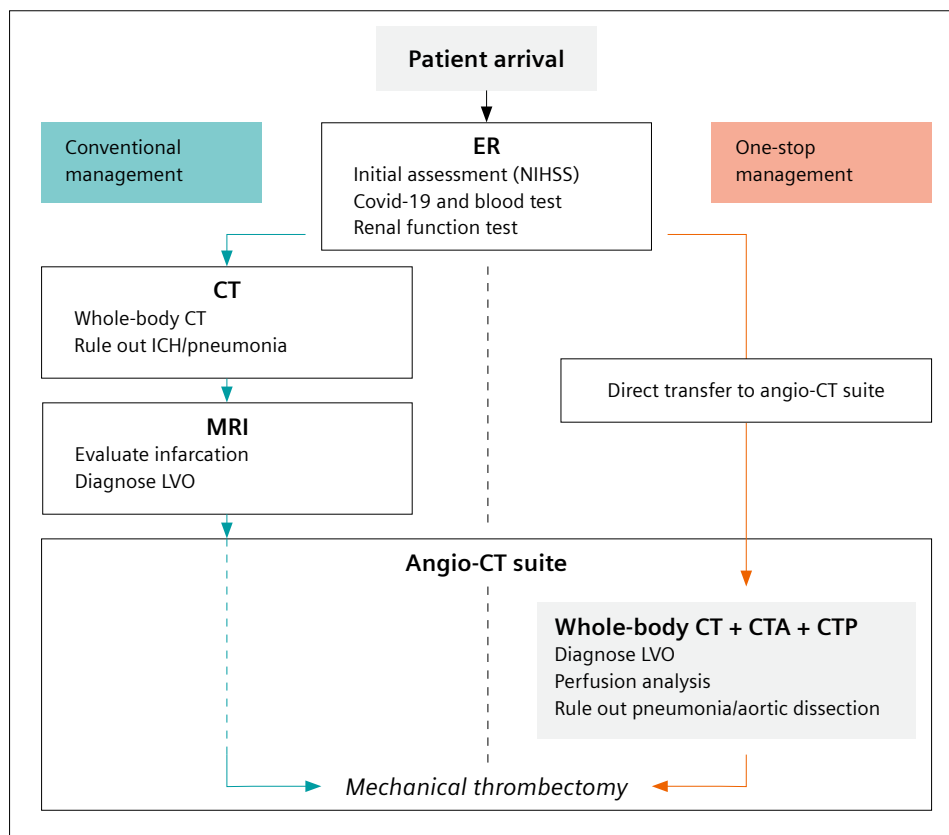
Introduction

The COVID-19 pandemic created significant challenges in managing acute ischemic stroke (AIS), as infection assessments and pneumonia screening — though essential for safety — often delayed diagnosis, treatment initiation, and onset-to-recanalization times [1–4]. To address this, protocols were modified to minimize delays while maintaining safety. Previous reports have emphasized the need to balance effective AIS treatment with infection prevention by integrating imaging, adapting workflows, and reducing transfers [5]. Although the public health emergency has ended, developing new protocols remains important to prepare for future pandemics.

Mechanical thrombectomy (MT) is highly effective for AIS and can be performed up to 24 hours after onset with perfusion imaging [6–12]. However, outcomes remain time-dependent, making rapid recanalization critical. Thus, even during the pandemic, minimizing delays while assessing infection status was essential for achieving optimal outcomes.

The Nexaris Angio-CT system, which combines biplane angiography and CT imaging in one suite, enables one-stop AIS management (Fig. 1), pneumonia assessment, perfusion analysis, and endovascular therapy without patient transfer. We demonstrate its impact on treatment efficiency and patient outcomes [13].

The information in this paper is based on research results that are not commercially available.



1 One-stop management workflow. After initial neurological assessment, the patient was transferred directly to the angio-CT suite, where whole-body CT, CT perfusion (CTP), and CT angiography (CTA) were performed to confirm large vessel occlusion and to exclude aortic dissection or pneumonia.

Angio-CT system

This angio-CT system consists of a biplane angiography unit (Artis zee biplane; Siemens Healthineers, Forchheim, Germany) and a CT scanner, separated by a movable wall. For suspected stroke, the wall was removed and the angiography table rotated 180° for CT use, enabling one-stop diagnosis and treatment (Fig. 2). The suite, located in the emergency department, is also used for trauma, acute myocardial infarction, and other urgent vascular diseases.

CT perfusion and 3D CT angiography

CT scans were performed on a SOMATOM Definition AS with Sliding Gantry (Siemens Healthineers, Forchheim, Germany). After excluding hemorrhage and pneumonia on non-contrast CT, we performed contrast-enhanced perfusion CT and 3D CT angiography. Contrast medium (35 mL, Iopamiron 370; Schering, Osaka, Japan) was injected at 6 mL/s, followed by saline. Imaging parameters were 80 kV, 200 eff mAs, 0.3 s rotation, and a 96 mm

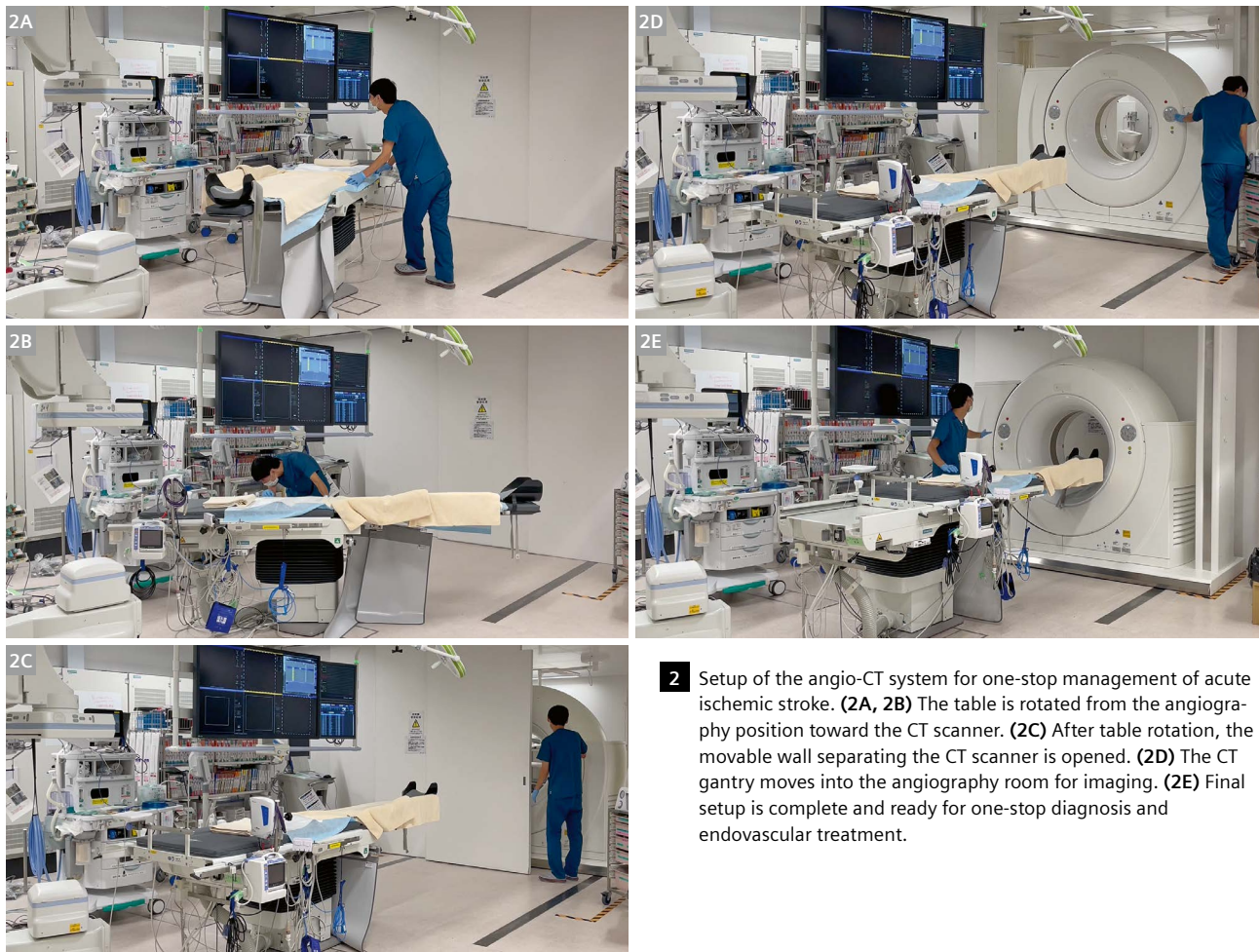
scan range. 3D CT angiography provided vascular information from the aorta to the intracranial arteries and ruled out aortic dissection.

Parameter analysis and treatment decision

All imaging data were transferred to a clinical workstation (syngo.via; Siemens Healthineers, Forchheim, Germany) and analyzed with syngo.CT Neuro Perfusion VB50 to generate multiparameter perfusion maps for ischemic core and penumbra assessment to guide treatment decisions.

Case presentation

A 64-year-old woman with a past medical history of hypertension presented to our hospital with sudden-onset left hemiparesis and dysarthria, 89 minutes after symptom onset. On arrival, her blood pressure was 238/134 mmHg and her cardiac rhythm was sinus. Neurological examination demonstrated left hemiparesis and left conjugate gaze deviation.

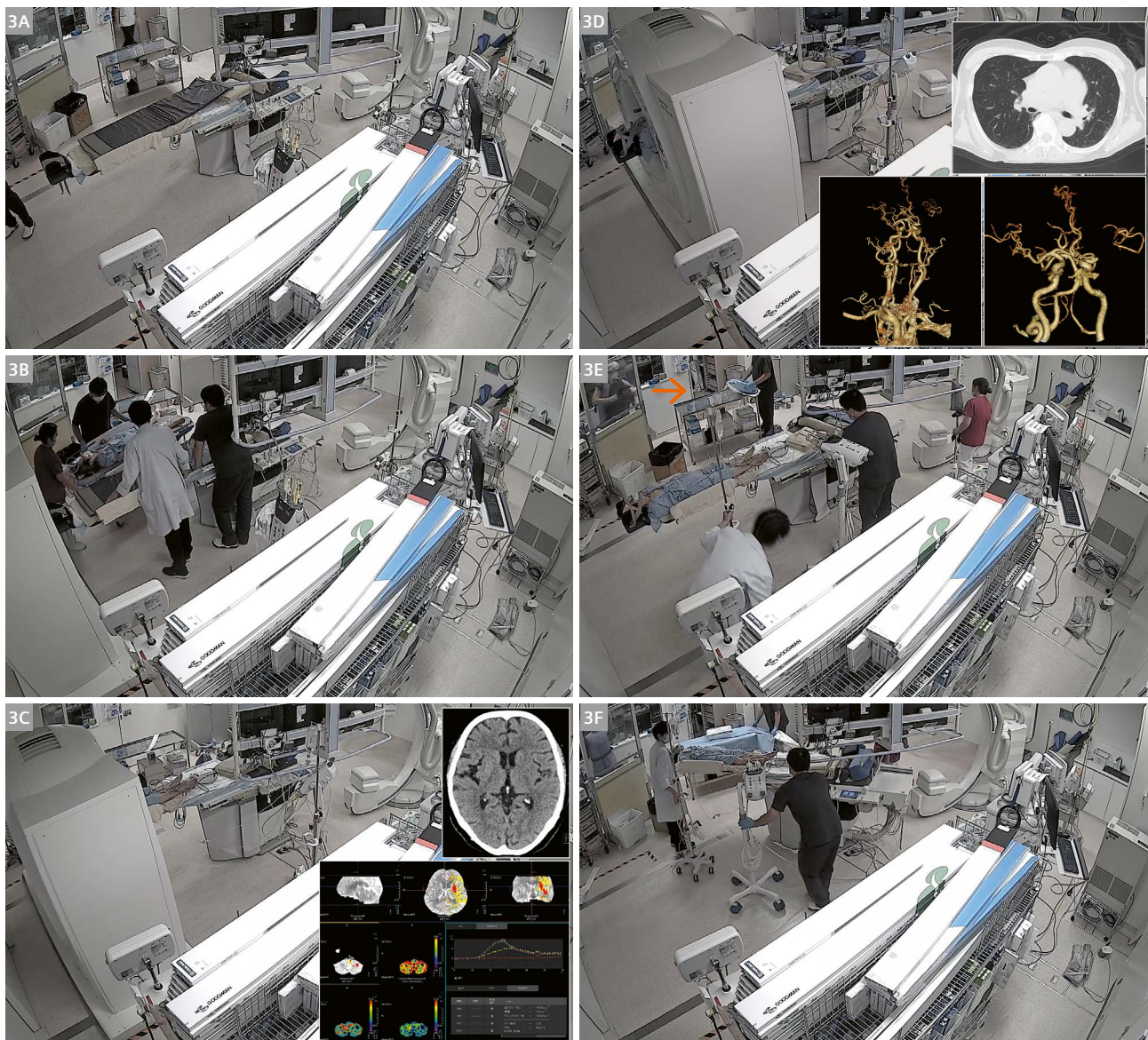


2 Setup of the angio-CT system for one-stop management of acute ischemic stroke. **(2A, 2B)** The table is rotated from the angiography position toward the CT scanner. **(2C)** After table rotation, the movable wall separating the CT scanner is opened. **(2D)** The CT gantry moves into the angiography room for imaging. **(2E)** Final setup is complete and ready for one-stop diagnosis and endovascular treatment.

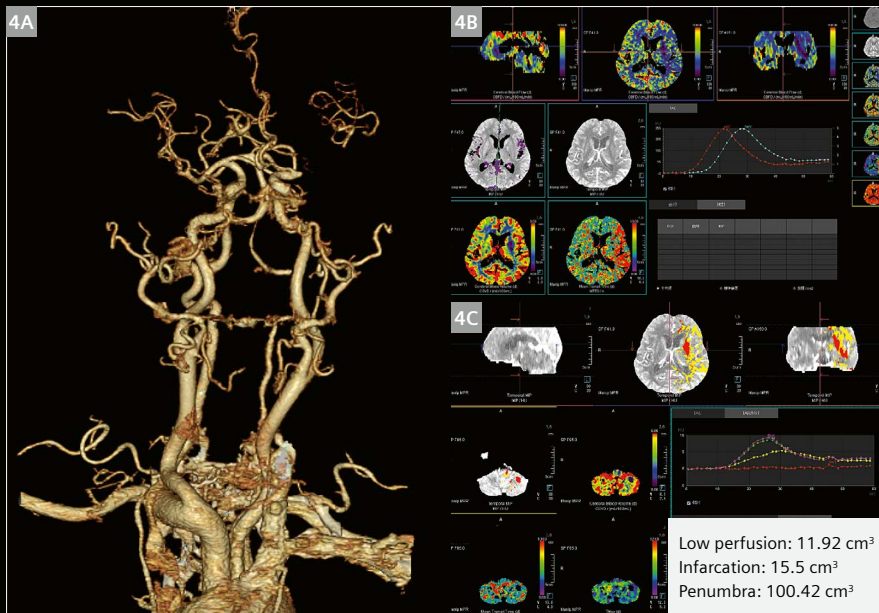
One-stop acute ischemic stroke management

After receiving a transport notification from the emergency medical services (EMS), the radiology technologist pre-rotated the angiography table in preparation for the patient's arrival. The patient arrived at 6:29 a.m. After neurological assessment, laboratory tests, and COVID-19 screening, imaging was initiated at 6:37 a.m. (Fig. 3). The patient was deemed eligible for MT based on initial

imaging, which revealed a left middle cerebral artery (M1) occlusion and a large ischemic penumbra (Fig. 4). Arterial puncture was performed at 6:58 a.m., and endovascular treatment with an aspiration catheter and stent retriever achieved complete recanalization (a Thrombolysis in Cerebral Infarction (TICI) score of 3) with a single pass at 7:32 a.m. (Figs. 5, 6).



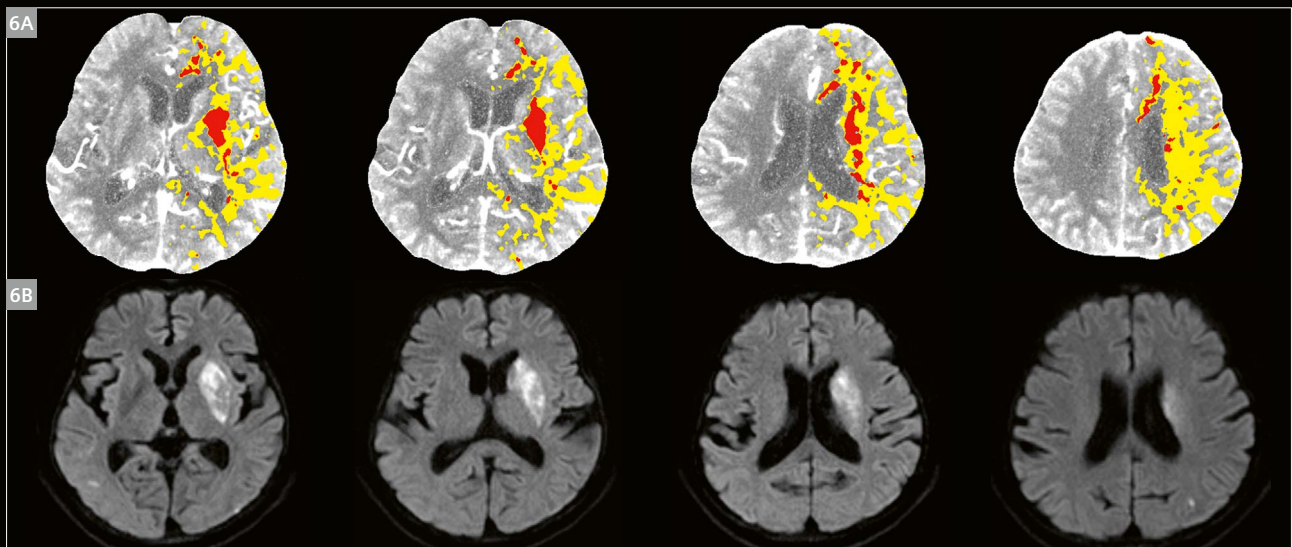
3 Imaging workflow of CT perfusion and 3D CT angiography in the angio-CT suite. **(3A)** The examination table is pre-rotated in preparation for the patient's arrival. **(3B)** The patient is transferred onto the angiography table. **(3C)** An initial non-contrast head CT is performed to rule out hemorrhage, followed by CT perfusion (approximately 1 minute and 20 seconds) to assess cerebral ischemia. **(3D)** A chest CT is performed to check for COVID-19-related pneumonia. While the chest CT is being acquired, the CT perfusion images are reviewed. A 3D CT angiography (approximately 2 minutes) is then performed to evaluate the aortic arch and intracranial vessels. **(3E, 3F)** After imaging, the examination table is rotated back to the treatment position, and preparation for endovascular treatment begins immediately (arrow). The time from patient arrival to the start of treatment preparation is approximately 12 minutes, and arterial puncture is achieved within 30 minutes of arrival.



4 Initial imaging findings in a representative case. 3D CT angiography and CT perfusion demonstrate a left middle cerebral artery (M1) occlusion (4A) with a large ischemic penumbra and a small infarction core (4B, 4C). On the perfusion map (4C), the infarction core is shown in red and the penumbra in yellow. The low-perfusion volume was 115.9 cm³, the infarction core volume was 15.5 cm³, and the penumbra volume was 100.4 cm³. Based on these findings, the patient was deemed eligible for mechanical thrombectomy.



5 Pre- and post-treatment angiographic findings. (5A) Pre-treatment angiogram showing occlusion of the left middle cerebral artery (M1) segment). (5B) Post-treatment angiogram demonstrating complete recanalization of the occluded vessel following mechanical thrombectomy.



6 Comparison of pre-treatment CT perfusion and post-treatment MRI findings. (6A) Pretreatment CT perfusion maps showing the ischemic core and penumbra. (6B) Diffusion-weighted imaging (DWI) obtained on the day after thrombectomy. The infarction area on DWI corresponds closely to the ischemic core identified on CT perfusion before treatment, confirming the accuracy of the perfusion-based assessment.

Post-treatment course

The patient's neurological symptoms improved immediately after the procedure, and she achieved full recovery without residual deficits within a few days. Transthoracic echocardiography revealed a patent foramen ovale, and paradoxical embolism was considered the cause of the stroke.

Discussion

This case highlights the effectiveness of one-stop management using an angio-CT system with biplane angiography for AIS. Integrating angiography and CT in a single suite enabled rapid diagnosis, perfusion assessment, and endovascular therapy without patient transfer, thereby streamlining the workflow in emergency settings.

Compared with flat-panel CT in direct-transfer-to-angio-suite (DTAS) protocols, our multidetector CT system provided higher-quality imaging of intra- and extracranial vessels as well as perfusion data, allowing for more reliable patient selection [14–16]. Perfusion imaging was particularly useful for patients with unknown onset time, consistent with evidence supporting thrombectomy in the extended window. The system was also applicable to patients contraindicated for MRI and did not increase procedural complications.

During the COVID-19 pandemic, angio-CT enabled simultaneous infection screening with whole-body CT, minimizing delays while maintaining safety. However, limitations include the need for contrast, which is unsuitable for some patients, and potential technical inaccuracies due to arrhythmia or arterial stenosis [17–19].

In summary, one-stop management using an angio-CT system provides a safe and efficient workflow that may improve outcomes in AIS and offers additional advantages in high-risk emergency settings.

References

- 1 Nguyen TN, Abdalkader M, Jovin TG, Nogueira RG, Jadhav AP, Haussen DC, et al. Mechanical Thrombectomy in the Era of the COVID-19 Pandemic: Emergency Preparedness for Neuroscience Teams: A Guidance Statement From the Society of Vascular and Interventional Neurology. *Stroke*. 2020;51(6):1896–1901.
- 2 Wang J, Chaudhry SA, Tahsili-Fahadan P, Altaweel LR, Bashir S, Bahiru Z, et al. The impact of COVID-19 on acute ischemic stroke admissions: Analysis from a community-based tertiary care center. *J Stroke Cerebrovasc Dis*. 2020;29(12):105344.
- 3 Nogueira RG, Qureshi MM, Abdalkader M, Ouriques Martins S, Yamagami H, Qiu Z, et al. Global Impact of COVID-19 on Stroke Care and IV Thrombolysis. *Neurology*. 2021;96(23):e2824–e2838.
- 4 World Health Organization. World health statistics 2022: monitoring health for the SDGs, sustainable development goals [Internet]. Geneva: World Health Organization; 2022 May 19 [cited 2025, Nov 03]. Available from: <https://www.who.int/publications/i/item/9789240051157>.
- 5 Pedicelli A, Valente I, Pilato F, Distefano M, Colosimo C. Stroke priorities during COVID-19 outbreak: acting both fast and safe. *J Stroke Cerebrovasc Dis*. 2020;29(8):104922.
- 6 Berkhemer OA, Fransen PSS, Beumer D, van den Berg LA, Lingsma HF, Yoo AJ, et al. A randomized trial of Intraarterial treatment for acute ischemic stroke. *N Engl J Med*. 2015;372(1):11–20.
- 7 Campbell BC, Mitchell PJ, Kleinig TJ, Dewey HM, Churilov L, Yassi N, et al. Endovascular therapy for ischemic stroke with perfusion-imaging selection. *N Engl J Med*. 2015;372(11):1009–18.
- 8 Goyal M, Demchuk AM, Menon BK, Eesa M, Rempel JL, Thornton J, et al. Randomized assessment of rapid endovascular treatment of ischemic stroke. *N Engl J Med*. 2015;372(11):1019–30.
- 9 Jovin TG, Chamorro A, Cobo E, de Miquel MA, Molina CA, Rovira A, et al. Thrombectomy within 8 hours after symptom onset in ischemic stroke. *N Engl J Med*. 2015;372(24):2296–306.
- 10 Saver JL, Goyal M, Bonafe A, Diener H-C, Levy EI, Pereira VM, et al. Stent-retriever thrombectomy after intravenous t-PA vs. t-PA alone in stroke. *N Engl J Med* 2015;372(24):2285–95.
- 11 Nogueira RG, Jadhav AP, Haussen DC, Bonafe A, Budzik RF, Bhuva P, et al. Thrombectomy 6 to 24 Hours after Stroke with a Mismatch between Deficit and Infarct. *N Engl J Med*. 2018;378(1):11–21.
- 12 Albers GW, Marks MP, Kemp S, Christensen S, Tsai JP, Ortega-Gutierrez S, et al. Thrombectomy for Stroke at 6 to 16 Hours with Selection by Perfusion Imaging. *N Engl J Med*. 2018;378(8):708–718.
- 13 Fujimoto M, Nakagami T, Yamazaki R, Okamoto N, Okonogi S, Kiyohira M, et al. Effectiveness of one-stop management using the Angio-CT suite: Impact on acute ischaemic stroke treatment amid and beyond the COVID-19 Era. *J Clin Neurosci*. 2025;138:111368.
- 14 Brehm A, Tsogkas I, Maier IL, Eisenberg HJ, Yang P, Liu JM, et al. One-Stop Management with Perfusion for Transfer Patients with Stroke due to a Large-Vessel Occlusion: Feasibility and Effects on In-Hospital Times. *AJNR Am J Neuroradiol*. 2019;40(8):1330–1334.
- 15 Powers WJ, Rabinstein AA, Ackerson T, Adeoye OM, Bambakidis NC, Becker K, et al. 2018 Guidelines for the Early Management of Patients With Acute Ischemic Stroke: A Guideline for Healthcare Professionals From the American Heart Association/American Stroke Association. *Stroke*. 2018;49(3):e46–e110.
- 16 Powers WJ, Rabinstein AA, Ackerson T, Adeoye OM, Bambakidis NC, Becker K, et al. Guidelines for the Early Management of Patients With Acute Ischemic Stroke: 2019 Update to the 2018 Guidelines for the Early Management of Acute Ischemic Stroke: A Guideline for Healthcare Professionals From the American Heart Association/American Stroke Association. *Stroke*. 2019;50(12):e344–e418.
- 17 Hofmann BB, Donaldson DM, Fischer I, Karadag C, Neyazi M, Piedade GS, et al. Blood Pressure Affects the Early CT Perfusion Imaging in Patients with aSAH Reflecting Early Disturbed Autoregulation. *Neurocrit Care*. 2023;39(1):125–134.
- 18 Garcia-Esperon C, Spratt NJ, Gangadharan S, Miteff F, Bivard A, Lillcrap T, et al. Computed Tomography Perfusion Identifies Patients With Stroke With Impaired Cardiac Function. *Stroke*. 2020;51(2):498–503.
- 19 Mosqueira AJ, Pumar JM, Arias S, Rodríguez-Yáñez M, Blanco Ulla M, Vázquez Herrero F, et al. False ischaemic penumbras in CT perfusion in patients with carotid artery stenosis and changes following angioplasty and stenting. *Neurologia (Engl Ed)*. 2020;35(1):24–31.

Contact

Michio Fujimoto, M.D., Ph.D.
Department of Neurosurgery
Shin-Yurigaoka General Hospital
255 Furusawa, Asao-ku
Kawasaki-shi, Kanagawa 215-0026
Japan
michio1974111@gmail.com



Predictive, personalized, data-driven: A new era in stroke care

Minimizing the time between symptom onset and reperfusion is the essence of acute stroke care. Technological advances are helping to shrink this gap: Innovations like mobile stroke units and direct-to-angio-suite protocols are among the most recent game changers in the field. And with more sophisticated solutions coming down the pipeline, a new era in stroke care is beginning.



Carlos Molina, MD

Director Stroke Unit,
Hospital Universitari Vall d'Hebron &
Head of Stroke Research Group,
Scientific Coordinator of UMBRELLA-IHI,
Vall d'Hebron Institute of Research,
Barcelona, Spain

Carlos Molina, MD, shares his insights on stroke alerts, how stroke care can become proactive, and what tomorrow holds for this dynamic field. We also spoke to him about UMBRELLA, a groundbreaking, collaborative initiative seeking to transform stroke care in Europe.

Dr. Molina, what would you say are the crucial factors in patient care during a stroke alert?

Time is our most precious currency during a stroke alert. Every minute of delay costs millions of neurons, so our top priorities are **rapid, accurate diagnosis** to differentiate between ischemic and hemorrhagic stroke; **streamlined decision-making** with immediate access to imaging, lab data, and medical history; **clear communication** between prehospital and hospital teams to prepare the pathway before the patient arrives; and **availability of reperfusion therapies** with no administrative or procedural bottlenecks. Innovations such as **mobile stroke units** that bring CT imaging, thrombolysis, and stroke expertise directly to the patient, and **direct-to-angio-suite protocols** for eligible large-vessel occlusion cases are both game changers. They allow us to move directly from diagnosis to reperfusion, dramatically improving functional outcomes. In short, stroke alerts need **seamless coordination**, from symptom recognition to restoring blood flow, whether in the ambulance, the emergency room, or the angiography suite.

What innovations can change the patient journey in stroke care, in your opinion?

Three key innovations can transform stroke care from a reactive emergency service to a proactive, continuous care pathway: The first is **integrated digital platforms** that bring together real-time patient data, imaging, and AI-driven decision support to guide clinicians at every stage of care. Then there are **federated learning models** — like those we are developing in UMBRELLA — that allow us to train predictive algorithms on large, diverse datasets without compromising



UMBRELLA

This pioneering project, supported by the Innovative Health Initiative (IHI), is using AI, real-world data, and cutting-edge digital technologies to enhance stroke care in Europe. Over 20 public and private organizations are involved in the project, which is being led by Vall d'Hebron Institute of Research and Siemens Healthineers.

patient privacy. Third, **personalized risk prediction and prevention tools** help us identify high-risk individuals and intervene before a stroke occurs.

You mentioned UMBRELLA: It's been a year since the project launched. What have been the most significant milestones and lessons so far?

In just one year, Umbrella has achieved what usually takes several years in large-scale collaborative projects. We've defined the foundations for a Stroke Common Data Model that will allow us to speak a common language across European stroke centers. This involved harmonizing data protocols and procedures for retrospective analyses and prospective studies. We're also aligning IT teams and data scientists with the clinical frontlines. And we're integrating digital solutions for diagnosis, treatment, management, and prevention into most of our centers. A key learning is that technology alone is not enough — success also depends on building trust and a shared vision among clinicians, engineers, and data scientists. Thanks to the enthusiasm and commitment of all our partners, UMBRELLA is more than a research project; it's a movement for transforming stroke care in Europe.

What do you think the future holds for stroke care?

I believe the future of stroke care is **predictive, personalized, and fully data driven**. AI tools will be able to forecast a patient's stroke risk days or even weeks in advance, facilitating preventive measures. Acute treatment will be faster, more precise, and tailored to the patient's biological profile. Rehabilitation will start earlier and be guided by neuroimaging and digital biomarkers to maximize recovery. And all of this will happen in a connected ecosystem where hospital care, primary care, and home-based monitoring form a single continuum. This year's World Stroke Congress is taking place in your home city of Barcelona. You are part of the organizing committee.

This year's World Stroke Congress is taking place in your home city of Barcelona. You are part of the organizing committee. What do you expect from the congress? What's your take-home message for the neuro community?

As local congress chairman, hosting the WSC in Barcelona is both an honor and an opportunity. I expect it to be a vibrant forum where cutting-edge science meets clinical practice, and where we foster lasting collaborations. I'm particularly proud that we've received a record number of scientific abstracts, for both the main sessions and the late-breaking sessions. This shows the vitality and innovation in our global stroke community. My take-home message to the neuro community is simple: We are entering a new era where data, technology, and human expertise converge to change the natural history of stroke. For this transformation to happen, we must work together across disciplines, countries, and sectors.

Thank you very much for talking to us, Dr. Molina.

Find out more at
[siemens-healthineers.com/stroke](https://www.siemens-healthineers.com/stroke)

The statements by customers of Siemens Healthineers described herein are based on results that were achieved in the customer's unique setting. Because there is no "typical" hospital or laboratory and many variables exist (e.g., hospital size, samples mix, case mix, level of IT and/or automation adoption) there can be no guarantee that other customers will achieve the same results.

The Distal Occlusion Tracker (DOT) Sign: A New Imaging Finding on Non-contrast DynaCT for the Detection of Remaining Vessel Occlusions After Mechanical Thrombectomy

Johannes Kaesmacher, Adnan Mujanovic, Daniel Windecker, Petra Cimflova, Sara Pilgram-Pastor, Lorenz Grunder, Philippe Breiding, Eike Piechowiak, Jan Gralla, Tomas Dobrocky

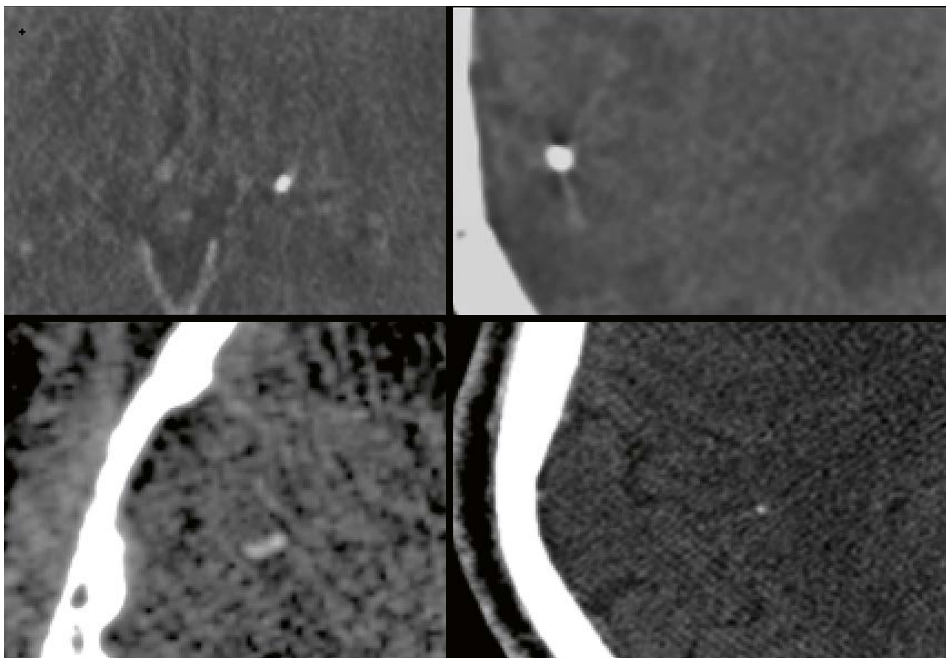
University Hospital Bern, Inselspital, University of Bern, Switzerland

Endovascular therapy (EVT) has revolutionized the treatment of acute ischemic stroke, yet achieving complete reperfusion remains a challenge. A significant proportion of patients may experience incomplete reperfusion due to residual distal vessel occlusions (DVOs). These smaller occlusions can be particularly difficult to identify using traditional two-dimensional digital subtraction angiography (DSA) alone, often leading to an overestimation of reperfusion success by the treating surgeon. Addressing this diagnostic gap is crucial, as incomplete reperfusion is strongly linked to poorer patient outcomes, and recent trials on intra-arterial thrombolysis suggest that patients with residual vessel occlusion benefit the most. Hence, appropriate selection seems warranted in the future [1].

In this context, the distal occlusion tracker (DOT) sign has emerged as a promising imaging marker to aid in the process of DVO detection after EVT [4]. The DOT sign can be evaluated on a standard non-contrast DynaCT, which is a technique that is available on multiple angiography systems, can be acquired rapidly, and does not require specific post-processing or contrast media injection.

Method

The conventional DynaCT is a planar rotation (planar: focal spot stays within a plane) over 200° with an angular increment of 0.4°, adding up to 496 projection images. The scan is from right anterior oblique (RAO) 100° to left



1 DOT signs in different shapes, sizes, and densities along the course of the distal intracranial arteries.

anterior oblique (LAO) 100°, and the craniocaudal angle stays at zero. In the new protocol syngo DynaCT Sine Spin there is slight cranial/caudal modulation, like a sine curve, with an amplitude of 10°, and the scan is over 220° from RAO 110° to LAO 110°. The scan starts at -110°/0°, goes to -55°/10°, then to 0°/0° and 55°/-10°, and finally to 110°/0°. The angular increment is 0.4°, adding up to 546 projections. Within the 7sDCT Sine Spin acquisition protocol, 4 × 4 binning and “HU smooth” are used.

The DOT sign

The DOT sign manifests as dot-like, round, or tubular hyperdensities along the course of the distal intracranial arteries (Fig. 1), often reflecting contrast media stagnation proximal to a residual occlusion, or possibly iodine-stained fragmented thromboembolism [3]. The DOT sign may be very dense or only slightly hyperdense, depending on the amount of contrast media stagnating before or penetrating the thrombus. In addition, the time from the last intra-arterial injection to acquisition of the DynaCT may play a role in the depiction of the DOT sign. In order to prevent false-positive ratings, pre-interventional scans should be screened for preexisting parenchymal or subarachnoid calcification, which could mimic the DOT sign.

Diagnostic performance in detecting residual distal vessel occlusion

The prevalence of the DOT sign on immediate post-procedural DynaCT varies across studies, appearing in around 40%–50% of the cases [3, 4]. The DOT sign has demonstrated valuable diagnostic capabilities in identifying residual DVOs. Studies indicate that it possesses high specificity, typically above 90%, meaning that if the DOT sign is present, it is highly likely that a residual occlusion exists and the reperfusion is very unlikely to be complete. However, its sensitivity for detecting residual DVO seems more moderate, often around 60%–80%, suggesting that while it is a strong indicator when present, it may not capture all existing occlusions [3, 4]. This variability in sensitivity might be attributed to factors such as clot composition or location, which could hinder contrast penetration into the clot or contrast stagnation proximal to the occlusion (e.g., in cases where one branch of a bifurcation is occluded without a proximal vessel stump, there is lack of contrast stagnation) [3]. In addition, this variation might be due to differing definitions of the DOT sign, study designs, imaging quality, or slice thickness. Despite these differences, adding flat-panel CT (FPCT) findings, including the DOT sign, to conventional DSA significantly increases the overall diagnostic accuracy for detecting residual DVOs.

Correlation with reperfusion success

The presence of a DOT sign correlates strongly with incomplete reperfusion. This is particularly significant in clinical practice, as surgeons frequently overestimate the degree of reperfusion when relying solely on 2D DSA, often in more than 25% of the treated cases. The integration of FPCT into reperfusion grading substantially reduces this overestimation, with false complete reperfusion gradings falling to around < 5% [3, 4]. For instance, in cases where surgeons initially graded complete reperfusion based on DSA alone, the presence of a DOT sign on FPCT led to a re-evaluation and often a downgrading of the thrombolysis in cerebral infarction (TICI) score, effectively preventing the misgrading of the final perfusion status.

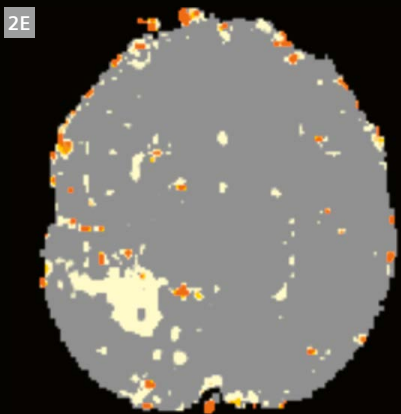
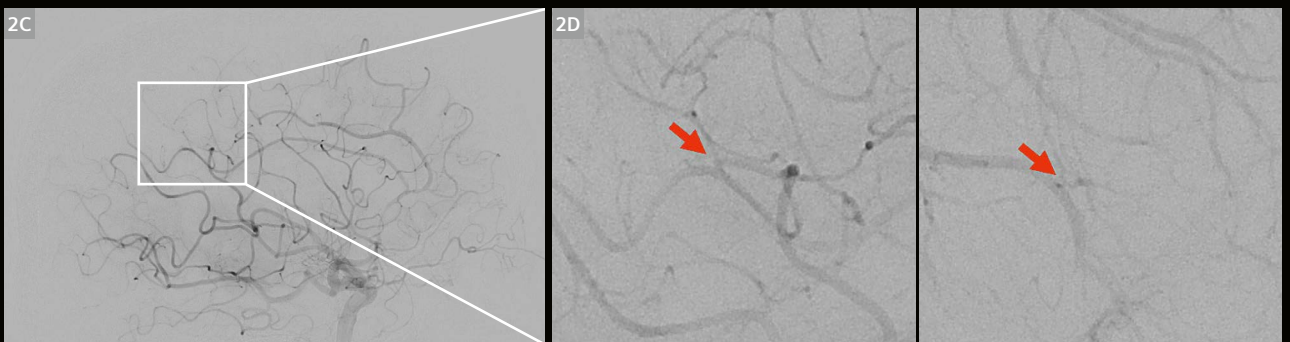
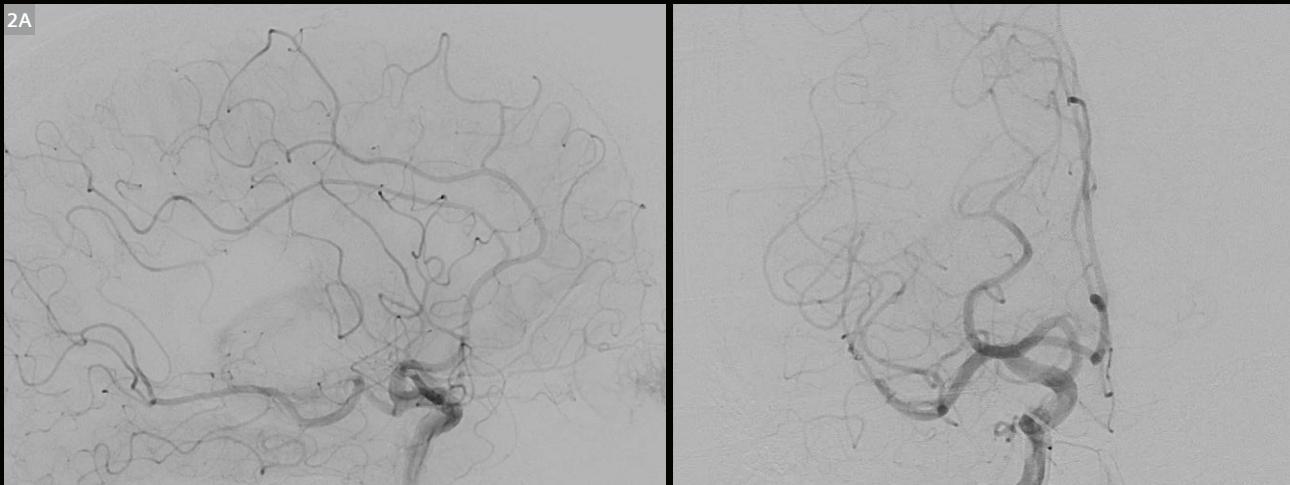
Beyond simply detecting missed occlusions, the DOT sign on FPCT provides crucial additional information. It offers a more intuitive 3D anatomical localization of clots, which is a challenge with 2D DSA images alone, due to issues like over-projection and motion sensitivity. This enhanced spatial understanding can aid surgeons in more accurately assessing the proximity or distal extent of an occlusion and its potential involvement in eloquent brain areas.

Correlation with persistent hypoperfusion and clinical outcome

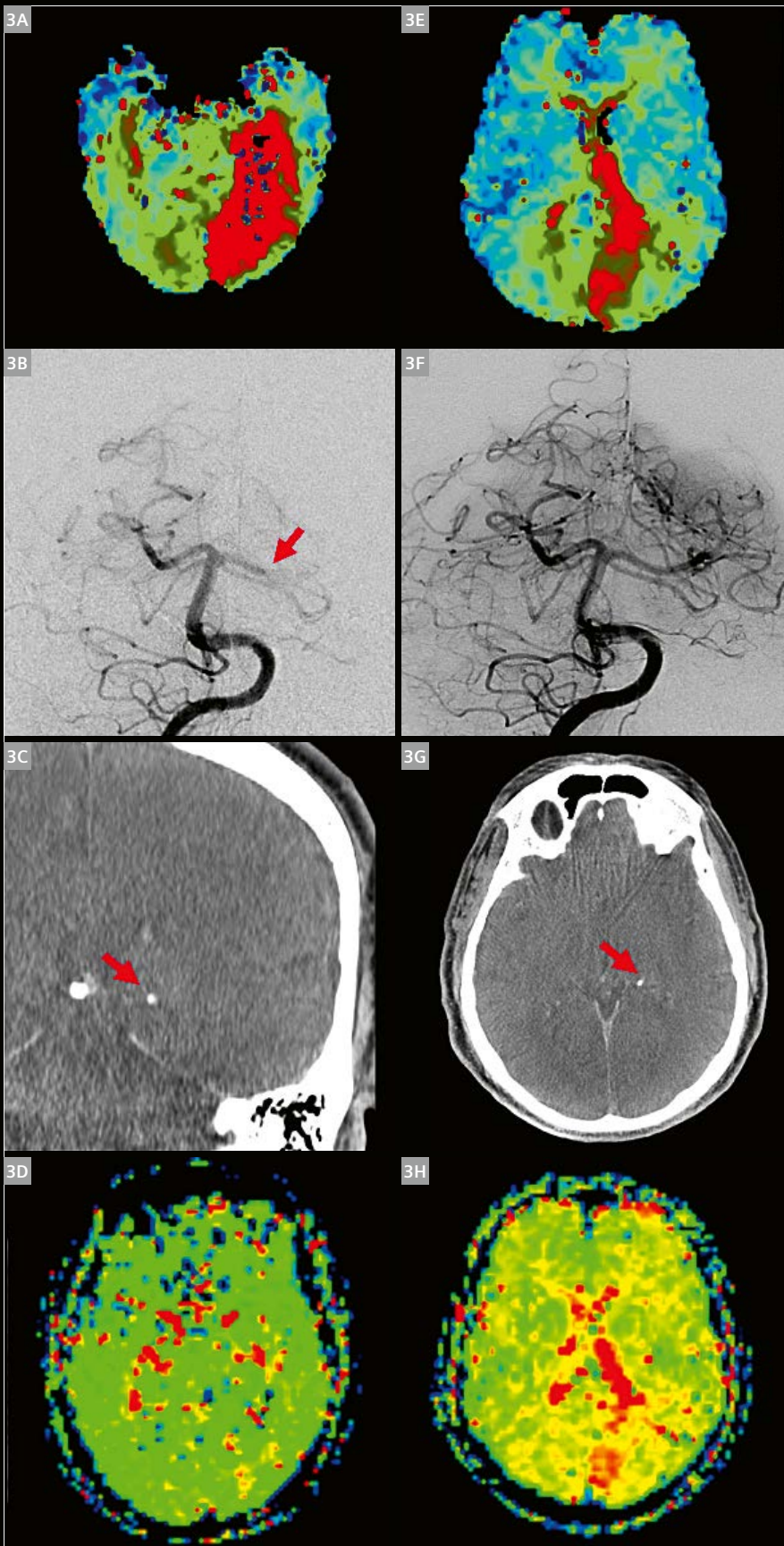
The DOT sign demonstrates clinical significance as it is associated with persistent hypoperfusion and worse long-term outcomes. Studies on 24-hour dual-energy (DE) CT imaging show that around 30% of patients still exhibit a DOT sign at 24 hours [5]. Even more clinically relevant, the presence of a DOT sign on immediate post-interventional FPCT is strongly associated with persistent hypoperfusion on 24-hour follow-up perfusion imaging [6]. This association remains consistent across all incomplete reperfusion grades. This suggests that patients with a DOT sign are more likely to have ongoing tissue ischemia despite initial reperfusion efforts [6].

The presence of a DOT sign is also an independent predictor of worse clinical outcomes, including acute symptom evolution (e.g., higher NIH Stroke Scale scores at 24 hours) and a lower likelihood of good functional status at three months [3, 5]. This adverse impact on outcome is observed independently of other factors, such as the degree of successful reperfusion, age, or baseline neurological severity.

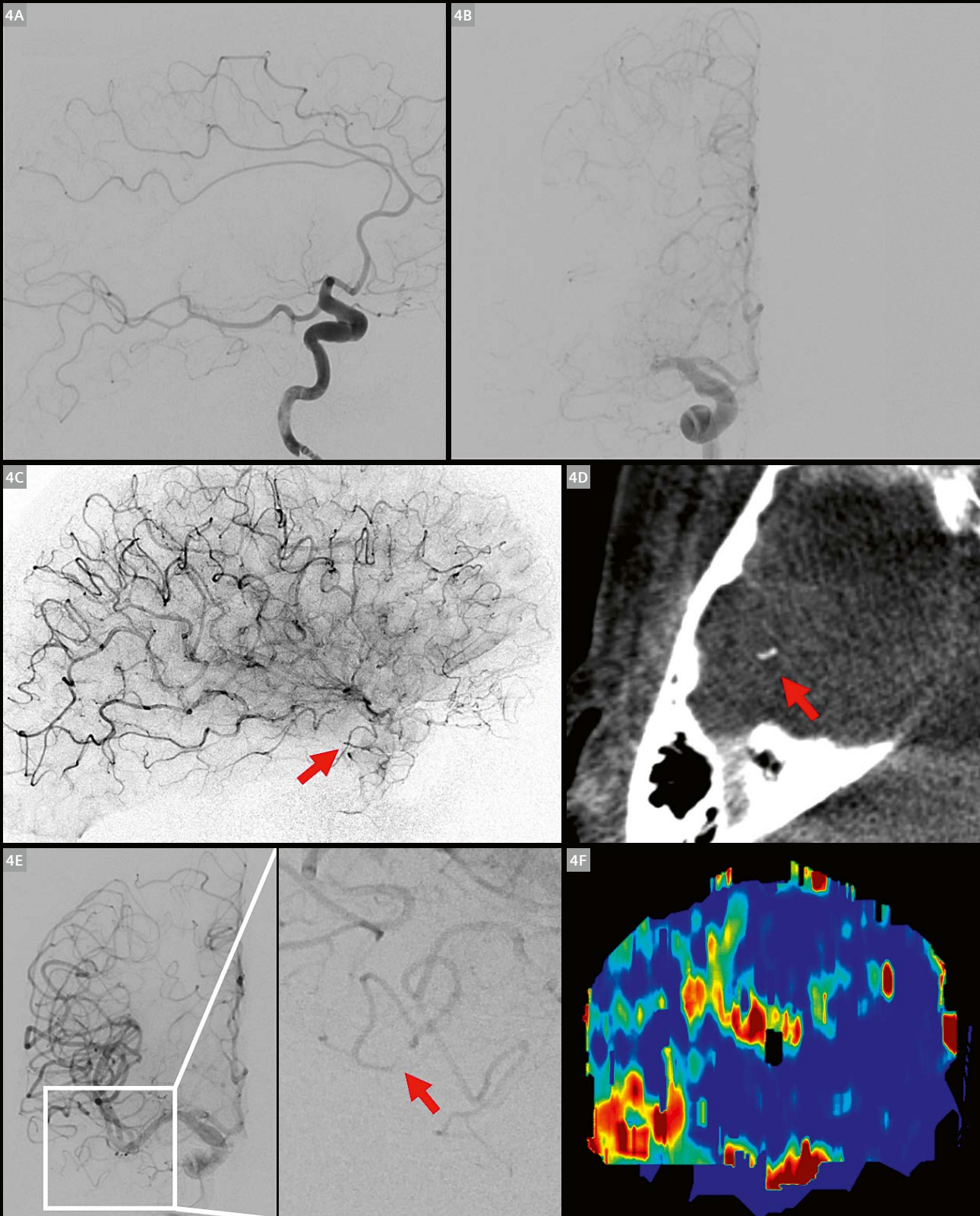
Therefore, the DOT sign is as an important indicator for the treating surgeon, suggesting a higher likelihood of persistent hypoperfusion and a poorer prognosis. This could help identify a subgroup of patients with incomplete reperfusion who may benefit from additional reperfusion attempts or closer monitoring.



2 A patient in his 70s presenting with an M2 occlusion (2A) treated with mechanical thrombectomy. The surgeon initially rated the reperfusion success as TIC1 3 on 2D DSA images (2C). However, a non-contrast DynaCT demonstrated a very dense DOT sign (2B, orange arrow), which retrospectively corresponded to a residual M4 occlusion post-centrally (2D, orange arrow). At 24 hours, this occlusion persisted, as evidenced by a wedge-shaped deficit on MR perfusion imaging (Tmax) (2E) within the region corresponding to the post-interventional capillary phase deficit, as well as the location of the DOT sign.



3 A patient in his 80s was treated for a P2 occlusion (**3B**, red arrow) with a large perfusion deficit involving the visual cortex (**3A**, **3E**). After mechanical thrombectomy, a P3 occlusion (**3F**) persisted that was supplying the superior posterior cerebral artery territory. Non-contrast CT shows a DOT sign along the course of the posterior cerebral artery, shortly before entering the quadrigeminal cistern (**3C**, **3G**). On 24-hour MR perfusion imaging (**3D**, **3H**), most of the initial hypoperfusion is normalized, but a perfusion delay persisted in the upper posterior cerebral artery territory, corresponding to the residual occlusion after mechanical thrombectomy, as evidenced by the DOT sign.



4 A patient in his 80s was treated for a right M1 occlusion (4A, 4B). After mechanical thrombectomy, the reperfusion success was rated as TIC1 3 (4C). On DynaCT, a small DOT sign (4D) could be detected, which correlated well with a residual temporal M4 branch occlusion (4E). Immediate post-interventional DynaCT perfusion imaging (4F) showed a hypoperfusion matching the territory of this small residual occlusion. This shows the correlation of DSA, DOT sign, and post-interventional flat-panel perfusion imaging.

Conclusion

The distal occlusion tracker (DOT) sign, an easily identifiable imaging finding on post-procedural FPCT, is a valuable adjunct to conventional DSA in the detection of residual distal vessel occlusions after endovascular therapy. It significantly improves the diagnostic accuracy of reperfusion assessment and helps mitigate the common overestimation of reperfusion success by surgeons. Furthermore, the presence of a DOT sign correlates strongly with persistent hypoperfusion and predicts poorer clinical outcomes, serving as an early indicator of ongoing tissue ischemia. By integrating assessment of the DOT sign into the acute workflow, neurointerventionalists can gain a more comprehensive understanding of reperfusion quality and potentially tailor post-procedural management strategies to improve patient outcomes.

References

- 1 Palaiodimou L, Papageorgiou NM, Turc G, Gory B, Theodorou A, Bakola E, et al. The Added Benefit of Intra-Arterial Thrombolysis After Successful Recanalization by Endovascular Treatment: A Systematic Review and Meta-Analysis of Randomized-Controlled Clinical Trials. *Eur J Neurol*. 2025;32(7):e70270.
- 2 Hsu CC-T, Watkins T, Kato K, Fomin I, Hapugoda S, Cheng J, et al. Iodine-stained fragmented thromboembolism. *Neuroradiol J*. 2019;32(6):445–451.
- 3 Mujanovic A, Windecker D, Serrallach BL, Kurmann CC, Almiri W, Meinel TR, et al. Connecting the DOTs: a novel imaging sign on flat-panel detector CT indicating distal vessel occlusions after thrombectomy. *J Neurointerv Surg*. 2024;17(e1):e47–e54.
- 4 Baik SH, Jung C, Kim JY, Kim DY, Kim N, Kim BJ, et al. Adjunctive Flat Panel CT-Based Reperfusion Grading after Endovascular Therapy: Enhanced Detection of Residual Distal Vessel Occlusion. *AJNR Am J Neuroradiol*. 2025. Epub ahead of print.
- 5 Francesco D. Distal Occlusion Tracker Sign in the 24 Hours Dual-Energy CT control after Thrombectomy: Significance and association with clinical outcome. In review.
- 6 Mujanovic A, Windecker D, Serrallach B, Kurmann CC, Rohner R, Auer E, et al. DOT sign indicates persistent hypoperfusion and poor outcome in patients with incomplete reperfusion following thrombectomy. *J Neurointerv Surg*. 2025;17(11):1242-1248.



Contact

Professor Dr. Johannes Kaesmacher, M.D., Ph.D.
 University Institute of Diagnostic and
 Interventional Neuroradiology
 University Hospital Bern, Inselspital
 Freiburgstrasse 18
 CH-3010 Bern
 Switzerland
johannes.kaesmacher@insel.ch

Effect of Copper Filtration on Radiation Dose in Cerebral 3D Rotational Angiography During Endovascular Aneurysm Treatment

Niclas Schmitt¹, Andreas Berting², Christian Herweh¹, Tim Hilgenfeld¹, Fabian Preisner¹, Lena Wucherpfennig³, Martin Bendszus¹, Dominik F Vollherbst^{*1}, Markus A Möhlenbruch^{*1}

*These authors share senior authorship.

¹ Department of Neuroradiology, Heidelberg University Hospital, Heidelberg, Germany

² Siemens Healthineers, Clinical Segment Interventional Radiology, Neurovascular, Forchheim, Germany

³ Department of Diagnostic and Interventional Radiology, Heidelberg University Hospital, Heidelberg, Germany

Background

Cerebral angiography remains the gold standard for the diagnostic and therapeutic management of cerebrovascular pathologies, particularly intracranial aneurysms [1, 2]. Among the available imaging techniques, three-dimensional rotational angiography (3D-RA) has become an indispensable tool for the precise visualization of complex vascular anatomy. Owing to its high spatial resolution and ability to generate volumetric reconstructions, 3D-RA enables a superior assessment of aneurysm morphology, branch configuration, and parent-vessel relationships compared with conventional two-dimensional digital subtraction angiography (2D-DSA) [3, 4]. With the growing use of non-invasive imaging modalities such as CT and MR angiography, small and incidental aneurysms are detected more frequently, further emphasizing the clinical value of 3D-RA for treatment planning and individualized risk stratification [1, 5–7]. However, despite its diagnostic advantages, 3D-RA contributes a relevant share of cumulative radiation exposure in neurointerventional procedures. Radiosensitive structures such as the eye lens are particularly at risk, as even relatively low doses may contribute to cataract formation [8–10]. In line with the ALARA principle (“as low as reasonably achievable”), dose optimization and reduction have therefore become central aims in neurointerventional imaging. Several technical innovations and workflow adaptations have been proposed, yet practical and universally applicable strategies remain limited [10–16]. Physical beam filtration offers a particularly efficient and technically simple means of reducing patient dose without altering acquisition parameters or

reconstruction settings. The present study evaluates such an approach, replacing the standard aluminum (Al) filter with a thinner 0.1 mm copper (Cu) filter in cerebral 3D-RA to significantly reduce radiation dose while preserving diagnostic image quality.

General acquisition parameters		
Acquisition time	4 s	
Projections	133 projections	
Angular increment	1.50°	
Coverage	200° (starting at 100° RAO and ending at 100° LAO)	
Filter-specific acquisition parameters		
	Al filter	Cu filter
Mean pulse width	7.06 ms	7.46 ms
Mean tube voltage	74.9 kV	75.5 kV
Mean tube current	425 mA	424 mA

Table 1: Overview of the general and filter-specific imaging parameters using the “4s DSA Head Micro” protocol on the ARTIS icono angiography system.

Al: aluminum; Cu: copper; kV: kilovolts; LAO: left anterior oblique; mA: milliamperes; ms: milliseconds; RAO: right anterior oblique; s: seconds

The presented concepts and results are based on research and are not commercially available.

Technique and methods

To explore the potential of physical beam filtration for dose optimization, cerebral 3D-RA was performed on an ARTIS icono biplane angiography system (Siemens Healthineers, Forchheim, Germany) equipped with a modified X-ray filtration setup. In this configuration, the conventional 0.8 mm Al filter positioned in the primary beam path was replaced by a 0.1 mm Cu filter, while all mandatory Al prefilters within the tube housing and detector assembly remained unchanged. This adjustment represents a purely hardware-based modification that can be integrated without altering system software or acquisition presets. The investigation included 40 consecutive patients who received endovascular treatment of unruptured anterior circulation aneurysms under general anesthesia. All examinations followed an identical standardized protocol to ensure comparability. Using the “4s DSA Head Micro” mode, each acquisition covered a 200° rotational range with 133 projections at 1.5° increments, generating both a native and a contrast-enhanced dataset. Subtracted 3D volumes were automatically reconstructed on the system workstation to visualize vascular anatomy in high spatial resolution. Radiation exposure metrics — including entrance

skin dose (mGy) and dose area product $\text{Gy} \cdot \text{cm}^2$ — were recorded directly from the angiography system for both the standard Al-filtered and the Cu-filtered configurations. Quantitative image quality was evaluated by calculating the contrast-to-noise ratio (CNR) within standardized regions of interest in the middle cerebral artery and background tissue. In addition, two blinded neuroradiologists with extensive experience in cerebral angiography independently performed qualitative assessments on a five-point diagnostic scale ranging from “fail” to “excellent.”

Results

The substitution of the 0.8 mm Al filter with a 0.1 mm Cu filter resulted in a substantial reduction in radiation dose without any loss of image quality. Considering the cumulative exposure from both the native and contrast-enhanced acquisitions, the mean entrance skin dose decreased from 110.63 ± 10.75 mGy in the Al group to 68.70 ± 6.03 mGy in the Cu group, corresponding to a relative reduction of 38% ($p < 0.001$). A similar trend was observed for the dose area product, which declined from 6.26 ± 1.57 $\text{Gy} \cdot \text{cm}^2$ in the Al group to 3.35 ± 0.67 $\text{Gy} \cdot \text{cm}^2$ in the Cu group,



1 3D rotational angiography (RA) datasets acquired with the 3D neurovascular native/contrast reconstruction (1A, 1B) alongside their volume-rendered 3D models acquired with the 3D neurovascular subtraction dataset (1C, 1D). The standard aluminum filter was applied to the images on the left (1A and 1C), while the copper filter was used for those on the right (1B and 1D).

representing a reduction of 46% ($p < 0.001$). Despite these pronounced dose savings, quantitative analysis confirmed that vessel contrast remained unchanged between both configurations. In the 3D neurovascular native/contrast dataset, the mean CNR was 20.72 ± 1.82 for the Al group and 20.66 ± 1.54 for the Cu group ($p = 0.93$). Similarly, in the 3D neurovascular subtraction dataset, mean CNR values were 21.40 ± 1.17 and 20.92 ± 1.24 , respectively ($p = 0.18$). Qualitative image analysis on the five-point scale likewise revealed no difference between the two filter setups. The mean scores were 4.55 ± 0.54 (Al group)

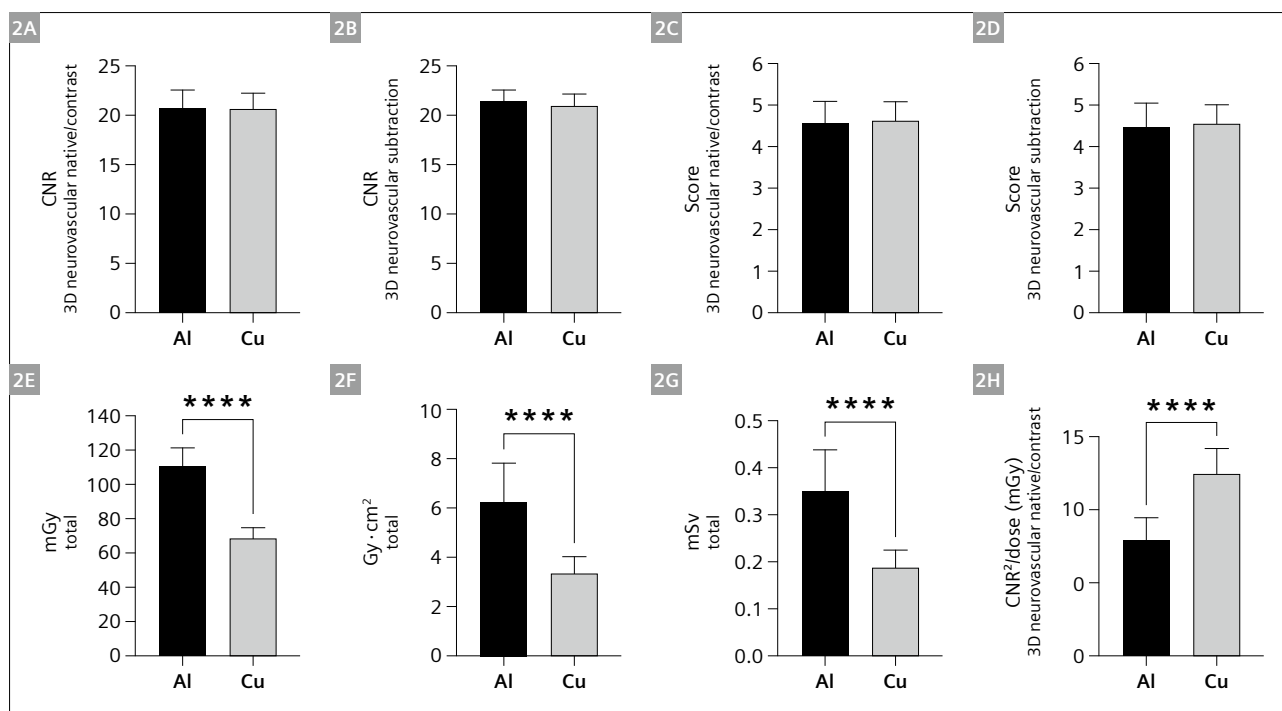
versus 4.63 ± 0.46 (Cu group; $p = 0.75$) for the 3D neurovascular native/contrast images, and 4.48 ± 0.57 versus 4.55 ± 0.46 ($p = 0.86$) for the subtraction datasets. Both groups consistently achieved ratings corresponding to “good” to “excellent” diagnostic image quality, with strong inter-reader agreement. Importantly, dose efficiency (CNR^2/dose) improved markedly when using the Cu filter, increasing from 7.9 ± 1.6 to 12.5 ± 1.7 ($p < 0.001$). This finding demonstrates that radiation energy was converted more effectively into diagnostically useful image information.

(A) Image quality			
	Al filter	Cu filter	p-value
Quantitative CNR <i>3D neurovascular native/contrast</i>	20.72 ± 1.82	20.66 ± 1.54	$p = 0.93$
Quantitative CNR <i>3D neurovascular subtraction</i>	21.40 ± 1.17	20.92 ± 1.24	$p = 0.18$
Qualitative score <i>3D neurovascular native/contrast</i>	4.55 ± 0.54	4.63 ± 0.46	$p = 0.75$
Qualitative score <i>3D neurovascular subtraction</i>	4.48 ± 0.57	4.55 ± 0.46	$p = 0.86$
(B) Radiation dose			
	Al filter	Cu filter	p-value
mGy <i>3D neurovascular native</i>	55.55 ± 5.41	34.21 ± 3.51	
mGy <i>3D neurovascular native/contrast</i>	55.09 ± 5.35	34.49 ± 2.89	
mGy <i>total</i>	110.63 ± 10.75	68.70 ± 6.03	$p < 0.001$
Gy · cm² <i>3D neurovascular native</i>	3.14 ± 0.79	1.68 ± 0.33	
Gy · cm² <i>3D neurovascular native/contrast</i>	3.12 ± 0.79	1.67 ± 0.33	
Gy · cm² <i>total</i>	6.26 ± 1.57	3.35 ± 0.67	$p < 0.001$
mSv <i>total</i>	0.35 ± 0.09	0.19 ± 0.04	$p < 0.001$
CNR²/dose (mGy) <i>3D neurovascular native/contrast</i>	7.91 ± 1.55	12.47 ± 1.72	$p < 0.001$

Table 2: Results of the statistical analyses

Summary of the statistical results for image quality (A) and radiation dose (B). Dose values in mGy represent the entrance surface dose as calculated by the angiography system at the patient entrance reference point (PERP). Both the entrance dose (mGy) and the dose-area product ($\text{Gy} \cdot \text{cm}^2$) are reported separately for the native acquisitions (3D neurovascular native), the contrast-enhanced acquisitions (3D neurovascular native/contrast), and the total of both. In addition, the effective radiation dose in mSv is provided for the total acquisitions and the dose efficiency (CNR^2/dose) for the contrast-enhanced acquisitions (3D neurovascular native/contrast). Data are presented as mean \pm standard deviation. Boldface type indicates statistical significance.

Al: aluminum; CNR: contrast-to-noise ratio; Cu: copper; $\text{Gy} \cdot \text{cm}^2$: gray-centimeters squared = dose-area product; mGy: milligray = entrance skin dose; mSv: millisievert



2 Summary of quantitative (2A, 2B), qualitative (2C, 2D), and dosimetric (2E–2G) results comparing the Al and Cu filter groups.

Quantitative image quality was assessed by CNR for the 3D neurovascular native/contrast (2A) and the subtraction (2B) datasets. Qualitative image quality assessments were performed for the same datasets: 3D neurovascular native/contrast (2C) and subtraction (2D). Radiation dose parameters for the total image acquisition (native + contrast-enhanced) are shown as entrance skin dose in mGy (2E) and dose area product in Gy·cm² (2F). In addition, the effective dose in mSv (2G) and the dose efficiency (CNR²/dose) (2H) are presented.

Bars: mean; whiskers: standard deviation; **** indicates statistical significance; Al: aluminum; CNR: contrast-to-noise ratio; Cu: copper; Gy·cm²: gray-centimeters squared = dose-area product; mGy: milligray; mSv: millisievert

Clinical relevance

The results underline that physical beam filtration using copper is a powerful yet straightforward method for meaningful dose reduction in cerebral angiography. Unlike protocol modifications or system-specific low-dose presets, Cu filtration does not require any changes to acquisition parameters, reconstruction settings, or operator workflow. It is a purely hardware-based adjustment that can be implemented without additional training or software updates. Because the Cu filter replaces only the supplemental 0.8 mm Al layer, statutory Al filtration is maintained, ensuring full compliance with regulatory requirements. The reduction in primary dose not only enhances patient safety but also lowers scatter radiation exposure for interventional staff — a relevant consideration in high-volume neurointerventional centers. In contrast to earlier phantom studies, these findings were derived from real-world patient data, reflecting the true clinical environment including contrast dynamics and patient anatomy [13]. The study therefore provides robust evidence that Cu filtration can achieve significant radiation savings while preserving image quality in routine clinical workflows.

Discussion and outlook

Substituting aluminum with copper filtration in 3D-RA is an immediate, low-cost, and technically straightforward strategy to achieve meaningful radiation dose reduction. The magnitude of dose savings observed in this study is comparable or superior to previously published studies that focused on low-dose protocols that required substantial adjustments to acquisition parameters or complex system modifications [10–16]. A key advantage of this approach lies in its simplicity and universality: Copper filtration can, in principle, be implemented on any modern angiography system equipped with standard X-ray filtration assemblies, independent of manufacturer or software platform. The modification preserves all statutory aluminum prefilters and does not interfere with image reconstruction algorithms or workflow, making it particularly attractive for routine clinical use and high-throughput environments. Clinically, the benefit of reduced radiation exposure is most relevant for patients who require repeated angiographic follow-up — such as those undergoing staged or post-treatment imaging after aneurysm embolization — and for younger or pediatric patients with increased radiosensitivity.

and longer life expectancy [17]. Lowering the primary dose also indirectly decreases scatter radiation to interventional staff, contributing to improved occupational safety. Future research may explore whether thicker copper filters (for example, 0.2 mm) or hybrid strategies combining Cu filtration with optimized acquisition protocols could further improve dose efficiency while maintaining diagnostic image quality. In addition, multicenter studies and cross-platform evaluations would help confirm the reproducibility of these findings and establish copper filtration as a broadly applicable method for reducing radiation dose in neurointerventional practice.

Conclusion

Replacing the standard 0.8 mm Al filter with a 0.1 mm Cu filter in cerebral 3D-RA achieves a substantial reduction in radiation dose while maintaining excellent diagnostic image quality. The modification requires no changes to workflow, acquisition protocols, or reconstruction settings and can be implemented easily within existing angiographic systems. As such, Cu filtration is a practical, low-cost, and operator-independent way of enhancing radiation safety in neurointerventional imaging. Its seamless integration and broad technical compatibility make it a promising step toward establishing more standardized and patient-centered dose optimization strategies across angiographic platforms.

References

- 1 Brisman JL, Song JK, Newell DW. Cerebral aneurysms. *N Engl J Med*. 2006;355(9):928–39.
- 2 Shaban S, Huasen B, Haridas A, Killingsworth M, Worthington J, Jabbour P, et al. Digital subtraction angiography in cerebrovascular disease: current practice and perspectives on diagnosis, acute treatment and prognosis. *Acta Neurol Belg*. 2022;122(3):763–780.
- 3 van Rooij WJ, Sprengers ME, de Gast AN, Peluso JP, Sluzewski M. 3D rotational angiography: the new gold standard in the detection of additional intracranial aneurysms. *AJNR Am J Neuroradiol*. 2008;29(5):976–9.
- 4 Abe T, Hirohata M, Tanaka N, Uchiyama Y, Kojima K, Fujimoto K, et al. Clinical benefits of rotational 3D angiography in endovascular treatment of ruptured cerebral aneurysm. *AJNR Am J Neuroradiol*. 2002;23(4):686–8.
- 5 White PM, Wardlaw JM, Easton V. Can noninvasive imaging accurately depict intracranial aneurysms? A systematic review. *Radiology*. 2000;217(2):361–70.
- 6 White PM, Teasdale EM, Wardlaw JM, Easton V. Intracranial aneurysms: CT angiography and MR angiography for detection prospective blinded comparison in a large patient cohort. *Radiology*. 2001;219(3):739–49.
- 7 Chappell ET, Moure FC, Good MC. Comparison of computed tomographic angiography with digital subtraction angiography in the diagnosis of cerebral aneurysms: a meta-analysis. *Neurosurgery*. 2003;52(3):624–31; discussion 30-1.
- 8 Shkumat NA, Shroff MM, Muthusami P. Radiation Dosimetry of 3D Rotational Neuroangiography and 2D-DSA in Children. *AJNR Am J Neuroradiol*. 2018;39(4):727–33.
- 9 Schueler BA, Kallmes DF, Cloft HJ. 3D cerebral angiography: radiation dose comparison with digital subtraction angiography. *AJNR Am J Neuroradiol*. 2005;26(8):1898–901.
- 10 Ryu JC, Yoon JT, Kim BJ, Kim MH, Moon EJ, Suh PS, et al. Impact of a selective lens dose reduction protocol in 3D rotational angiography on radiation exposure to the eye lens during cerebral angiography: a randomized controlled trial. *J Neurointerv Surg*. 2024;16(10):1021–1026.
- 11 Ryu JC, Yoon JT, Kim BJ, Kim MH, Moon EJ, Suh PS, et al. Reduction of Radiation Dose to Eye Lens in Cerebral 3D Rotational Angiography Using Head Off-Centering by Table Height Adjustment: A Prospective Study. *Korean J Radiol*. 2023;24(7):681–689.
- 12 Ki HJ, Kim BS, Kim JK, Choi JH, Shin YS, Choi Y, et al. Low-Dose Three-Dimensional Rotational Angiography for Evaluating Intracranial Aneurysms: Analysis of Image Quality and Radiation Dose. *Korean J Radiol*. 2022;23(2):256–263.
- 13 Ki HJ, Kim BS, Kim JK, Choi JH, Shin YS, Choi Y, et al. Low-Dose 3D Rotational Angiography in Measuring the Size of Intracranial Aneurysm: In Vitro Feasibility Study Using Aneurysm Phantom. *Neurointervention*. 2021;16(1):59–63.
- 14 Oberstar EL, Speidel MA, Davis BJ, Strother CM, Mistretta CA. Feasibility of reduced-dose three-dimensional/four-dimensional-digital subtraction angiogram using a weighted edge preserving filter. *J Med Imaging (Bellingham)*. 2017;4(1):013501.
- 15 Pearl MS, Torok C, Katz Z, Messina SA, Blasco J, Tamargo RJ, et al. Diagnostic quality and accuracy of low dose 3D-DSA protocols in the evaluation of intracranial aneurysms. *J Neurointerv Surg*. 2015;7(5):386–90.
- 16 Pearl MS, Torok CM, Messina SA, Radvany M, Rao SN, Ehtiati T, et al. Reducing radiation dose while maintaining diagnostic image quality of cerebral three-dimensional digital subtraction angiography: an in vivo study in swine. *J Neurointerv Surg*. 2014;6(9):672–6.
- 17 Bosch de Basea M, Thierry-Chef I, Harbron R, Hauptmann M, Byrnes G, Bernier MO, et al. Risk of hematological malignancies from CT radiation exposure in children, adolescents and young adults. *Nat Med*. 2023;29(12):3111–3119.

Contact

PD Dr. Niclas Schmitt, M.D., MHBA, EdiR
Department of Neuroradiology
Heidelberg University Hospital
Im Neuenheimer Feld 400
69120 Heidelberg
Germany
Tel.: +49 6221 567566
Niclas.Schmitt@med.uni-heidelberg.de



Niclas Schmitt, M.D.



Prof. Markus A Möhlenbruch, M.D.

ARTIS icono Ultra-High-Resolution Cone-Beam Computed Tomography for Depiction of Basilar Artery Brainstem Perforators Prior to Stent Placement: A Short Case Report

Philippe Breiding, M.D.

Department of Neurosurgery, University of Bern, Inselspital, Bern, Switzerland

Case presentation

A 68-year-old male patient presented to the emergency department with symptoms of fluctuating dysarthria and left-sided weakness (National Institutes of Health Stroke Scale, NIHSS 2). Magnetic resonance imaging (MRI) revealed an occlusion of the mid basilar artery and signs of acute ischemia of the right-sided pons. The distal basilar artery showed adequate collateralization from bilateral posterior communicating arteries, and we postulated that atherosclerotic disease or an underlying vessel stenosis may have been the culprit. The patient was initially treated conservatively with dual antiplatelet therapy; however, fluctuating neurologic symptoms persisted so we opted for endovascular therapy on day 13 of hospitalization.

Digital subtraction imaging (Figure 1)

Selective intra-arterial digital subtraction angiography (DSA) was performed under general anesthesia on a biplane, high-resolution angiographic system (ARTIS icono, Siemens Healthineers, Forchheim, Germany) using iodinated contrast (Iopamiro 300, Iopamidol, Bracco, Switzerland) for vessel opacification. ARTIS icono provides excellent spatial resolution using the as40HDR flat-panel detector with a 49 cm diagonal entrance plane, an active imaging size of 398 × 293 mm, and an active matrix size of 2586 × 1904 pixels. DSA images were obtained with 2.5 frames per second in the arterial phase, a focal spot size of 0.3 mm, and an edge enhancement reconstruction algorithm. A flat-detector zoom format of 32 × 32 cm in each plane was used.



1 Anteroposterior (1A) and lateral (1B) DSA images prior to angioplasty and stent placement demonstrating a high-grade stenosis of the middle third of the basilar artery (arrow).

ARTIS icono 3D ultra-high-resolution cone beam computed tomography imaging (Figure 2)

Arterial phase ultra-high-resolution cone beam computed tomography (UHR-CBCT) was performed for treatment planning. A diagnostic catheter was placed at the origin of the dominant vertebral artery. The catheter was connected to a double-head contrast agent injector (Accutron HP-D, Medtron AG, Saarbrücken, Germany) using a designated Y-pressure line with two check valves (Medtron AG) after having purged all air bubbles with sterile saline solution. The contrast injection was performed under apnea.

During image acquisition, a mixture of non-ionic contrast agent (15 mL) and sterile saline solution (30 mL) was injected with a flow of 3 mL/s (total volume 45 mL, contrast agent concentration 33%, injection time 15 s). The amount of contrast agent was adapted to allow adequate vessel opacification during the entire run and prevent any beam-hardening artifacts. Continuous fluoroscopic monitoring at a rate of 1 frame/s was used for contrast appearance in the basilar artery to trigger the rotational run. Upon appropriate opacification, a dedicated UHR CBCT run with a scan time of 14 s focusing on the posterior circulation was performed. During the run, the C-arm rotates around the patient over 200 degrees to create a circumferential run of the region of interest. In each run, 500 images with a resolution of 0.14 mm were obtained. The raw data was then transferred to a dedicated workstation and analyzed.

Endovascular therapy

The UHR-CBCT was crucial to precisely locate the atherosclerotic plaque along the ventral aspect of the basilar artery and the brainstem perforators originating

exclusively from the dorsal aspect of the basilar artery. With this information, we were able to assess the potential risk of angioplasty and stent placement. Since the atherosclerotic plaque was not located in close proximity to the perforator ostia, the risk of a perforator stroke secondary to plaque displacement after angioplasty / stent placement was considered low. A 7F guiding catheter was placed in the distal V2 segment of the left vertebral artery. First, an angioplasty with a 2.5 × 15 mm balloon (Fig. 3A) was performed. Due to recoiling of the vessel, a self-expanding stent was delivered (Wingspan 4.0 × 15 mm, Stryker Neurovascular, Fremont, CA, USA, Fig. 3B) covering the culprit lesion in the mid-basilar artery. The final DSA shows good stent expansion with a residual < 50% stenosis and an ulcerating plaque, which was adequately covered by the stent (Figs. 3C and 3D). No changes in neurologic function were noted after endovascular therapy, and the patient was discharged into neurorehabilitation with a mild persistent left-sided hemisyndrome and mild dysarthria.

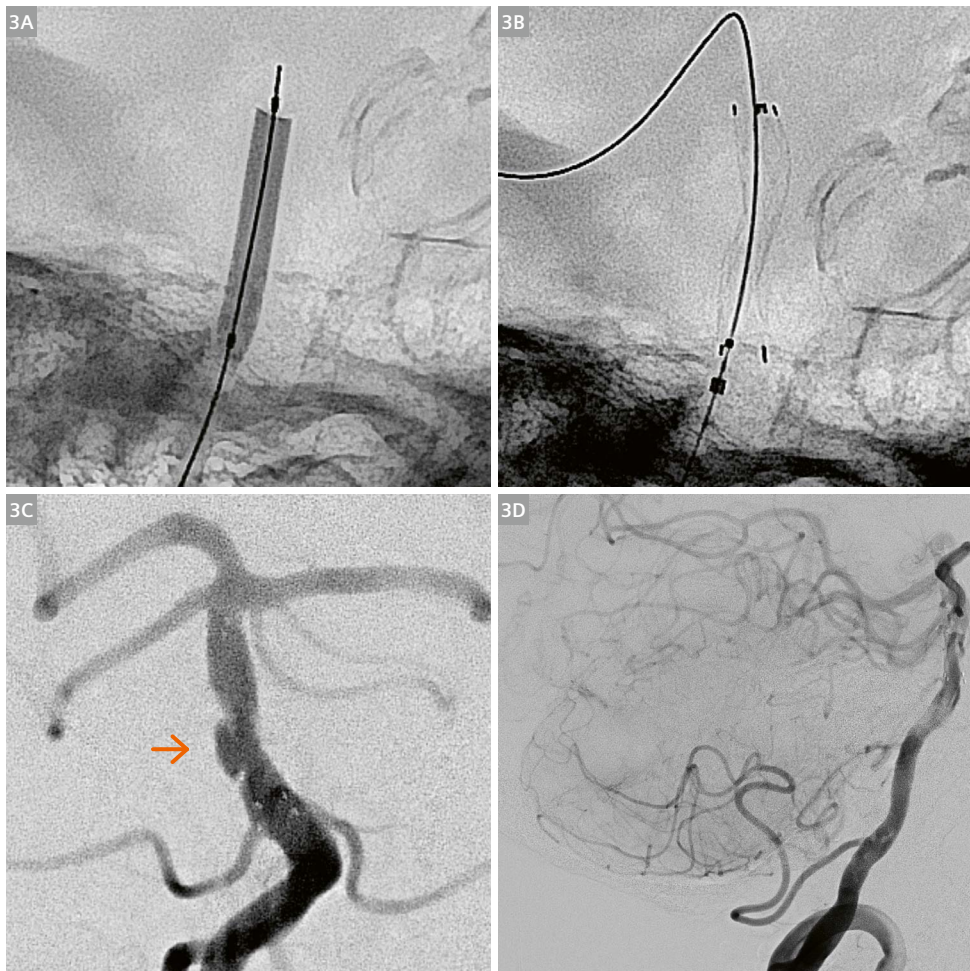
Discussion

The improved spatial resolution available with the newest generation of angiographic systems incorporating cone beam CT technology provides valuable insight into the perforator and neurovascular microanatomy, and helps with decision-making and treatment planning.

Perforating arteries arising from the basilar artery play a crucial role in supplying the brainstem, and their compromise may lead to ischemia that affects respiratory, cardiac, motor, and sensory function. Endovascular manipulations, especially in atherosclerotic vessels within the posterior fossa, may cause obliteration of small perforating vessels by plaque migration and may result in devastating consequences for the patient. It is therefore of the utmost



2 (2A–2C) UHR-CBCT images with maximal intensity reconstructions demonstrating focal stenosis of the basilar artery resulting from an atherosclerotic plaque in the ventral aspect of the basilar artery (**arrow, 2A**). Note the accurate depiction of several deep pontine perforators originating solely from the dorsal aspect of the basilar artery (**2A, 2B**). Superficial brainstem perforators are also visualized, originating from the posterior aspect of the basilar artery (**2B**).



3 Images acquired during endovascular therapy of a symptomatic basilar artery stenosis. Balloon angioplasty with 2.5 × 15 mm (**3A, 3B**). Dedicated “neurodevice” DSA depicts the most delicate device structures (**3A, 3B**). Deployment of a self-expanding stent (Wingspan 4.0 × 15 mm, **3B**). DSA images after stent deployment (**3C, 3D**) showing < 50% residual stenosis and an ulcerating plaque (**arrow, 3C**).

importance to understand the detailed vascular anatomy of the patient prior to treatment initiation.

In general, brainstem perforators are poorly appreciated on standard cross-sectional imaging, including CT angiography (CTA) and conventional 1.5 and 3 Tesla MR angiography (MRA) techniques. UHR CBCT enables a better understanding of the vascular pathology and therefore has important implications for therapy [1]. Implementing it in clinical routine for selected pathologies is useful.

Conclusion

UHR-CBCT enables a better understanding of vascular anatomy and depiction of small brainstem perforating

arteries. Implementing it in clinical routine has important implications with regard to endovascular treatment planning and patient outcome.

Reference

- 1 Dobrocky T, Piechowiak EI, Goldberg J, Barvulsky Aleman E, Nicholson P, Lynch J, et al. Absence of pontine perforators in vertebrobasilar dolichoectasia on ultra-high resolution cone-beam computed tomography. *J Neurointerv Surg.* 2021;13(6):580–584.

The information presented in the case report is for illustration only and is not intended to be relied upon by the reader for instruction as to the practice of medicine. Any health care practitioner reading this information is reminded that they must use their own learning, training and expertise in dealing with their individual patients. This material does not substitute for that duty and is not intended by Siemens Healthineers to be used for any purpose in that regard. The treating physician bears the sole responsibility for the diagnosis and treatment of patients.



Contact

Philippe Breiding, M.D., EBIR
Department of Neurosurgery
University of Bern, Inselspital
Rosenbühlgasse 25
CH-3010 Bern
Switzerland
Tel.: +41 31 632 13 77
Philippe.Breiding@insel.ch

Optimizing Acute Stroke Diagnostics with Photon-counting CT: Balancing Multiphase CT Angiography, Perfusion, and Cardioembolic Assessment

Adrian Szum^{1,2}, Patrik Nowik³, Alina Stenke⁴

¹ Department of Clinical Neuroscience, Karolinska Institutet, Stockholm, Sweden

² Department of Neuroradiology, Karolinska University Hospital, Stockholm, Sweden

³ Siemens Healthineers, Stockholm, Sweden

⁴ Siemens Healthineers, Forchheim, Germany

Background

Traditionally, stroke imaging has been a fragmented process involving trade-offs between speed, coverage, and image resolution. The need to rule out hemorrhage, identify occlusions, assess collaterals, and evaluate salvageable hypoperfused brain tissue often required multiple scan sequences and time-consuming post-processing. Furthermore, identifying the embolic source usually required separate downstream investigations. This is a critical diagnostic step for selecting the appropriate secondary-prevention treatment. Research indicates that 27.7% of first-ever ischemic strokes are of cardioembolic origin. Additionally, 10.8% of strokes are classified as an embolic stroke of undetermined source (ESUS); a clinical entity describing strokes of likely embolic origin where the source remains undetected despite standard workups [1].

Siemens Healthineers have introduced photon-counting CT technology in clinical practice with the introduction of the NAEOTOM Alpha. This CT scanner combines the advantages of the photon-counting detector, including high spatial and contrast resolution [2, 3], with the fast acquisition speed of a dual source scanner. This combination makes this scanner interesting for neuroimaging, which is why the dual source NAEOTOM Alpha at Karolinska University Hospital is the Stockholm region's main CT scanner for stroke diagnostics.

At Karolinska University Hospital, the approach to acute stroke imaging has evolved within 10 years, from a reliance on simple non-enhanced CT (NECT) and single-phase CT angiography (CTA), to a more comprehensive diagnostic protocol: After the traditional NECT, a multiphase

CTA (mCTA) is performed, with the first phase also covering the heart. This extended scan range helps identify certain cardiac etiologies during the initial workup, facilitating earlier triage. Finally, a CT perfusion (CTP) is added where needed. Thus, the combination of NECT + mCTA (including the heart) + CTP is used as a "one-stop" shop style protocol.

Karolinska University Hospital's philosophy of mCTA versus CTP is not binary, but rather a stratified approach. The mCTA acts as the robust workhorse for the majority of stroke cases, providing rapid acquisition and sufficient physiological data, e.g. to assess collaterals. CTP serves as a critical problem-solving tool to provide further clinical information, especially for wake-up strokes, complex cases, and stroke mimics.

The stroke protocol takes advantage of various automated features. For the NECT, patient positioning is supported by the FAST 3D camera, which automatically identifies the optimal patient positioning in the isocenter. The scan and reconstruction regions are planned manually to ensure appropriate coverage. After scanning, multi-planar reconstructions (MPRs and MIPs) are automatically created by the *syngo.via* server (Rapid Results Technology*). Based on our experience, all results are available in PACS within 6 minutes; specifically, CTP volumetric maps, including penumbra, core infarct, and mismatch ratio are ready in just 2.5 minutes.

The automated post-processing removes the traditional workflow bottleneck and provides specific benefits for each exam: For NECT, it ensures that reconstructions are standardized regarding angulation and settings across

different scanners. For mCTA, the system enables thick maximum intensity projections (MIPs) in axial, coronal, and sagittal reconstructions as needed, which facilitates quick viewing and is useful for demonstration during future patient rounds. For perfusion imaging, the process runs fully automatically in the vast majority of patient cases, including automatic identification of the reference vessel (superior sagittal sinus) and the arterial input function (AIF).

This article begins with an overview of the different components of Karolinska University Hospital's stroke protocol, followed by three patient cases that each illustrate the value of a specific element: mCTA, perfusion imaging, and the integrated cardiac assessment included in the mCTA acquisition.

The Karolinska stroke protocol

Stroke patients at Karolinska University Hospital in Solna are primarily diagnosed with the NAEOTOM Alpha CT scanner. The scan protocol is designed to be fast and effective, and consists of three main parts, the NECT, mCTA and CTP. The NECT and the mCTA are always included and used, while the CTP is skipped if bleeding is detected. In such cases, the mCTA is used to exclude potential vascular malformations (e.g., aneurysms, arteriovenous malformations, arteriovenous fistulas) as the source of the bleeding. Furthermore, when bleeding is detected, the mCTA covers all three phases over the brain only, as it is not necessary to additionally scan from the heart.

A summary of the scan protocol for stroke is shown in Table 1. The separate series and their corresponding reconstructions are discussed in this section.

Series	Topogram PA (550 mm)	Topogram LAT (550 mm)	NECT	Premonitoring	Monitoring	mCTA Phase 1	mCTA Phase 2	mCTA Phase 3	CTP
Scan range	Vertex to diaphragm	Diaphragm to vertex	Skull base to vertex	Level of aortic arch	Level of aortic arch	Diaphragm to vertex	Skull base to vertex	Skull base to vertex	11 cm shuttle range
Scan mode	QuantumSn	QuantumSn	Quantum-Plus	Quantum	Quantum	Quantum	Quantum	Quantum	Quantum
Tube potential [kV]	Sn140	Sn140	120	90	90	90	90	90	70
(phantom diameter) CTDIvol [mGy]	SPR (16 cm) 0.11	SPR (16 cm) 0.11	(16 cm) 38.5	(32 cm) 0.84	(32 cm) 37.8	(32 cm) 6.96	(32 cm) 6.96	(32 cm) 6.96	(16 cm) 109
DLP [mGy*cm]	6.1	6.1	747	0.4	18.9	344	116	116	1,399
Exam time [s]	3.03	3.03	6	0.25	35.45	2.63	1.74	1.74	45.9
Start delay: Intended [s]	2	2	2	2	8	Trigger	22	28	6
CARE Dose4D & CARE keV	N/A	N/A	Off	Manual kV, IQ level 22	Manual kV, IQ level 22	Off	Off	Off	IQ level 45
Effective mAs / mA	55 mA	55 mA	228 mAs	33 mAs	33 mAs	250 mAs	250 mAs	250 mAs	97 mAs
Pitch	N/A	N/A	0.35	N/A	N/A	1.6	1.6	1.6	0.5
Rotation time [s]	N/A	N/A	0.5	0.25	0.25	0.25	0.25	0.25	0.25

Table 1: Karolinska University Hospital's scan protocol for stroke on the NAEOTOM Alpha. The detailed protocol is freely available for download here: github.com/karolinskaimaging

CTDIvol = Volume CT Dose Index, CTP = CT perfusion, IQ level = Image Quality level, LAT = lateral projection, mCTA = multiphase CT angiography, N/A = not applicable, NECT = non-enhanced CT, PA = posteroanterior projection, Sn = tin-filtered, SPR = Scan Projection Radiograph dose reference

1. Non-enhanced CT (NECT): Spectral intelligence

The stroke protocol begins with two long topograms, used for planning and potential exclusion of metal in case the patient needs to be transferred to the MRI suite. This is followed by a NECT at a standard 120 kVp with a CTDIvol of 38.5 mGy. Photon-counting CT technology allows Karolinska University Hospital to access spectral information in every baseline scan. Reconstructions always include Virtual Non-Contrast (VNC) and Iodine (1 mm Qr44 QIR4) to provide an immediate assessment of early ischemic changes, even if intravenous contrast medium was previously given, e.g., during coronary angiography or other interventional procedures. Multiplanar reconstructions (MPRs) are created from a soft reconstruction (0.8 mm Hr40 QIR4 512 × 512 67 keV) automatically via Rapid Results Technology in *syngo.via*. A sharp reconstruction (0.4 mm Hr72 QIR2 768 × 768 T3D) is stored for bone evaluation.

2. Multiphase CTA (mCTA): Head and heart coverage

The mCTA is the cornerstone of this stroke protocol. Performed at a locked 90 kVp (dual source) for improved iodine contrast visualization of intracranial vessels, this sequence is divided into three phases to assess both flow and perfusion dynamics without delay or the need for complex calculations. Compared to CTP, mCTA offers higher spatial resolution while still providing a temporal sampling of 3 images per study. This is achieved with a highly optimized radiation profile: The total effective dose for the mCTA is approximately 4.6 mSv. Crucially, the radiation “cost” of obtaining this time-resolved data is minimal, with the second and third phases contributing only ~ 0.6 mSv each. This design transforms a standard static angiogram into a dynamic flow assessment with a negligible increase in biological risk. In contrast, while CTP carries a slightly lower effective dose (3.1 mSv), it deposits a significantly higher cumulative dose concentrated exclusively within the intracranial volume (CTDIvol 109 mGy versus 21 mGy for CTP and mCTA respectively).

Evaluation is based on the application of a single intravenous contrast bolus. Scanning is performed in dual source mode with a slightly reduced pitch of 1.6, a parameter chosen for several critical reasons: First, higher pitch values over 1.6 result in higher acceleration and deceleration of the table, which would prolong the interval between phases. A pitch of 1.6 maintains the short 6-second interval. Second, a higher pitch limits patient positioning along the z-plane, risking scan range cut-off. Finally, compared to higher pitch values, a pitch of 1.6 provides more sinogram information with improved sampling, reducing artifacts such as windmill artifacts from high-attenuating materials like contrast, bone, or arms within the scan field.

The reconstructions (0.4 mm Hv56 QIR4 T3D) are automatically reformatted into MIPs via *syngo.via*. Further, a separate reconstruction (5 mm Qr44 QIR4 53 keV, recently changed to 2 mm Hr36) is made for reading the dynamic iodine uptake in the parenchyma.

Using these settings, a short interval timing of 6 seconds is achieved that allows the reduction of the total bolus injection time and the overall amount of intravenous contrast medium. The contrast injection protocol for the mCTA on the dual source NAEOTOM Alpha consists of 80 ml of Visipaque 320 (GE Healthcare) at 6 ml/s over 13.3 seconds, compared to 100 ml at the same rate over 16.7 seconds on other CT systems, followed by a saline chaser of 80 ml NaCl (9 mg/ml) at 8 ml/s.

Phase 1 (early arterial): Unlike standard protocols that stop at the aortic arch, Phase 1 extends to include the entire heart. In early mCTA articles [4, 5], this Phase 1 often resembled a late arterial phase; however, Karolinska University Hospital has decided to perform an earlier phase, making it easier to distinguish arteries from veins. Optimized for rapid acquisition, the scan is performed from the diaphragm to the skull vertex using a high pitch of 1.6 and no ECG-gating or triggering, minimizing setup time. By leveraging both the acquisition speed of the dual source system and the high spatial and contrast resolution of the photon-counting detector, a good to excellent cardiac image quality is generally achieved [6].

As we demonstrated in a recent cohort study [6], this enables immediate detection of potential cardioembolic findings, notably cardiac thrombi and aortic valve vegetations, while also revealing other management-relevant cardiothoracic findings such as patent foramen ovale; severe valvular calcifications were also observed. However, image quality may occasionally be insufficient for cardiac evaluation, or findings may remain inconclusive. The rates observed in our cohort study were around 3%, which is comparable to those reported for ECG-gated energy-integrating dual source CT [7]. False positives were rare, and false negatives may occur, both of which need to be further investigated by comparison with diagnostic reference standards.

Overall, this scan allows identification of cardioembolic stroke sources during routine comprehensive stroke imaging with virtually no additional time or cost to patient management. This may reduce the need for subsequent investigations, ultimately improving patient flow and lowering healthcare costs, and may also shorten diagnostic timelines, potentially enabling earlier targeted secondary prevention.

Phases 2 & 3 (venous / late): These phases are restricted to the head to minimize the overall radiation dose while capturing the temporal evolution of contrast. This allows for robust collateral scoring, which is essential for predicting outcomes in thrombectomy candidates. These

phases are included to visualize flow dynamics while assessing more distal vessels without the post-processing delay of perfusion maps in standard cases.

3. CT perfusion (CTP): Automated volumetry

This scan is performed at 70 kVp, acquiring 30 volumes over 45 seconds. The factory protocol was adjusted to achieve the target image quality at a reduced radiation dose, utilizing the highest iterative reconstruction level (5 mm Hr40 QIR4 T3D). This reduced the radiation dose by more than 40%, compared to the factory protocol, yielding a CTDIvol of 109 mGy. The CTP data provides critical insight into the physiological and pathophysiological status of the brain tissue.

As described in the introduction, Karolinska University Hospital relies on fully automated processing using Rapid Results Technology to eliminate delays. By the time the patient is moved from the table, the PACS has already received the penumbra and core infarct volumes as well as the mismatch ratios. For automatic post-processing of CTP data we used motion correction, 4D noise reduction, smoothing filter 10 mm, AIF vessel threshold 12% and increased the width of the brain parenchyma segmentation to 23 HU and 500 HU in order to accommodate the preceding CTA. The ischemic penumbra (tissue at risk) is defined as tissue with a time-to-maximum (Tmax) delay of > 6 seconds. The infarct core (non-viable tissue) is defined as tissue with a relative cerebral blood flow (rCBF) of < 20% compared to the contralateral healthy hemisphere. Vessel suppression is applied to the final parametric maps to improve tissue visualization. For quantitative analysis, images are reconstructed at a slice thickness of 5 mm with a 3 mm interval.

The standard contrast injection for CTP is 42 ml of Visipaque 320 (GE Healthcare) at 7 ml/s, with a saline chaser of 80 ml NaCl (9 mg/ml) at 8 ml/s.

Patient cases

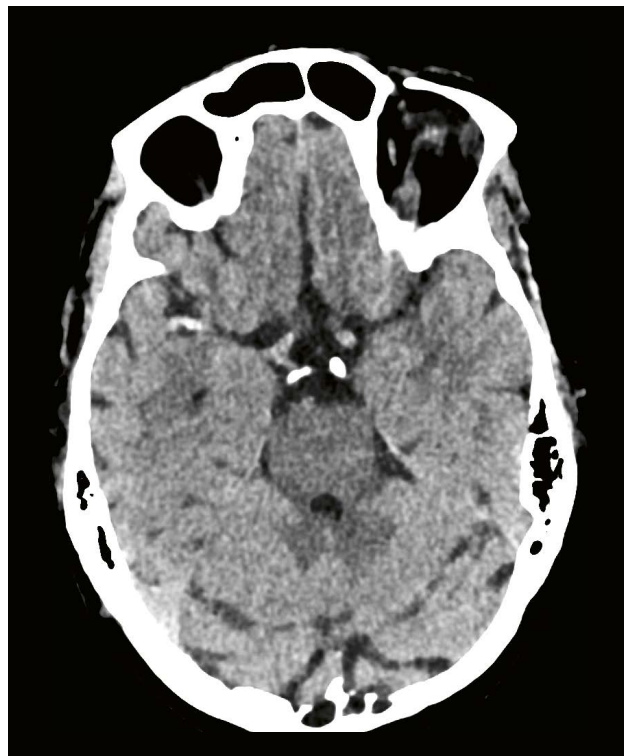
Three cases are presented in this article. Case 1 is an example of a stroke case where the mCTA showed a clear M1 occlusion and the patient could be sent directly for thrombectomy without requiring immediate review of the CTP maps. Case 2 is an example where the first mCTA phase clearly demonstrates a thrombus in the heart, and therefore shows the advantage of including the heart in phase 1 of the mCTA. Case 3 is a complicated stroke patient with findings in the mCTA which were difficult to interpret. CTP helped to correctly read the case.

Case 1: The “clear” large vessel occlusion (mCTA is sufficient)

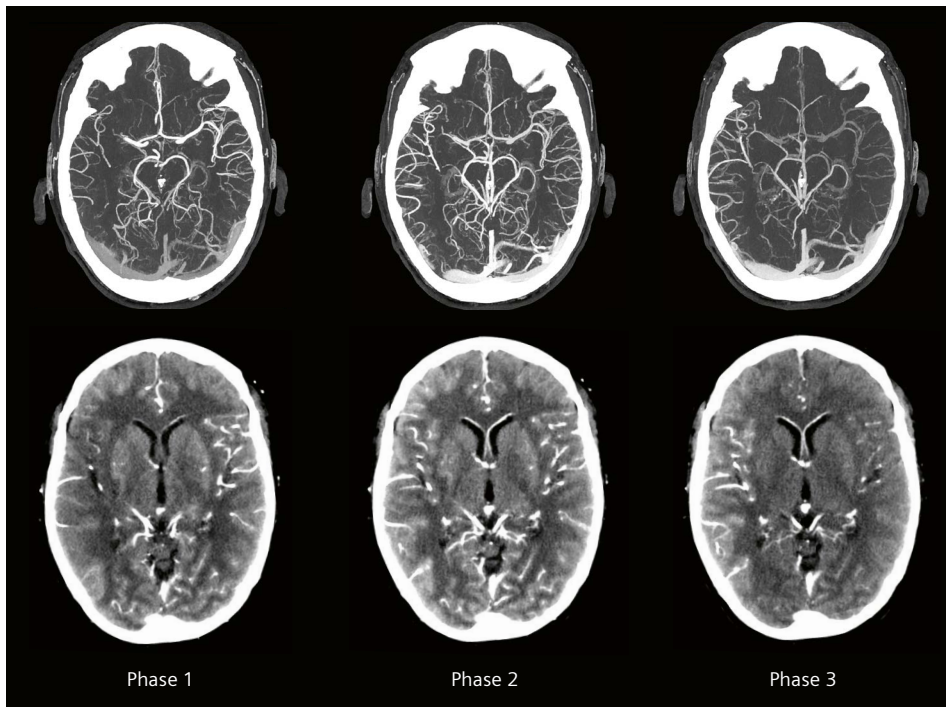
An elderly patient presented with a new-onset left-sided hemiparesis. NECT demonstrated no intracranial hemorrhage and no early infarct demarcation but revealed a 1.5 cm long dense vessel sign in the right middle cerebral artery (MCA) (see Figure 1).

Key finding (mCTA): A subsequent mCTA confirmed an occlusion in the right MCA, distally in the M1 segment with extension into the proximal M2 branches. Figure 2 shows the mCTA images as they are typically displayed in our PACS. The right MCA territory exhibits delayed contrast filling with good opacification in the later phases. This represents a favorable collateral status, indicating salvageable penumbra.

Clinical impact: The patient was immediately referred for thrombectomy. This case illustrates how in standard large vessel occlusions, mCTA alone provides all information necessary for rapid decision-making, representing a highly efficient workflow. In this case, additional perfusion imaging would increase time and radiation exposure without adding clinically relevant information.



1 Axial non-enhanced CT. Note the dense vessel sign in the distal right M1 segment. No hemorrhage or acute infarct demarcation.



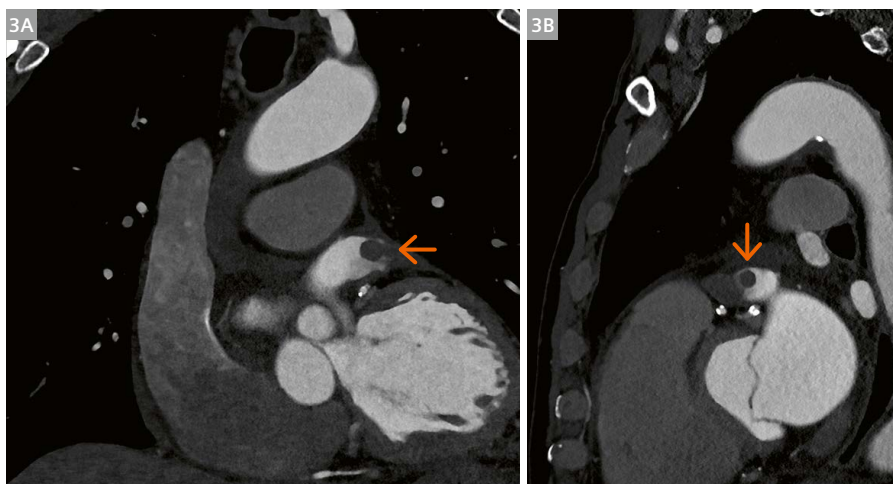
2 Multiphase CT angiography (mCTA) in three phases. The upper row shows maximum intensity projections (MIPs) with 25 mm slice thickness at the level of the circle of Willis, and the lower row shows parenchymal images with 5 mm slice thickness at the level of the basal ganglia. From left to right, early arterial (phase 1), arteriovenous (phase 2), and venous (phase 3) acquisitions are shown respectively. Note the occlusion of the right middle cerebral artery (MCA) in the distal M1 segment. There is delayed contrast filling in the right middle MCA territory with a one-phase delay compared to the left side, but with good contrast filling in later phases.

Case 2: The cardioembolic source (the “heart” scan)

An 82-year-old patient presented with a witnessed acute onset of dysarthria and right-sided hemiparesis, most pronounced in the arm. Initial NECT, performed one hour after symptom onset, demonstrated no hemorrhage or acute infarction.

Key finding (mCTA): The intracranial component of the mCTA demonstrated an occlusion in a frontal M4 vessel on the left side. In addition, the extended thoracic field of view acquired without ECG-gating revealed a thrombus within the left atrial appendage (LAA), providing a likely cardiac source of embolism (see Figure 3).

Clinical impact: The patient, who had atrial fibrillation, was treated with intravenous thrombolytics. Identifying the stroke etiology directly on the extended-range CT scan allowed clinicians to decide on secondary-prevention strategies immediately, rather than waiting for a transesophageal echocardiogram days later. This demonstrates the practical value of including an extended thoracic field of view in acute stroke imaging. In our recent cohort study of 193 patients, we identified clinically relevant cardiothoracic findings in every third patient and specific cardioembolic findings in 4.7% of patients, with cardiac thrombi and vegetations found exclusively in the subgroup with confirmed infarction [6]. This supports the role of extended-range CT in efficiently uncovering cardioembolic sources.



3 Cardiac images from the multiphase CT angiography. Images acquired during the early arterial phase of the multiphase CT angiography, extended to a non-gated thoracic scan. Coronal (3A) and sagittal (3B) reconstructions clearly demonstrate the thrombus in the left atrial appendage (arrow).

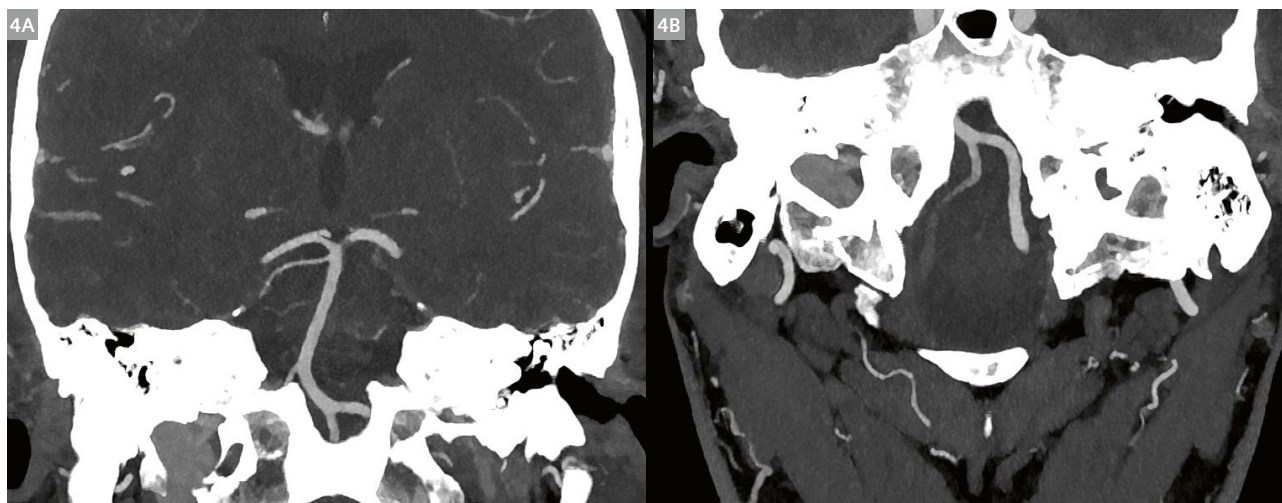
Case 3: The “complex” presentation (CTP is decisive)

A 40-year-old male presented with an acute onset right-sided weakness, numbness, and right hemianopsia. Upon arrival, motor symptoms had transiently improved, but visual field deficits and oculomotor dysfunction persisted (NIHSS 4).

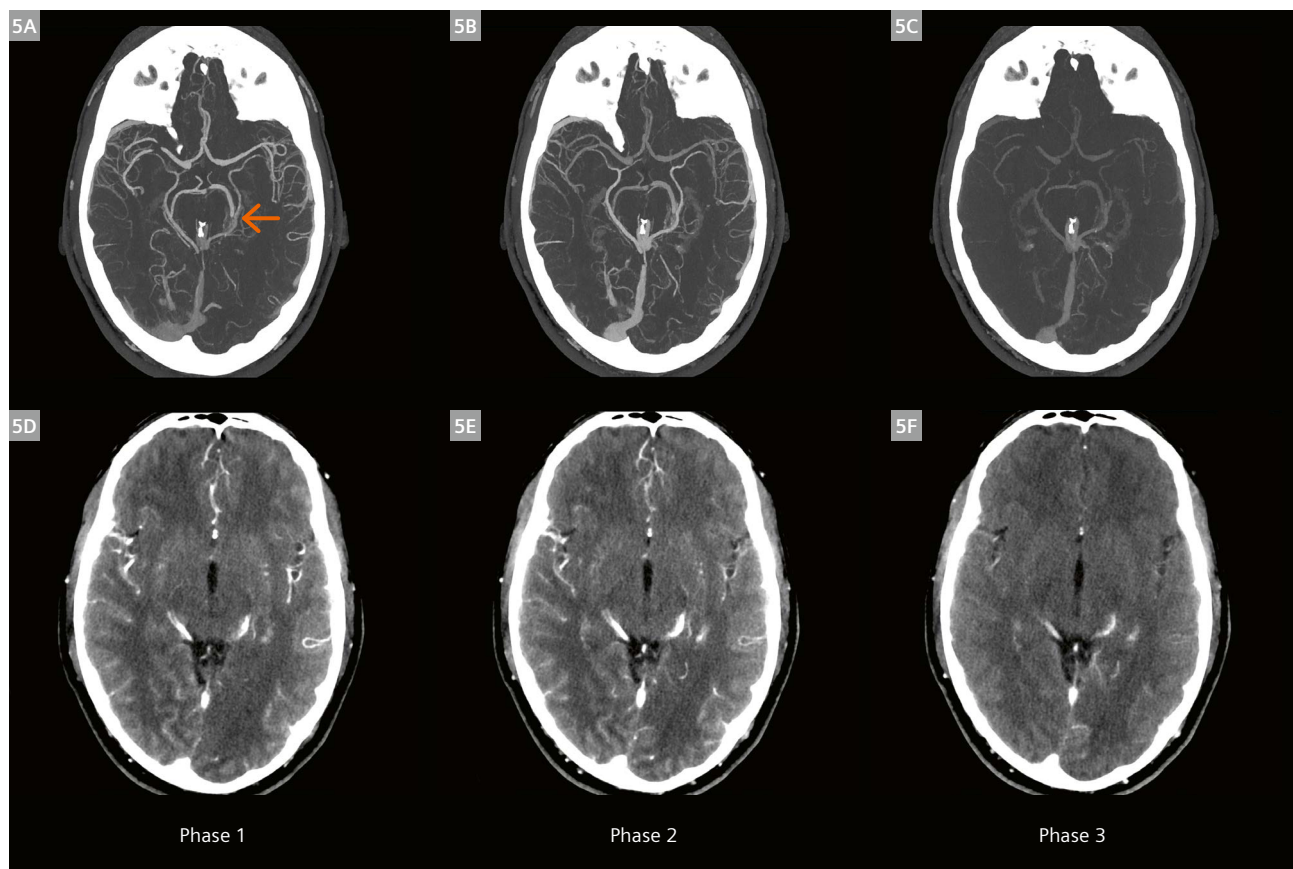
Initial imaging (NECT & mCTA): The NECT showed only a subtle hypoattenuation in the left lingual gyrus, suggestive of early ischemia but otherwise unremarkable. The mCTA, however, revealed a highly complex vascular landscape that was difficult to immediately interpret. It showed a proximal dissection of the right vertebral artery (VA) with irregular caliber and lack of antegrade flow, showing some retrograde filling of the most distal portion (see Figure 4). Conversely, distal occlusions were found contralateral: an occlusion of the left superior cerebellar artery (SCA), and the left posterior cerebral artery (PCA) with a thrombus surrounded by contrast medium in a short, stenotic P1 segment (see Figure 4), followed by an occlusion at the left P2/P3 transition (see Figure 5).

Key finding (CTP): While the mCTA identified the vessel patency issues and delineated perfusion deficits in the left occipital lobe and parts of the left temporal lobe, it was difficult to fully evaluate the hemodynamic impact on the brainstem (see Figure 5). Here, CTP provided critical additional information. Crucially, the perfusion maps delineated deficits not only in the left occipital and temporal lobes (PCA territory) and left cerebellum (SCA territory), but also in the right pons and medulla oblongata (vertebrobasilar territory), confirming the risk of critical ischemia in the brainstem and extensive salvageable cortical tissue (see Figure 6).

Clinical impact: The CTP was instrumental in the interventional neuroradiologist’s planning, as it delineated the perfusion deficits resulting from the right VA dissection and the contralateral left PCA and SCA occlusions. This justified an immediate mechanical thrombectomy despite the low NIHSS. The procedure was performed via the intact left VA, thereby avoiding the dissected right VA. The interventionalist performed four passes with a stent retriever, successfully opening the inferior temporal branch and achieving a substantial reperfusion result (grade TIC1 2b). Follow-up MRI confirmed small, scattered infarcts in the cerebellum and occipital lobe, partly matching the CTP prediction, but primarily the patient was spared potentially larger infarcts in the posterior circulation (see Figure 7).



4 CT angiography for vessel evaluation. Oblique coronal maximum intensity projections (MIPs) from the early arterial phase of the multiphase CT angiography: **(4A)** 10 mm MIP, demonstrating the markedly stenotic P1 segment of the left posterior cerebral artery and the occluded left superior cerebellar artery, reconstructed with 10 mm slice thickness. **(4B)** 4 mm MIP of the basilar and vertebral arteries, showing retrograde filling of the distal right vertebral artery.



5 Multiphase CT angiography (mCTA) in three phases. From left to right, images in early arterial (phase 1), arteriovenous (phase 2), and venous (phase 3) acquisitions at the level of the circle of Willis. The upper row shows maximum intensity projections (MIPs) of 25 mm slice thickness, and the lower row shows the corresponding parenchymal images with 5 mm slice thickness. The arrow in (5A) indicates the occlusion of the left posterior cerebral artery. In the downstream vascular territory, a phase shift of the contrast is observed across two phases, with all vessels present but not completely filling the entire area. The parenchymal images demonstrate delayed perfusion in the left occipital region and partly in the temporal region.

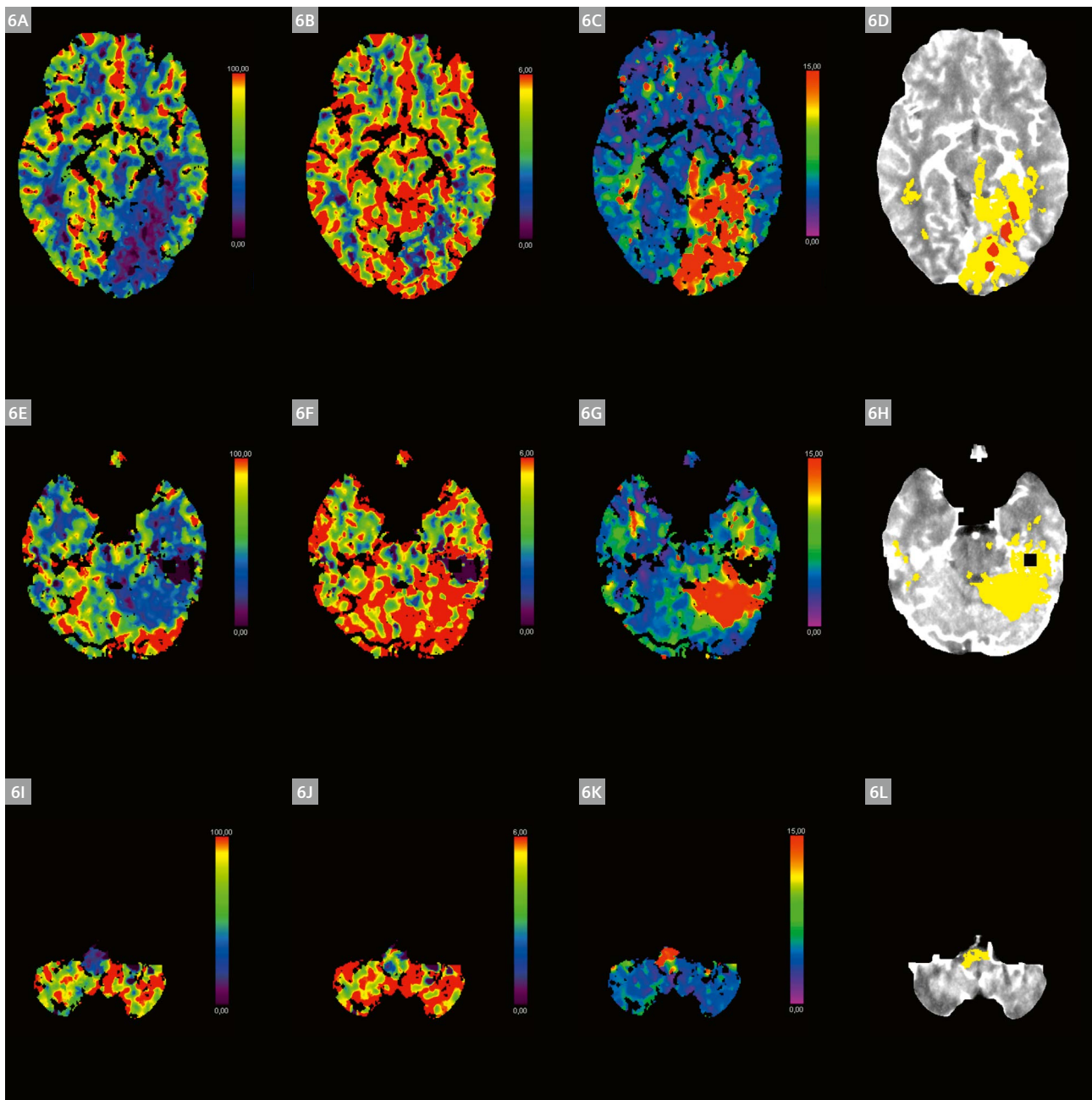
Discussion

The stroke imaging protocol implemented at Karolinska University Hospital in Solna, using the dual source NAEOTOM Alpha photon-counting CT, offers an integrated diagnostic workflow designed to reduce fragmentation in acute stroke care. By combining spectral NECT, comprehensive dual source mCTA extending from the diaphragm to the vertex, and CTP in selected cases, the protocol aims to optimize the “time is brain” window while maximizing diagnostic yield. The cases presented herein demonstrate the clinical efficacy of this stratified approach, suggesting that optimized protocol design may be as important as the underlying technology in improving patient management.

The transition from single-phase to multiphase CTA is central to this protocol’s utility. Based on our experience and as illustrated in Case 1, a standard large vessel occlusion (LVO) often requires no further imaging than the CTA to guide clinical decision-making. While CTP provides high temporal resolution, it incurs a higher radiation dose and

generates large data volumes that can be time-consuming to process and review. The mCTA protocol offers a favorable trade-off, providing the flow dynamic information necessary for assessing collateral status without the radiation burden associated with perfusion imaging. Consequently, CTP is reserved for cases requiring more detailed physiological clarification.

The technical capabilities of the photon-counting detector and dual source technology facilitate this comprehensive approach. Achieving the three mCTA scan phases, including thoracic coverage, with a total effective dose of approximately 4.6 mSv, suggests that increased diagnostic information does not necessitate a prohibitive rise in radiation exposure. The use of a high pitch (1.6) allows for rapid acquisition, ensuring separation of temporal windows (early arterial, arteriovenous, venous). This enables the radiologist to assess tissue viability based on collateral filling delays, facilitating immediate triage for thrombectomy in straightforward cases.



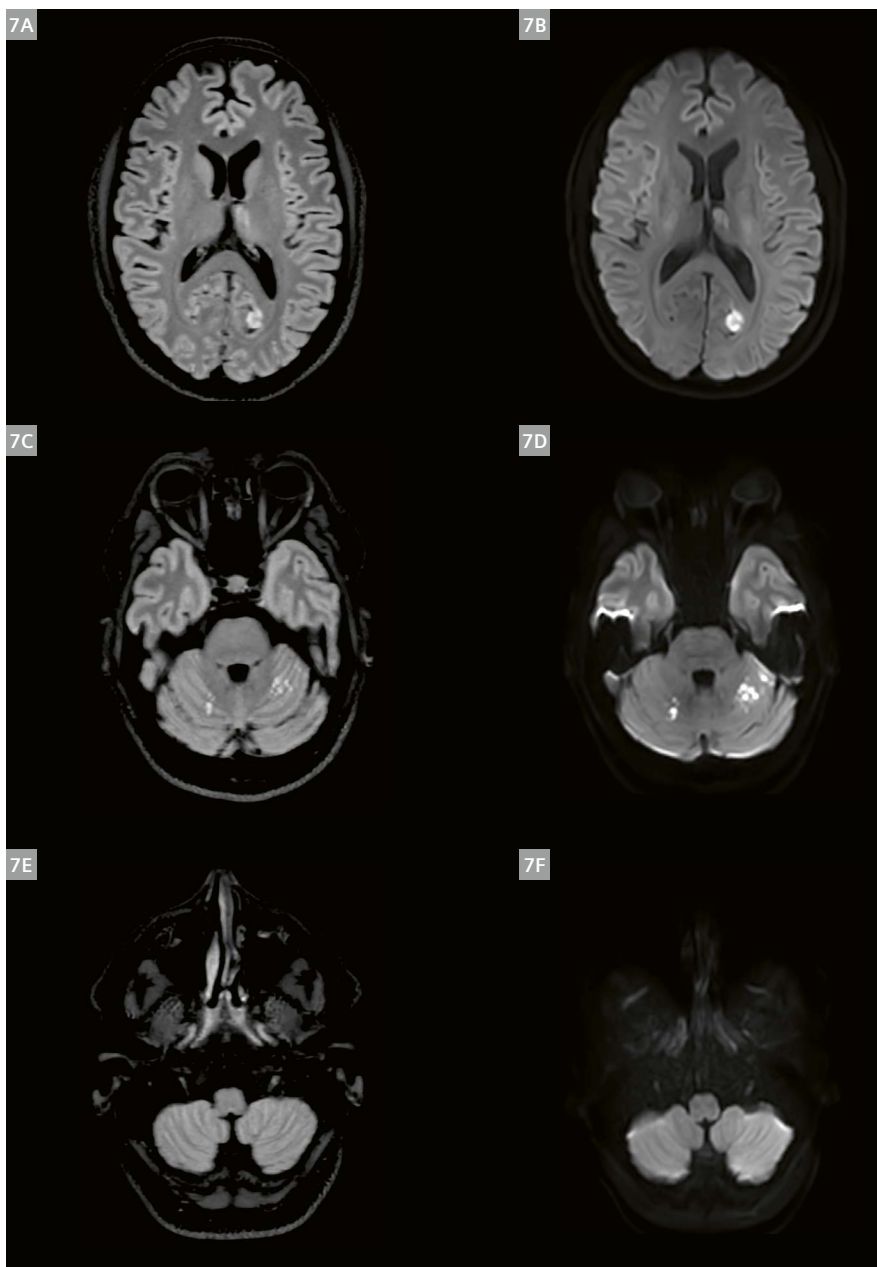
6 Selected CT perfusion maps at three axial levels, showing cerebral blood flow (CBF), cerebral blood volume (CBV), time to drain (TTD) and automated penumbra/core in columns from left to right respectively. **(6A–6D)** shows a large perfusion-impaired area in the left occipital lobe extending into the medial temporal lobe, with decreased CBF and increased CBV, consistent with penumbra. The middle row **(6E–6H)** demonstrates perfusion impairment in the left cerebellum, likewise with reduced CBF and increased CBV, consistent with penumbra. The bottom row **(6I–6L)** shows perfusion impairment on the right side of the medulla oblongata, with decreased CBF and normal CBV, also representing penumbra. A smaller perfusion disturbance medially on the right side in the pons is not shown.

Integrated cardiac assessment

A distinct feature of this protocol is the inclusion of the heart during the initial arterial phase. A significant proportion of ischemic strokes are cardioembolic or classified as an embolic stroke of undetermined source (ESUS). Traditionally, identifying the embolic source is a downstream process involving echocardiography and telemetry, which may be delayed by days. By extending the scan range to the diaphragm, the search for etiology is shifted to the acute phase.

Case 2 highlights the clinical utility of this extended coverage. The identification of the embolic source, such

as left atrial appendage thrombi or aortic vegetations during the initial workup, allows for the immediate tailoring of secondary prevention strategies, including the timing of anticoagulation. Although the scan is non-gated to prioritize speed, the high temporal resolution of the dual source system sufficiently mitigates motion artifacts to render diagnostic images in the majority of patients. As reported by Ståhl et al. [6], clinically relevant cardioembolic findings were detected in 4.7% of patients using this specific non-gated high-pitch protocol, with incidental thoracic findings that could affect patient management observed in nearly one-third of the scans. These findings



7 Post-thrombectomy MRI confirming small infarctions at three axial levels. Follow-up MRI after mechanical thrombectomy. Each row shows diffusion weighted imaging (DWI, left) and fluid-attenuated inversion recovery (FLAIR, right) at corresponding axial levels. Small scattered hyperintensities, consistent with acute infarction, are seen in the left occipital lobe and thalamus (7A–7B) as well as in the cerebellum (7C–7D), while the brainstem is spared (7E–7F). The infarct burden is markedly smaller than the perfusion abnormalities observed on the pre-thrombectomy CT perfusion study, supporting successful reperfusion.

suggest that the diagnostic yield of extended coverage outweighs the minimal increase in acquisition time and radiation, potentially reducing the need for subsequent transesophageal echocardiography.

Stratified use of CT perfusion

The protocol employs a stratified, rather than a binary approach, to perfusion imaging. While mCTA serves as the primary diagnostic tool, Case 3 demonstrates that CTP remains a valuable complement to complex presentations. In this case, CTP provided the diagnostic confidence required to intervene in a complex vascular scenario where mCTA findings were equivocal. This confirms that CTP should not be discarded but reserved for cases where mCTA flow dynamics are complex to determine tissue viability. Such situations include wake-up strokes where physiological perfusion parameters may provide necessary adjunctive information. The integration of automated post-processing further supports this strategy. With core infarct and mismatch maps generated automatically, the inclusion of CTP data does not significantly delay the workflow.

Implementation considerations

Implementing this protocol requires specific considerations regarding patient selection and interpretation. First, the patient population at a comprehensive stroke center is often pre-triaged with a higher pre-test probability of LVO, justifying the comprehensive nature of our default protocol. In centers with lower LVO probabilities, the yield of extended protocols must be balanced against throughput requirements. Second, while non-gated scanning covering the heart is effective for screening, it does not replace dedicated cardiac CT; for example, small thrombi may be obscured by motion artifacts in patients with high heart rates, though the high-pitch technique significantly reduces this risk. Finally, while spectral NECT (using Virtual Non-Contrast and Iodine maps) aids in differentiating hemorrhage from contrast staining, it requires radiologist familiarity with spectral datasets.

Conclusion

The Karolinska Stroke Protocol leverages the acquisition speed, spatial and contrast resolution, as well as spectral capabilities of a dual source photon-counting CT to address the traditional trade-offs between coverage, resolution, and time. By extending the mCTA to include the heart at a comprehensive stroke center, the protocol allows for the simultaneous assessment of vessel occlusion and embolic etiology. Combined with the selective use of CTP for complex scenarios, this approach aims to expedite acute revascularization and potentially streamlines the pathway from admission to secondary prevention.

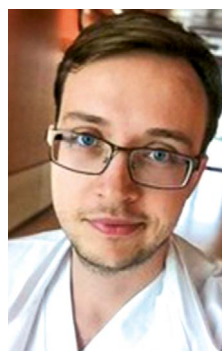
References

- 1 Bembenek JP, Karlinski MA, Kurkowska-Jastrzebska I, Czlonkowska A. Embolic strokes of undetermined source in a cohort of Polish stroke patients. *Neurol Sci*. 2018 June;39(6):1041–7.
- 2 Schwartz FR, Sodickson AD, Pickhardt PJ, Sahani DV, Lev MH, Gupta R. Photon-Counting CT: Technology, Current and Potential Future Clinical Applications, and Overview of Approved Systems and Those in Various Stages of Research and Development. *Radiology*. 2025 Mar;314(3):e240662. doi: 10.1148/radiol.240662. Erratum in: *Radiology*. 2025 Apr;315(1):e259006. doi: 10.1148/radiol.259006. PMID: 40067107; PMCID: PMC11950899.
- 3 Madhavan AA, Bathla G, Benson JC, Diehn FE, Nagelschneider AA, Lehman VT. High yield clinical applications for photon counting CT in neurovascular imaging. *Br J Radiol*. 2024 May 7;97(1157):894–901. doi: 10.1093/bjrt/qae058. PMID: 38460543; PMCID: PMC11075996.
- 4 Menon BK, d'Esterre CD, Qazi EM, Almekhlafi M, Hahn L, Demchuk AM, Goyal M. Multiphase CT Angiography: A New Tool for the Imaging Triage of Patients with Acute Ischemic Stroke. *Radiology*. 2015 May;275(2):510–20.
- 5 Goyal M, Demchuk AM, Menon BK, Eesa M, Rempel JL, Thornton J, Roy D, et al. Randomized Assessment of Rapid Endovascular Treatment of Ischemic Stroke. *N Engl J Med*. 2015 Mar 12; 372(11):1019–30.
- 6 Ståhl F, Szum A, Damlin A, Planken RN, Coutinho JM, Granberg T, Lundberg J. Nongated Photon Counting Computed Tomography Angiography Detects Cardioembolic Stroke Sources and Thoracic Pathology: A Retrospective Cohort Study. *Stroke Vasc Interv Neurol*. 2025;5(6):e001927.
- 7 Rinkel LA, Guglielmi V, Beemsterboer CFP, Groeneveld NS, Lobé NHJ, Boekholdt SM, et al. Diagnostic Yield of ECG-Gated Cardiac CT in the Acute Phase of Ischemic Stroke vs Transthoracic Echocardiography. *Neurology*. 2022;99(14):e1456–e1464.

The statements by customers of Siemens Healthineers described herein are based on results that were achieved in the customer's unique setting. Since there is no "typical" hospital and many variables exist (e.g., hospital size, case mix, level of IT and/or automation adoption) there can be no guarantee that other customers will achieve the same results.

The products/features (mentioned herein) are not commercially available in all countries. Their future availability cannot be guaranteed.

** Rapid Results Technology refers to tasks from post-processing applications provided by Siemens Healthineers. These tasks may be displayed on syngo.via or via the scanner user interface, depending on configuration or nature of the related task. syngo.via is a separate device and not part of the CT scanner.*



Contact

Adrian Szum, M.D., M.Sc.
Department of Neuroradiology
Karolinska University Hospital
171 76 Stockholm
Sweden

Department of Clinical Neuroscience
Karolinska Institutet
Tomtebodavägen 18 A
171 77 Stockholm
Sweden
adrian.szum@ki.se

Flat-Panel CT Perfusion Imaging in the Angiography Suite to Assess Reperfusion Quality after Thrombectomy

Adnan Mujanovic¹, Thomas Meinel², Barbara Birner², Jan Gralla¹, Tomas Dobrocky¹, Johannes Kaesmacher^{1,3,4}

¹ Department of Diagnostic and Interventional Neuroradiology, University Hospital Bern, Inselspital, University of Bern, Switzerland

² Department of Neurology, University Hospital Bern, Inselspital, University of Bern, Switzerland

³ Diagnostic and Interventional Neuroradiology, CIC-IT 1415, CHRU de Tours, France

⁴ Le Studium Loire Valley Institute for Advanced Studies, Orléans, France

Introduction

Reperfusion success after endovascular therapy (EVT) is assessed with 2D digital subtraction angiography (DSA) imaging and is typically graded according to the Thrombolysis in Cerebral Infarction (TICI) scale at the end of an intervention. Presently, all international guidelines advise achieving complete reperfusion (TICI 3), i.e., complete filling of all the vessels in the downstream target territory, including capillaries.

Overestimation of the reperfusion success (i.e., final TICI score) is a well-known phenomenon among operators. Aside from operator-overestimation, factors such as the location of residual perfusion deficit or interventions performed outside of regular working hours may also lead to false rates of complete reperfusion (TICI 3). This is a significant limitation, as it may result in the failure to identify potentially salvageable perfusion deficits at the crucial time point of the intervention. Moreover, there is a growing body of evidence that patients with complete reperfusion (TICI 3) may experience microcirculatory hypoperfusion, or the no-reflow phenomenon, which is not detectable on 2D DSA images and may result in worse patient outcome and higher costs of long-term stroke care.

Multiphase DynaCT is a new imaging modality to assess the collateral vessels. The multiphase data has been used to perform qualitative perfusion imaging with a prototype. This perfusion qualification post-processing SW can be performed directly after mechanical thrombectomy [1].

Flat panel computed tomography perfusion imaging (FPCT-PI) has the potential to provide three-dimensional and time-resolved perfusion maps with an accurate three-dimensional presentation of the location and extent of residual perfusion deficits. It can quantify cerebral blood flow and volume, and allow for a thorough risk-benefit assessment (e.g., brain eloquence grading) when guiding clinical decision-making. We propose a new interventional workflow integrating FPCT-PI at the end of an intervention. This workflow could potentially enhance the detection of residual perfusion deficits and aid operators in making informed decisions.

Methods

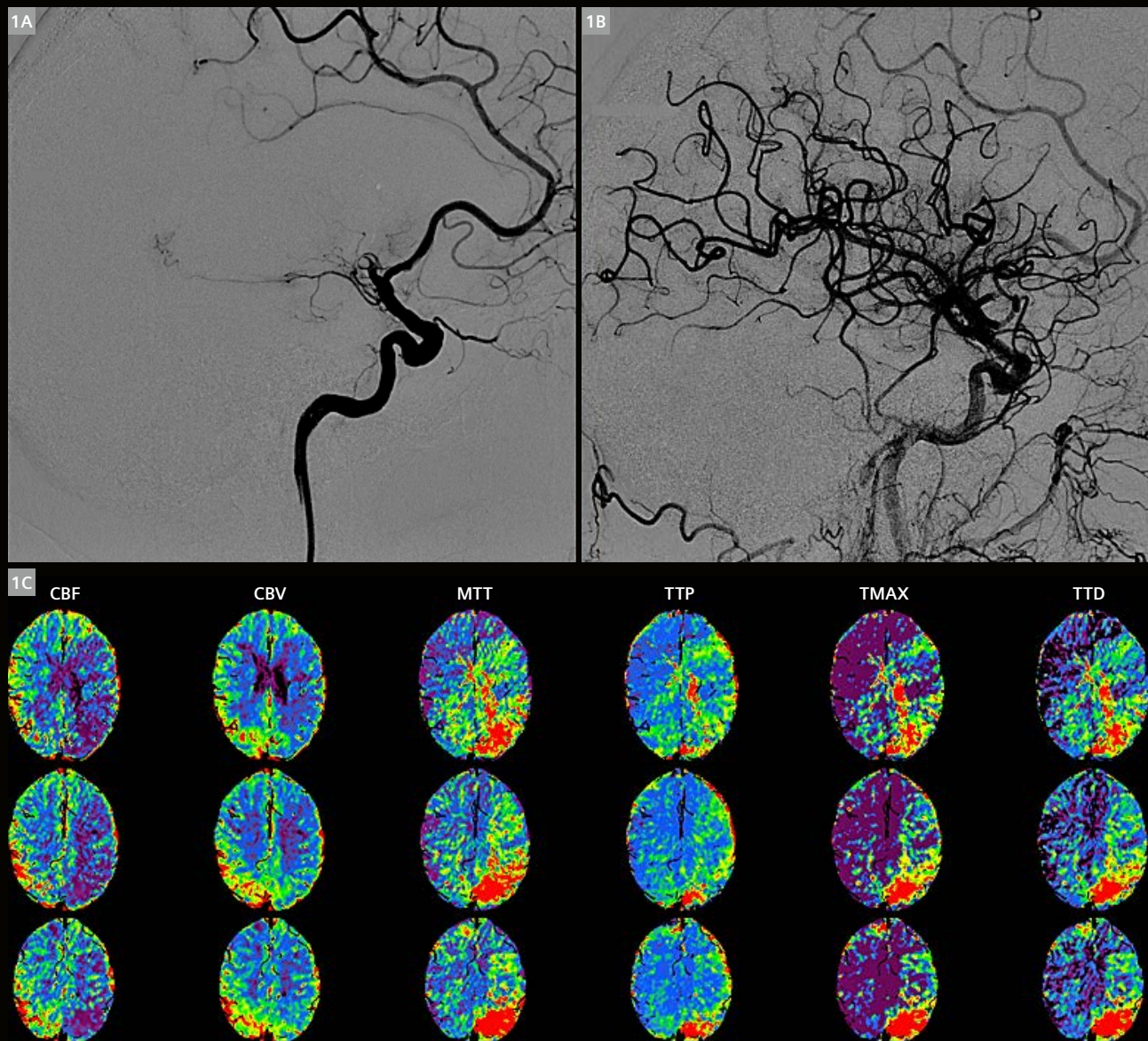
FPCT-PI acquisition

Biplane flat-panel detector angiographic systems (ARTIS icono, Siemens Healthineers, Forchheim, Germany) were used to acquire imaging data for the whole brain. Out of the ten sweeps, the first two rotations served as a mask run, while the following eight were used to record inflow and outflow of contrast agent (60 mL Iopamiro 400 or 300), creating time-density curves with eight time points. Contrast agent injection via an 18 G cubital venous line was started simultaneously with the first mask run. All contrast agents were flushed with saline (40–60 mL) with an injection rate of 5 mL/s via a dual-head power injector.

Case 1

A 90-year-old male patient presented to the emergency department with a right-side hemiplegia and right-side facial paresis (National Institutes of Health Stroke Scale: NIHSS 15). Magnetic resonance imaging (MRI) on admission revealed an occlusion of the proximal middle cerebral artery (MCA) on the left side, with an acute ischemia of the basal ganglia area and without any hemorrhagic transformation. The patient was immediately transferred to the angiography suite, where EVT was performed. The first angiography run showed an M1 occlusion of the MCA

(Fig. 1A). It was decided to use the combined thrombectomy approach with stent retriever (Solitaire 6 x 40 mm; Medtronic, Minneapolis, MN, USA) and aspiration catheter (RED 72, Penumbra, Inc., Alameda, CA, USA). After one maneuver, there was a recanalization of all the intracranial vessels (Fig. 1B). The operator rated the case as complete reperfusion (TICI 3). However, the immediate follow-up FPCT-PI showed evidence of demarcated hypoperfusion in the occipital lobe that was missed on the DSA (Fig. 1C). No further adjunctive attempts were performed in this case.



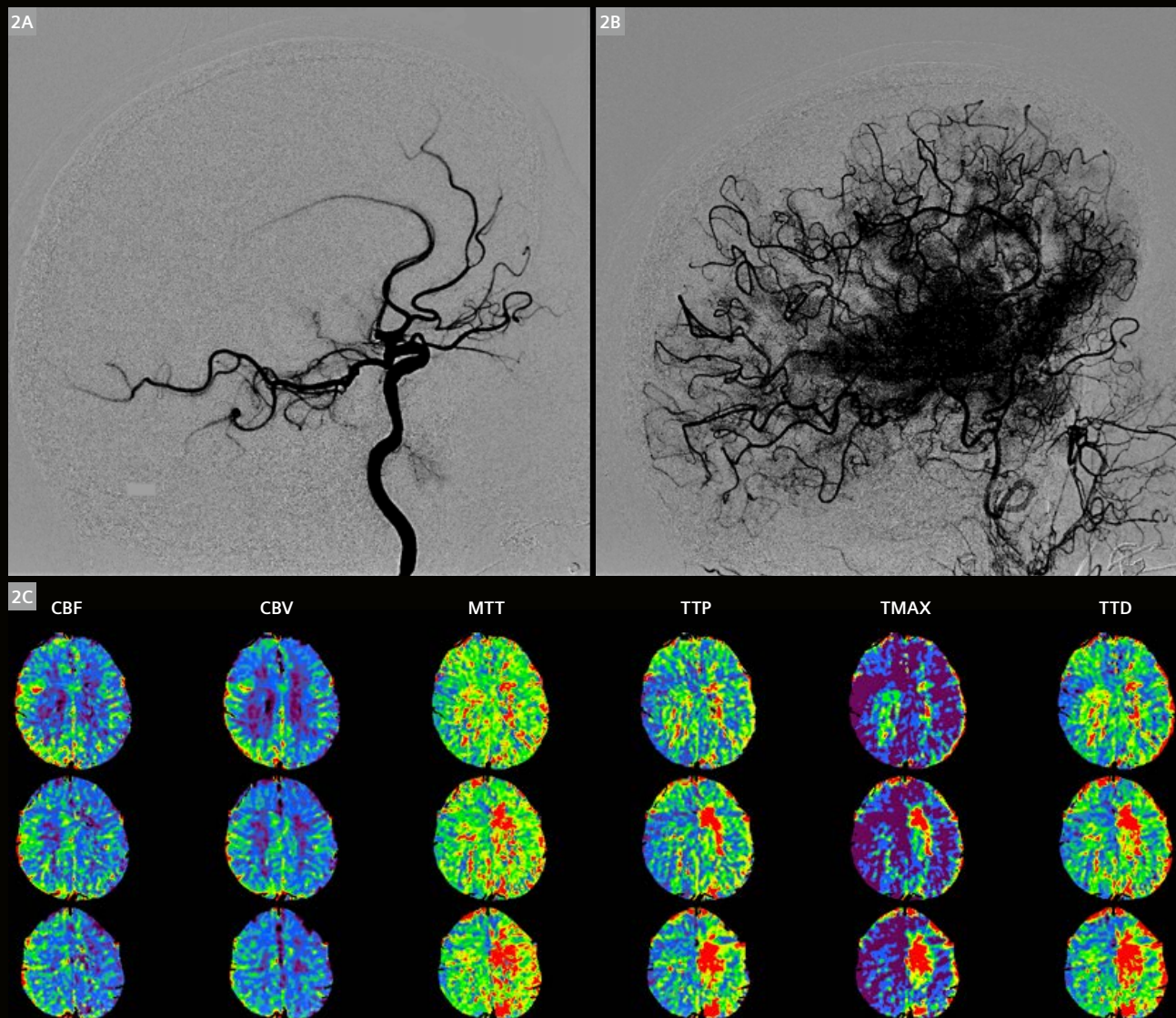
1 (1A) First DSA imaging shows an occlusion of the M1 MCA segment. (1B) Final DSA imaging shows reperfusion of the MCA branch and was rated as complete reperfusion (TICI 3) by the operator. (1C) The immediate postinterventional FPCT-PI shows a clear hypoperfusion deficit in the parietal region, which was missed on final DSA.

DSA: digital subtraction angiography; MCA: middle cerebral artery; TICI: Thrombolysis in Cerebral Infarction scale; FPCT-PI: flat-panel computed tomography perfusion imaging

Case 2

A 65-year-old male patient presented to the emergency department with a right-side hemiplegia, right-side facial paresis, and aphasia (NIHSS 17). Computed tomography (CT) on admission revealed an occlusion of the proximal MCA on the left side, with a perfusion mismatch in the entire MCA region and without any hemorrhagic transformation. The patient was immediately transferred to the angiography suite, where EVT was performed. The first angiography run showed an M1 occlusion of the MCA (Fig. 2A). Mechanical thrombectomy was performed

with a stent retriever (Solitaire 4 x 40 mm; Medtronic, Minneapolis, MN, USA), and complete recanalization was achieved after one maneuver (Fig. 2B). The operator rated the case as complete reperfusion with complete capillary filling of the distal vessels in the downstream territory (TICI 3). However, the immediate follow-up FPCT-PI showed evidence of emboli in the new territory of the A4 segment of the anterior cerebral artery (ACA), which was missed on the DSA (Fig. 2C). No further adjunctive attempts were performed in this case.



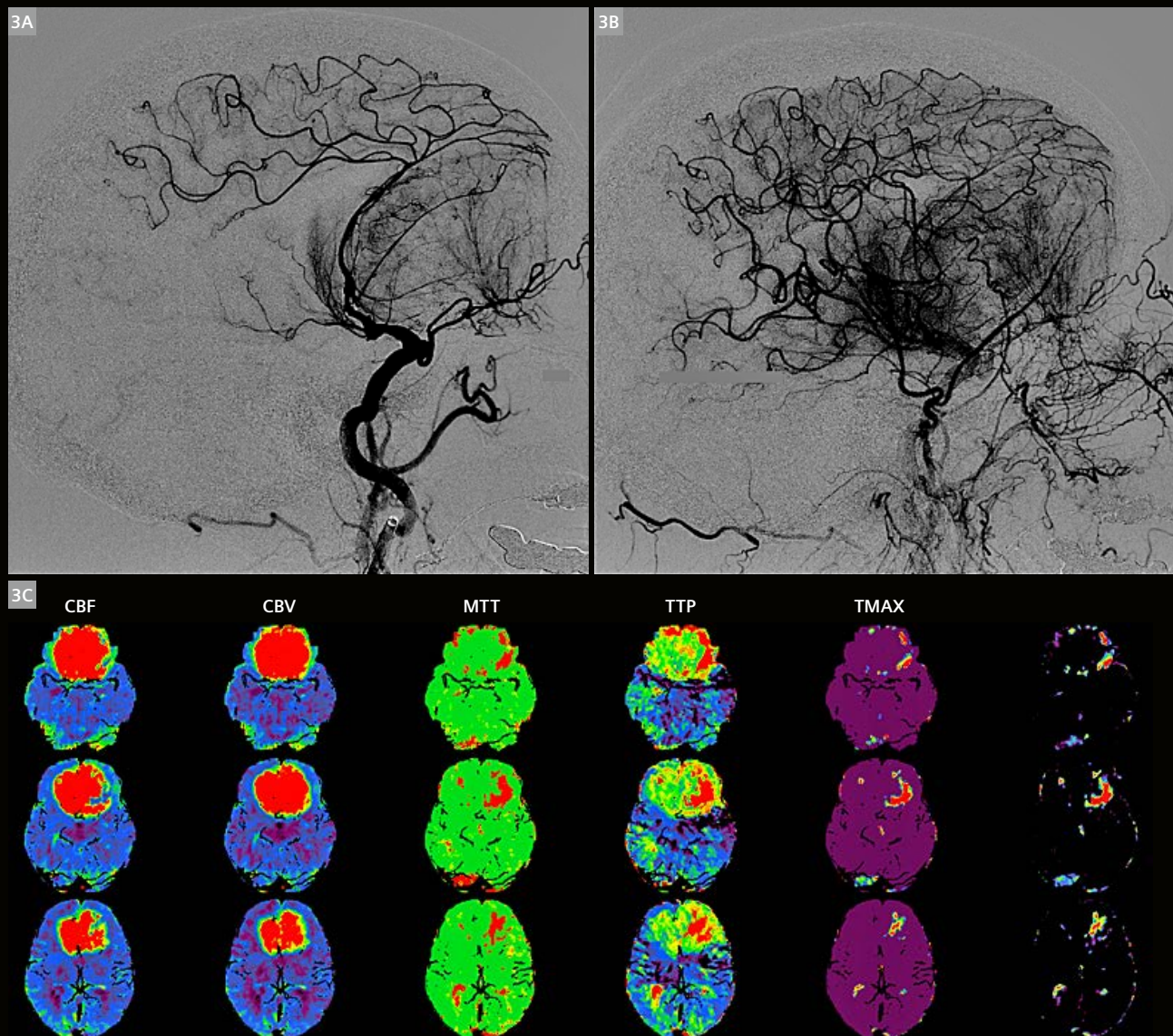
2 (2A) First DSA imaging shows an occlusion of the M1 MCA segment. (2B) Final DSA imaging shows reperfusion of the MCA branch and was rated as complete reperfusion (TICI 3) by the operator. (2C) The immediate postinterventional FPCT-PI shows a newly noted perfusion deficit which corresponded to the ACA territory. Upon re-inspection of the final DSA image, emboli were confirmed in the new territory of the A4 ACA segment.

DSA: digital subtraction angiography; MCA: middle cerebral artery; TICI: Thrombolysis in Cerebral Infarction scale; FPCT-PI: flat-panel computed tomography perfusion imaging; ACA: anterior cerebral artery

Case 3

A 94-year-old female patient presented to the emergency department with a right-side hemiplegia, hemi-inattention, and unresponsiveness to questions (NIHSS 25). CT on admission revealed an occlusion of the MCA on the left side, with an expansive mass on frontal basis (6 x 6 x 7 cm). The patient was immediately transferred to the angiography suite, where EVT was performed. The first angiography run showed an M1 occlusion of the MCA (Fig. 3A). In addition, there was a pronounced displacement of the vessels and capillary blush in the frontal part. Mechanical

thrombectomy was performed with a stent retriever (Solitaire 4 x 40 mm) and aspiration catheter (RED 62, Penumbra, Inc., Alameda, CA, USA). After one thrombectomy maneuver, a complete reperfusion was achieved (TICI 3, Fig. 3B). The immediate follow-up FPCT-PI showed a large hyperperfused mass at the base of the anterior cranial fossa, which would not directly correspond to the M1 MCA vascular territory (Fig. 3C). On the follow-up examination, the expansive mass was confirmed to be an olfactory meningioma.



3 (3A) First DSA imaging shows an occlusion of the M1 MCA segment, and there is a pronounced capillary blush in the frontal part. (3B) Final DSA imaging shows reperfusion of the MCA branch and was rated as complete reperfusion (TICI 3) by the operator (3C). The immediate follow-up FPCT-PI shows a strong perfusion signal in both frontal lobes with a strong increase in cerebral blood flow (CBF) and cerebral blood volume (CBV) in the corresponding area. This area of increased reperfusion corresponded to newly diagnosed meningioma. DSA: digital subtraction angiography; MCA: middle cerebral artery; TICI: Thrombolysis in Cerebral Infarction scale; FPCT-PI: flat-panel computed tomography perfusion imaging

Each acquired rotation was reconstructed individually using the filtered back projection algorithm available on the clinical system (ARTIS icono VE20, Siemens Healthineers, Forchheim, Germany). The reconstruction algorithm includes system-specific steps to correct for scatter radiation, beam hardening, projection image truncation, and ring artifacts [2]. The reconstruction parameters were 0.48 mm voxel size, 512 x 512 matrix, 378 slices, 0.48 mm slice thickness, and a “HU Normal” reconstruction kernel.

FPCT-PI post-processing

First, 3D-3D registration was performed between the first acquired volume and all remaining volumes to compensate for potential head motion during the acquisition. Accordingly, all volumes were automatically aligned to the orbitomeatal line and spatially resampled to a 0.96 mm voxel size. The two mask volumes were used to subtract the anatomical background from the remaining eight contrasted volumes. Noise reduction via non-linear filtering was performed on the contrasted subtracted volumes. Time-concentration curves with a temporal sampling of one second were extracted from the subtracted volume series by resampling via temporal spline interpolation. Afterwards, automated detection of the arterial input function was performed and voxels containing air, bone, or vascular structures were excluded by thresholding. Perfusion maps were computed using deconvolution-based perfusion analysis (Siemens Healthineers, Forchheim, Germany) [3].

Discussion

Flat-panel detector technology was designed to improve the quality of standard radiography through increased absorption efficiency and a wider dynamic range. When integrated into a rotating C-arm system in the angio suite, multi-phase FPCT-PI offers superior spatial resolution and allows the acquisition of time-resolved perfusion maps such as time-to-peak (TTP), time-to-maximum (Tmax), cerebral blood flow (CBF), and cerebral blood volume (CBV) maps.

Several studies have shown good correlation between perfusion maps on standardized CT and MR imaging protocols and FPCT-PI, including a multicenter analysis [4]. The implementation of time-resolved whole-brain FPCT-PI seems to be technically feasible, and both qualitative and quantitative perfusion results align with those obtained using conventional perfusion imaging.⁴ A recent proof-of-concept study evaluated the value of FPCT-PI performed during or immediately after the endovascular procedure. In total, more than one third of patients showed additional clinically relevant information on FPCT-PI, which was not noted on the 2D DSA [1].

One advantage of FPCT-PI is that it offers a simple workflow. This technique enables the assessment of tissue reperfusion status at an arbitrary time point during a thrombectomy case, while options for adjunctive intra-arterial treatment (e.g., intra-arterial lytics or secondary thrombectomy) are still available. Based on preliminary data, FPCT-PI demonstrates high sensitivity in detecting residual vessel occlusions, considering collateral circulation from various territories and identifying the anatomical location of hypoperfused regions. While these results are promising, a systematic prospective investigation of this new imaging technique is urgently needed to justify widespread implementation in clinical routine.

References

- 1 Mujanovic A, Kurmann CC, Manhart M, Piechowiak EI, Pilgram-Pastor SM, Serrallach BL, et al. Value of Immediate Flat Panel Perfusion Imaging after Endovascular Therapy (AFTERMATH): A Proof of Concept Study. *AJNR Am J Neuroradiol.* 2024;45(2):163–170.
- 2 Kurmann CC, Kaesmacher J, Cooke DL, Psychogios M, Weber J, Lopes DK, et al. Evaluation of time-resolved whole brain flat panel detector perfusion imaging using RAPID ANGIO in patients with acute stroke: Comparison with CT perfusion imaging. *J Neurointerv Surg.* 2023;15(4):387-392. Epub 2022 Apr 8.
- 3 Struffert T, Deuerling-Zheng Y, Kloska S, Engelhorn T, Lang S, Mennecke A, et al. Dynamic Angiography and Perfusion Imaging Using Flat Detector CT in the Angiography Suite: A Pilot Study in Patients with Acute Middle Cerebral Artery Occlusions. *AJNR Am J Neuroradiol.* 2015;36(10):1964–70.
- 4 Serrallach BL, Mujanovic A, Ntoulis N, Manhart M, Branca M, Brehm A, et al. Flat-panel Detector Perfusion Imaging and Conventional Multidetector Perfusion Imaging in Patients with Acute Ischemic Stroke: A Comparative Study. *Clin Neuroradiol.* 2024;34(3):625–635.

Contact

Adnan Mujanovic, M.D., Ph.D.
Department of Diagnostic and
Interventional Neuroradiology
University Hospital Bern, Inselspital
Freiburgstrasse 18
3010 Bern
Switzerland
adnan.mujanovic@insel.ch



This manuscript reflects ongoing research conducted at the University Hospital Bern Inselspital on the use of flat-panel CT perfusion imaging in the treatment of acute ischemic stroke patients. The concepts and information presented in this article are based on research and are not commercially available. Healthcare practitioners are reminded to rely on their own clinical expertise, training, and judgment when treating patients. This material does not substitute professional medical advice or treatment decisions. The responsibility for diagnosis and treatment lies solely with the treating physician. Siemens Healthineers supported the research, but this content is not intended to provide medical advice or direct clinical guidance.

Pictorial Essay of Cerebral CT Angiographies in the Era of Photon-Counting CT

Why do photon-counting CT systems produce cerebral CT angiography data that is so different from conventional CT systems? Why can photon-counting CT resolve the vessels and devices shown in the cases presented here? A short technical explanation.

This pictorial essay focuses on cerebral CT angiography (CCTA) in neurovascular pathologies. Specifically, it addresses the ability to image fine anatomical alterations of cerebral vessels of interest and especially devices after interventional procedures. The CCTA data acquired by photon-counting computed tomography (PCCT), as presented in the NAEOTOM Alpha systems, differs from the CCTA data acquired on conventional CT systems. The differences are mainly due to the ability of PCCT to provide both high resolution and high radiation sensitivity with its photon-counting detector [1, 4].

In addition, the PCCT detector material (cadmium telluride, CdTe) is more homogeneously sensitive to X-ray energies than conventional energy-integrating detectors (EID) are. In particular, the material is more sensitive to the lower energies emitted from the X-ray tube. This means that for the same tube and at identical tube settings, the CdTe-based PCCT detector will show a shift toward events measured at the lower energy spectrum and will therefore achieve a higher attenuation of iodine than the conventional detector.

The physics behind the attenuation curve of iodine and the principles of low-kV imaging and low-kiloelectron-volt (keV) spectral reconstruction are not changed by the different sensitivity of the detector material. However, this is of special interest for some of the images presented in this essay because, for the highest resolution of this detector generation and for the higher kVp settings used for the X-ray tube in these cases (e.g., 120 or 140 kVp with the consequence of less prominent artifacts, mainly beam hardening, and therefore improved overall image quality compared to low-kVp tube settings, e.g., 70 kVp), the data for the individual pixel is not used to calculate monoenergetic images. This is available for the data incorporating the information from the smallest cluster of the pixelated anodes of the detector, which represents a real physical resolution of approximately 0.4 mm in the z-axis and the x-/y-axes. Otherwise, the usable minimal isotropic resolution is approximately $0.2 \times 0.2 \times 0.2 \text{ mm}^3$ and the achievable contrast depends on the kVp setting and the detector sensitivity.

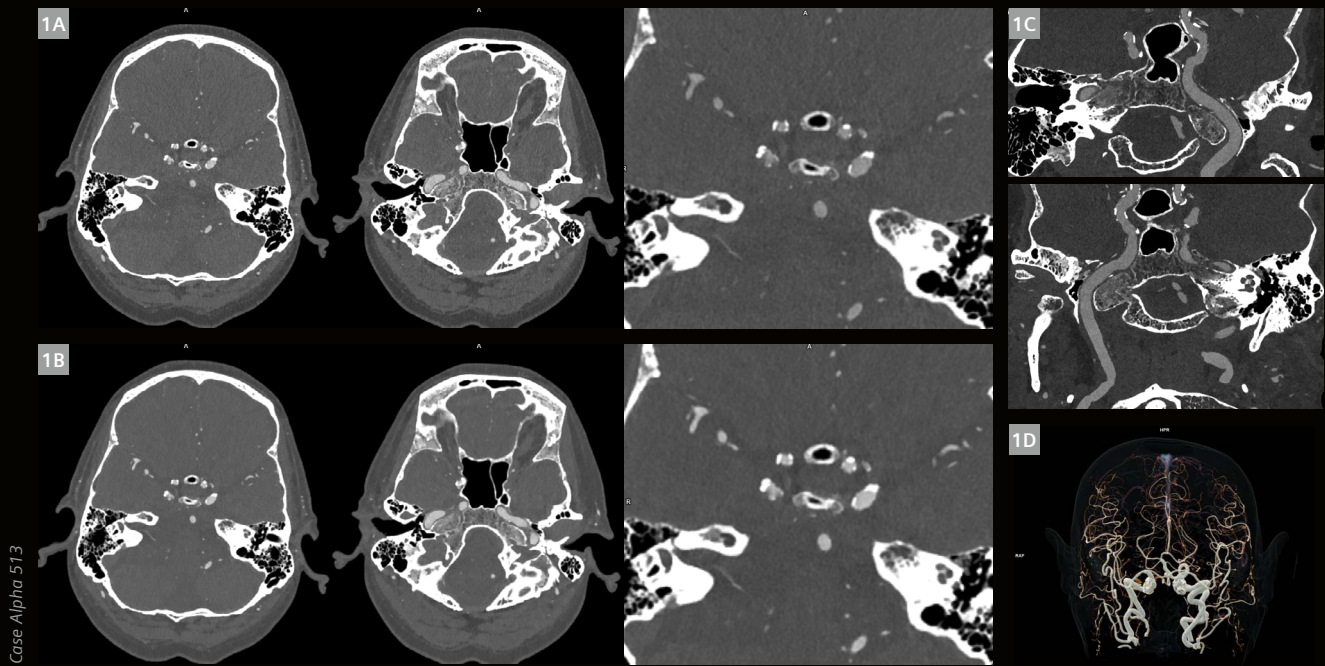
Note that resolution does not come for free: All images shown here match the new level of intrinsic resolution

with adjustments to the image sharpness and the matrix size of the reconstructed images. Higher resolution introduced by sharper kernel reconstruction will change the noise within the image. Even the signal-to-noise ratio determined by the radiation dose applied to measure the structures is kept constant compared to less aggressive kernel settings. Furthermore, and similar to the fact that higher resolution requires higher radiation levels, the volume/iodine delivery rate of contrast media must be adjusted, as the iodine load within these small anatomical structures will determine their detectability. In other words, for the same applied radiation level, smaller structures are visualized compared to a conventional CT system. Regarding the resolution, the differentiation between artificially increased resolution by post-processing and the physical resolution as provided by the PCCT scanner is important to mention also in the context of radiation.

Besides the detectability of small vessels, the combination of high resolution and the different handling of kernels and tube currents compared to conventional (low-kV) CCTA changes how blooming of calcium and beam hardening (e.g., by metallic structures) is controlled. However, the need to further enhance edges using sharp kernels can also aggravate signal alterations and cause more prominent artifacts, even when using a kVp tube setting that is higher than it would have been in the previous era of low-kV CCTA.

When reviewing these CCTA data sets, it is crucial to critically review the impact of the devices and their effects on the ability to detect, for instance, intra-luminal remodeling after stenting, or mimicry of luminal changes by the kernels when visualizing stenosis after anastomosis.

This pictorial essay is not intended to provide an overview of the scientific evidence for how this new detector technology may change clinical routine in CCTA. To gain further insights into how PCCT detectors can change CCTA performance, consider reading the articles by Diehn et al. [1] and He et al. [2]. De Beukelaer et al. [3] compare PCCT angiography with conventional digital subtraction angiography for imaging intracranial stents. Madhavan et al. [4] provide a broader statement on the potential of PCCT to change neurovascular imaging.



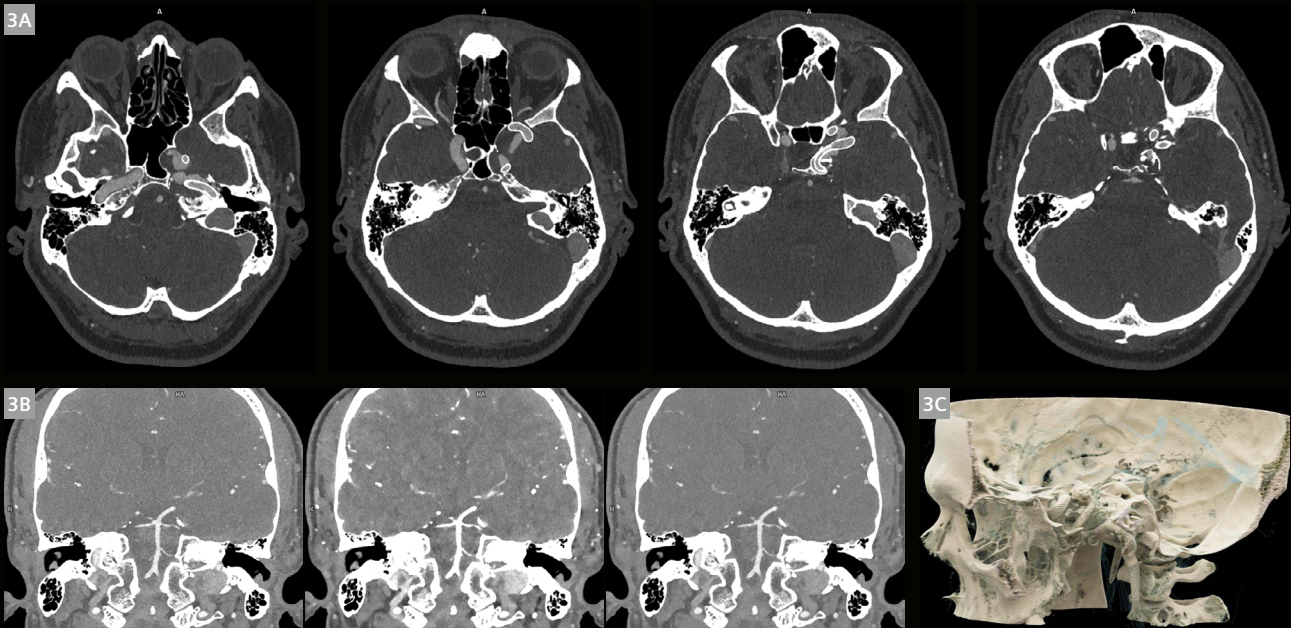
Case Alpha 513

1 Impact of resolution on calcium blooming. **(1A)** Axial 0.2 mm slices (T3D conventional image reconstruction (conv. recon.) | Hv60 kernel) and corresponding zoomed reconstruction; **(1B)** axial 0.4 mm slices (55 keV | Hv56 kernel) and corresponding zoomed reconstruction; **(1C)** curved multiplanar reconstruction (MPR) based on zoomed 0.2 mm slices; **(1D)** cinematic volume rendering technique (VRT). Images courtesy of Jones Radiology, SAHMRI clinic, Adelaide, SA, Australia.



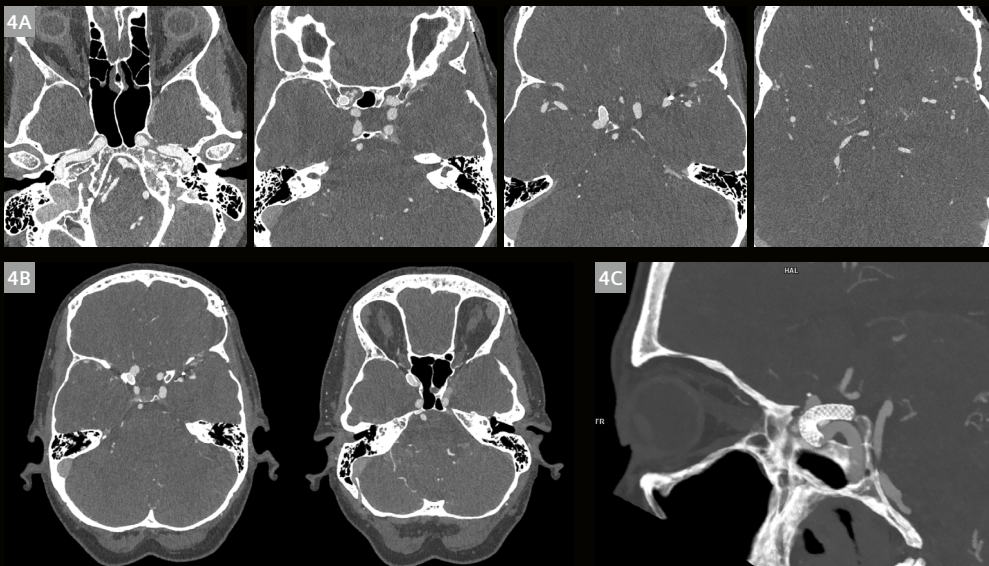
Case Alpha 375

2 Device example 1. **(2A)** Axial 0.2 mm slices (T3D conv. recon. | Hv60 kernel); **(2B)** corresponding curved MRP; **(2C)** corresponding maximum intensity projection (MIP); **(2D)** cinematic VRTs. Images courtesy of Jones Radiology, SAHMRI clinic, Adelaide, SA, Australia.



Case Alpha 373

3 Device example 2 with spectral versus T3D MPR and contrast-to-noise ratio (CNR). **(3A)** Axial 0.2 mm slices (T3D conv. recon. | Hv60 kernel); **(3B)** coronal oblique MPRs based on T3D (Hv60), and comparison with 45 and 70 keV reconstructions (comparable to conventional 120 kVp image contrast); **(3C)** cinematic VRT. Images courtesy of Jones Radiology, SAHMRI clinic, Adelaide, SA, Australia.



4 Device example 3 with resolution and zoomed imaging. **(4A)** Axial 0.2 mm slices (T3D conv. recon. | Hv60 kernel | zoomed reconstruction at 1024 matrix); **(4B)** axial 0.4 mm slices (T3D | Hv60 kernel | standard field of view (FOV) at 1024 matrix); **(4C)** corresponding MIP; **(4D)** cinematic VRTs. Images courtesy of Jones Radiology, SAHMRI clinic, Adelaide, SA, Australia.



Case Alpha 381

Further reading

- 1 Diehn FE, Zhou Z, Thorne JE, Campeau NG, Nagelschneider AA, Eckel LJ, et al. High-Resolution Head CTA: A Prospective Patient Study Comparing Image Quality of Photon-Counting Detector CT and Energy-Integrating Detector CT. *AJNR Am J Neuroradiol.* 2024;45(10):1441–1449.
- 2 He N, Zhang Y, Li Z, Xu Z, Lyu H, Li J, et al. Ultrahigh-Resolution Photon-Counting Detector CTA of the Head and Neck: Image Quality Assessment and Vascular Kernel Optimization. *AJR Am J Roentgenol.* 2025;224(1):e2431763.
- 3 De Beukelaer F, Wuyts L, De Beukelaer S, Van Hedent S, Nikoubashman O, Wiesmann M, et al. Photon-counting CT-angiography in comparison to digital subtraction angiography for assessing intracranial aneurysms after coiling or clipping. *Neuroradiology.* 2025;67(8):2021–2030.
- 4 Madhavan AA, Bathla G, Benson JC, Diehn FE, Nagelschneider AA, Lehman VT. High yield clinical applications for photon counting CT in neurovascular imaging. *Br J Radiol.* 2024;97(1157):894–901.

**Contact**

Matthias Lichy, MD, MSc.
Siemens Healthineers
DI CT M&S CMS
Healthcare Building 1
Siemensstr. 3
91301 Forchheim
Germany
Matthias.Lichy@siemens-healthineers.com

The entire editorial staff at University Hospital Bern, Inselspital, University of Bern, Switzerland, and at Siemens Healthineers extends their appreciation to all the radiologists, technologists, physicists, experts, and scholars who donate their time and energy — without payment — in order to share their expertise with the readers of *The Role of Imaging Along the Stroke Pathway*.

Imprint

© 2026 by Siemens Healthineers AG,
All Rights Reserved

Publisher:

Siemens Healthineers AG
Magnetic Resonance,
Karl-Schall-Str. 6, D-91052 Erlangen, Germany

Guest Editor:

Professor Dr. Johannes Kaesmacher, M.D., Ph.D.
University Institute of Diagnostic and Interventional
Neuroradiology
University Hospital Bern, Inselspital
Freiburgstrasse 18
CH-3010 Bern
Switzerland
johannes.kaesmacher@insel.ch

Editor-in-chief:

Antje Hellwich
SHS DI MR M&S CSM
antje.hellwich@siemens-healthineers.com

Associate Editor:

André Fischer, Ph.D.
SHS DI MR M&S CSM
andre.fischer@siemens-healthineers.com

Editor for CT content:

Alina Stenke
SHS DI CT M&S CE
alina.stenke@siemens-healthineers.com

Editor for AT content:

Stephanie Hench
SHS AT IR M
stephanie.hench@siemens-healthineers.com

Copy Editing:

Sheila Regan, Jen Metcalf, UNIWORKS,
www.uni-works.org
(with special thanks to Kylie Martin)

Layout:

Agentur Baumgärtner,
Friedrichstr. 4, D-90762 Fürth, Germany,
www.agentur-baumgaertner.com

PrePress and Image Editing, Production:

Sandra Birner, Andrea tom Felde,
Jennifer Klanar, Paul Linssen,
Siemens Healthineers AG

Note in accordance with § 33 Para.1 of the German Federal Data Protection Law: Dispatch is made using an address file which is maintained with the aid of an automated data processing system.

The statements and views of the authors in the individual contributions do not necessarily reflect the opinion of the publisher.

The information presented in these articles and case reports is for illustration only and is not intended to be relied upon by the reader for instruction as to the practice of medicine. Any health care practitioner reading this information is reminded that they must use their own learning, training, and expertise in dealing with their individual patients. This material does not substitute for that duty and is not intended by Siemens Healthineers AG to be used for any purpose in that regard. The drugs and doses mentioned herein are consistent with the approval labeling for uses and/or indications of the drug. The treating physician bears the sole responsibility for the diagnosis and treatment of patients, including drugs and doses prescribed in connection with such use. The Operating Instructions must always be strictly followed when operating a system. The sources for the technical data are the corresponding data sheets. Results may vary.

The written consent of the authors and publisher is required for partial reproduction in printed form or for reprinting of an article.

We welcome your questions and comments about the editorial content of this edition. Please contact us at magnetomworld.team@siemens-healthineers.com.

Manuscripts as well as suggestions, proposals and information are always welcome; they are carefully examined and submitted to the editorial board for attention. MAGNETOM Flash is not responsible for loss, damage, or any other injury to unsolicited manuscripts or other materials. We reserve the right to edit for clarity, accuracy, and space. Include your name, address, and phone number and send to the editors, address above.

***The Role of Imaging Along the Stroke Pathway* is also available online:**
magnetomworld.siemens-healthineers.com/publications/mreadings

Not for distribution in the US

On account of certain regional limitations of sales rights and service availability, we cannot guarantee that all products included in this brochure are available through the Siemens Healthineers sales organization worldwide. Availability and packaging may vary by country and is subject to change without prior notice. Some/All of the features and products described herein may not be available in the USA.

The information in this document contains general technical descriptions of specifications and options as well as standard and optional features which do not always have to be present in individual cases, and which

may not be commercially available in all countries. Due to regulatory reasons their future availability cannot be guaranteed. Please contact your local Siemens Healthineers organization for further details.

Siemens Healthineers reserves the right to modify the design, packaging, specifications, and options described herein without prior notice. Please contact your local Siemens Healthineers sales representative for the most current information.

Note: Any technical data contained in this document may vary within defined tolerances. Original images always lose a certain amount of detail when reproduced.

Siemens Healthineers Headquarters

Siemens Healthineers AG
Siemensstr. 3
91301 Forchheim, Germany
Phone: +49 9191 180
siemens-healthineers.com